Optimization of Acidic Post-translational Modification Detection and Natural Product Biosynthetic Enzyme Analysis with Dual Polarity nLC/FT-ICR Mass Spectrometry

by

Phillip J. McClory

A dissertation submitted in partial fulfillment
of the requirements for the degree of
Doctor of Philosphy
(Chemistry)
in the University of Michigan
2017

Doctoral Committee:

        Professor Kristina I. Håkansson, Chair
        Professor Robert T. Kennedy
        Associate Professor Brandon T. Ruotolo
        Professor David H. Sherman

mcclory@umich.edu

ORCID iD: 0000-0002-7804-5191

2017

To my family, for love and support

Acknowledgements

Over the last 5 years I have grown as a person and a scientist thanks to many people. I would first like to thank my wife Michelle for her support, love, and honesty about me and my studies. I couldn't have completed this dissertation without her understanding and sense of humor. Next, my parents Tom and Donna. I sincerely appreciate the opportunities they have provided for me in my life, allowing me to continue my education after undergraduate studies. I would also like to thank my In-Laws Steve, Laura, Scott, and Doug, for all of your support and help with seemingly endless housing moves. Without my dog and cat, Shadow and Leo, I would have been absurdly stressed and would not have made it these 5 years without them.

I would like to sincerely thank my advisor Dr. Kristina Håkansson for support throughout my research. I appreciate the scientific flexibility and banter she has had with me from theoretical experiments to future career options. Also, her positive attitude even when our instruments did not function was enough to keep me motivated, even when it was bleak. Finally, her willingness to send us to conferences to learn and present greatly helped me expand my scientific horizons.

I would also like to thank my committee members, Prof. Brandon Ruotolo, Prof. Robert Kennedy, and Prof. David Sherman, for their insightful commentary and clever suggestions to push my research forward. Also, their willingness to let me borrow valuable instrumentation, materials, and mass spectrometers in their respective laboratories despite our lab's run of bad luck, allowed me to complete this dissertation in a timely fashion. I am grateful for these opportunities and collaborations.

Over the years, I have relied on many of my fellow graduate students and post-docs for advice and help. I appreciate all of the help Dr. Jessica Rabuck-Gibbons and Dr. Richard Kerr provided me with the Waters Micromass LCT Premier and Synapt G1 instrumentation. Dr. Jenny Wong provided me with expertise in nESI needle pulling and fabrication. I am grateful for all of her help

and time spent on the needle puller. Also, I would like to thank Sam Slocum for his dedication and tenacity with the Bryostatin project.

The Håkansson lab is always a fun and exciting place to be, even if our instruments do not always behave. I believe this is due to the warm culture that has previously been established by its members. Without Dr. Wendi Hale, Dr. Ning Wang, Dr. Tao Jiang, Dr. Nick Borotto, Dr. Hye Kyong Kweon, Kevin Ileka, and Emma Wang, I don't think it would have been nearly as great of place to work. Without all of your helpful discussions and coffee runs, I would have been much less productive.

Phil McClory

July 22, 2017

Ann Arbor, MI

Table of Contents

List of Figures

xiv

List of Abbreviations

ACP	Acyl Carrier Protein
AT	Acyl Transferase
ATP	Adenosine Triphosphate
BryAM3	Bryostatin A Module 3
CID	Collision Induced Dissociation
CRM	Charged Residue Model
CZE	Capillary Zone Electrophoresis
DBA	Dibutylamine
DDA	Data Dependent Acquisition
DEA	Diethylamine
DIA	Data-independent Acquisition
DPA	Dipropylamine
ECD	Electron Capture Dissociation
EDD	Electron Detachment Dissociation
EID	Electron Induced Dissociation
ESI	Electrospray Ionization
ETD	Electron Transfer Dissociation
FA	Formic Acid
FID	Free Induction Decay
FT-ICR	Fourier Transform-Ion Cyclotron Resonance
GELFrEE	Gel-Eluted Liquid Fraction Entrapment
i.d.	Inner Diameter
IEM	Ion Ejection Model
IMAC	Immobilized Metal Affinity Chromatography
KirCAT	Kirromycin Acyl Transferase
KS	Ketosynthase

MOAC	Metal Oxide Affinity Chromatography
MS	Mass Spectrometry
MS/MS	Tandem Mass Spectrometry
nESI	Nanoelectrospray Ionization
NETD	Negative Electron Transfer Dissociation
niECD	Negative Ion Electron Capture Dissociation
nLC	Nanoflow Liquid Chromatography
NRPS	Nonribosomal Peptide Synthetase
PAPS	Adenosine 3'-Phosphate 5'-Phosphosulfate
Pipe	Piperidine
PKS	Polyketide Synthase
PTM	Post-translational Modification
Ppant	Phosphopantetheine
PPTases	4′-Phosphopantetheine Transferases
Q-TOF	Quadrupole-Time-of-Flight
SCX	Strong Cation Exchange
SEC	Size Exclusion Chromatography
SNAC	N-acetylcysteamine
SWATH	Sequential Isolation Window Acquisition
TBA	Tributylamine
TEA	Triethylamine
TEOA	Triethanolamine
TFE	Trifluoroethanol
TP	Thiophenol
TPA	Tripropylamine
TPST	Tyrosylprotein Sulfotransferase Enzyme
UVPD	Ultraviolet Photodissociation
WAX	Weak Anion Exchange

Abstract

Chair: Kristina I. Håkansson

Mass spectrometry-based proteomic protocols can identify thousands of expressed proteins with widely varying concentrations. However, acidic post-translational modifications (PTMs), e.g., phosphorylation and sulfation, are difficult to examine, due to the reduced ionization efficiency of highly acidic peptides with positive ion mode nanoelectrospray ionization (nESI). This thesis presents methods for improved detection of acidic, modified peptides and natural product biosynthetic active site peptides in both positive and negative ion mode.

Trace addition of trifluoroethanol (TFE) to aqueous samples suppresses corona discharge typically observed in negative ion mode nESI experiments. TFE greatly (~8 fold) improves nESI spray stability without altering observed protein, peptide, and small molecule charge states. This phenomenon is likely due to the highly electronegative fluorine atom's ability to scavenge electrons, thus stemming plasma formation. In negative ion mode nanoflow liquid chromatography-mass spectrometry (nLC-MS) experiments, TFE addition increases the number of identified peptides by 18%. The relatively simple addition of TFE to sample solutions for improved negative ion mode nESI can be readily employed for improved analysis of widely varied compounds in direct infusion and nLC-MS experiments.

The demonstrated compatibility of TFE with nLC-MS allowed for systematic examination of mobile phase and detection polarity effects on peptide identifications. Regardless of mobile phase pH and detection polarity, overall sequence coverage for a six protein digest was similar. However, multiply phosphorylated peptides were only detected at pH 11 in negative ion mode and sulfopeptides were detected most effectively (~55 fold improvement) in negative ion mode and with maximum ion abundance at pH 11. This work demonstrates that alkaline pH separations coupled with negative ion mode nESI provides an efficient method for the detection of highly

acidic multiply phosphorylated peptides and sulfopeptides in a background of tryptic peptides typically examined in most proteomic studies.

Under typical positive ion mode analysis, sulfopeptides undergo proton mediated loss of the PTM, hampering identification and detection. Alkylamines were found to selectively adduct to sulfopeptides in positive ion mode nESI, allowing for discernment of isobaric phosphorylation and sulfation PTMs without the need for high resolution instrumentation. Alkylamine ion-pairing occurs at 98-99% efficiency regardless of solution pH or base concentration. Characteristic [SO_3+alkylamine] neutral losses are observed upon slight collisional activation. This unique transition enables sulfopeptide identification and discovery with positive ion mode data-independent nLC tandem MS. Experiments to discover four sulfopeptide standards in a background of tryptic peptides resulted in 17 sulfopeptide identifications. To our knowledge, the work presented is the first protocol developed for positive ion mode sulfopeptide discovery without the need for tedious chemical modification of a sample proteome prior to analysis.

Optimization of tryptic digestion and separation conditions were imperative for MS detection of covalently tethered intermediates in the polyketide synthase (PKS) bryostatin A, module 3 (BryAM3), which introduces a unique beta-branch and O-methylation in the biosynthesis of bryostatin-1, a potent protein kinase C inhibitor. BryAM3 was successfully (98%) phosphopantetheinylated to generate holo acyl carrier protein (ACP). Malonyl extender unit loading on holo ACP was also successfully achieved (68%) utilizing a non-native kirromycin C trans acyl transferase (KirCAT). Unexpectedly, KirCAT also catalyzed malonation of BryAM3 non-active site cysteine residues and direct ACP loading of thiophenol-activated substrates was observed. These experiments indicate that great care must be taken when performing in vitro studies with this and potentially other trans PKSs.

Chapter 1

Introduction

1.1 Modern Proteomics

Proteomics refers to the study of expressed cellular proteins and their impact on, e.g., cellular signaling, interactions, disease states, and the overall organism.[1-4] While the aims of a specific proteomic experiment can be varied, several challenges exist across most investigations. These challenges include greatly varied protein expression levels, hundreds of post-translational modifications (PTMs), dynamic low concentration PTM states, and sample isolation and processing.[1-3, 5-8] Protein microarrays can successfully profile thousands of proteins via immobilization to a chip, then subsequent detection with fluorescence microscopy.[9-11] The generation of microarrays that can selectively bind thousands of proteins is often challenging due to the widely varied structure and function of expressed cellular proteins. Antibodies are often used as binding agents, greatly increasing cost and chip-to-chip variability in binding efficiencies and affinities.[9, 12]

Recent developments in nanoflow liquid chromatography (nLC) and robust mass spectrometry (MS) instrumentation have enabled the current explosion in global proteomic analysis without the need for tedious substrate generation.[6, 13] MS can successfully address many of these concerns due to its incredible speed (µs–ms) and high sensitivity (<zeptomole).[6, 14-16] Also, due to the robustness and mass accuracy of modern MS, interrogation of incredibly complex samples can be completed in minutes and hundreds of samples can be examined over weeks without significant instrument maintenance.[5, 17] The mass accuracy of modern mass spectrometers, such as Orbitraps, time-of-flight (TOF), or Fourier transform ion-cyclotron resonance (FT-ICR) instruments can routinely

reach 2 ppm, allowing for highly reliable proteomic information to be gathered.[17-19] Most MS-based proteomic analyses are similar in experimental design: 1) proteins are digested and resulting peptides of interest are possibly enriched, 2) peptides are then separated to maximize proteomic coverage, 3) gas-phase ions are generated via nanoelectrospray ionization, and 4) MS detection and subsequent peptide fragmentation is completed.[1, 6]

1.1.1 Protein Digestion

Three major types of proteomic experiments can be performed; bottom-up, top-down, and middle-down analysis.[20, 21] In a bottom-up experiment, a complex mixture of cellular proteins are digested by a protease, typically trypsin, to create an exponentially more complex mixture of peptides.[20, 22] The resulting peptides in the bottom-up experiment are approximately 400-3,000 Da in size and can be efficiently separated by reversed-phase C18 chromatography.[17, 23, 24] The digestion from intact proteins to smaller peptides is completed to limit charge heterogeneity, improve sample separation, and increase detection sensitivity.[6, 21, 22, 25] However, digestion of proteins can cause significant loss of proteome information rarely reach 100% protein sequence coverage in complex samples. Due to the highly dynamic nature of PTMs, unique proteoforms cannot be accurately assigned in a complex mixture of proteolytic peptides.[26, 27] While the protease trypsin is highly specific for arginine and lysine residues, incomplete and erroneous protein cleavage can occur, resulting in an even more complex peptide mixture, and making successful peptide identification more difficult.[22, 28] Even with these complications, bottom-up proteomics is routinely able to identify thousands of unique proteins in a single experiment.[23, 24]

The shortcomings of bottom-up proteomics are addressed in top-down analysis. Here, the digestion step is omitted and intact proteins are directly subjected to MS detection and fragmentation.[27, 29, 30] Typically, proteins with mass <40 kDa are detected and interrogated with this method.[31, 32] Top-down MS excels at detection and sequencing of individual proteoforms.[33-35] While bottom-up proteomics can be completed on most modern MS instruments, top-down analysis requires high resolution MS platforms, such as Orbitrap and FT-ICR, to successfully resolve protein fragment ions.[35, 36] In early implementations of top-down MS, proteins were isolated and purified prior to direct infusion, i.e., without on-line LC, analysis. More recently, on-line intact protein separation and detection have been completed with combinations of reversed-phase separation, isoelectric focusing, gel-eluted liquid fraction entrapment electrophoresis (GELFrEE), capillary zone

electrophoresis (CZE), and size exclusion chromatography (SEC).[33, 37-41] While these separation techniques have proven successful, their limited robustness has prevented widespread use. Also, limited fragmentation for intact proteins can limit protein identifications and PTM site assignments. Furthermore, even with modern MS platforms, the current top-down bioninformtic tools are less developed than comparable tools for bottom-up analyses.[30-32, 42] Despite these difficulties, top down approaches can routinely identify hundreds of unique proteoforms present in a sample.[33-35]

A melding of the top-down and bottom-up methods has recently been adopted, mainly for the study of antibodies and histones.[21, 43, 44] Middle-down proteomics attempts to retain the proteoform-specific PTM identifications of top-down methods and the improved separation, MS detection, and sample handling of bottom-up experiments.[20] Proteins are digested by proteases such as IdeS, OmpT, or trypsin to create 2–10 kDa peptides.[45-47] This resulting proteolytic mixture is less complex than the alternative bottom-up strategy, allowing for improved proteome coverage.[48, 49] These peptides can also be readily separated utilizing standard C18 methods stationary phases.[50, 51] The attempt to combine the advantages of bottom-up and top-down experiments has proven successful, but is a rather new approach for the study of proteomes. Improvements and optimization of the middle-down workflow are needed to approach the current sensitivity of bottom-up analysis and the proteoform-specific PTM localization and proteoform identification capabilities of top-down experiments.[5, 21, 31]

1.1.2 Reversed-phase Nanoflow Liquid Chromatography (nLC) for Peptide Separations

In the context of a bottom-up proteomic experiment, optimized nLC is important to increase proteome depth and coverage, especially for low-level modified peptides. Modern reversed-phase nLC is the separation technique of choice for maximum peptide detection and reduction of ion-suppression. Also, reversed-phase separation can be readily multiplexed with other common orthogonal peptide separations such as ion exchange, affinity, or electrophoretic chromatography. Typically, columns of 30–100 µm inner diameter (i.d.) are slurry packed with 2 – 5 µm reversed-phase C18 particles.[23] Specialized liquid handling pumps and valves are necessary in nLC systems, as column pressures and flow rates can routinely reach 500–1,000 bar and 100–500 nl/min respectively.[52-55] The Van Deemter equation (Equation 1) describes the optimum column and flow parameters for maximum separation.[56, 57]

Equation 1.1: $H = A + \dfrac{B}{\mu} + (C_S + C_M)\mu$

The plate height, H, describes the overall separation efficiency of the column and should be minimized. The A term describes the Eddy diffusion, or the different ways two similar molecules can migrate through the separation column (Random Walk Model). This term is affected by the quality and uniformity of stationary phase particles and column packing. The B term is related to longitudinal diffusive band-broadening of the sample and can be minimized by increasing the mobile phase flow rate, μ. However, the counteracting C terms describe the diffusion resulting from the repetitive adsorption and desorption of analyte onto and off of the stationary phase. Stagnant mobile phase, resulting from solvent adsorbed in/on stationary phase particles, is also accounted for in the C terms. The C terms are often reduced by decreasing packing particle sizes and by utilizing low viscosity mobile phases for fast analyte adsorption/desorption. Also, while not included explicitly in the Van Deemter equation, small bore capillary nLC columns are able to effectively disperse the heat created from the forced mobile phase flow, reducing diffusional broadening due to temperature/viscosity differences in column.[58]
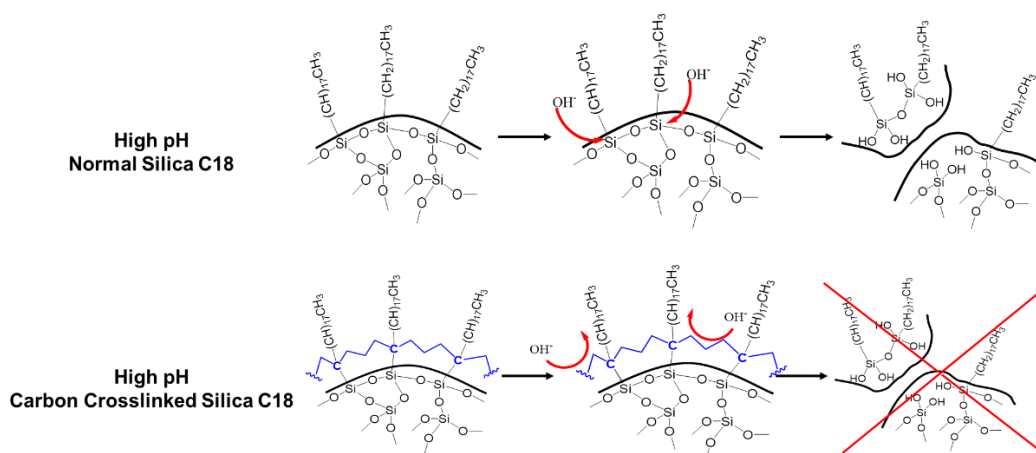
Figure 1.1: Example of standard (Top) and crosslinked (Bottom) C18 silica stationary phases under alkaline separation conditions.

Typical reversed-phase stationary phases utilized in proteomic separations are made of a silica core modified by octadecyl silane (C18) groups.[6, 58] These materials are robust for the separation of peptides under the acidic conditions typically found in proteomic experiments. Also, in-column cast silica frits effectively retain packing materials at the high pressures generated in an nLC system.[59] Above pH 7-8, these stationary phase and frit materials begin to degrade and dissolve (Figure 1.1), resulting in degradation of the column.[60, 61] For improved C18 separation at elevated

pHs, several manufacturers of silica reversed-phase particles have generated carbon protected C18 materials. These materials, such as the Waters Xbridge C18 particles used in this dissertation, are carbon crosslinked to protect the silica-based particles, preventing hydroxyl attack and eventual dissolution (Figure 1.1) (Waters). To retain the crosslinked material within the column at elevated pHs, stainless steel fitted end connections must be used to prevent silica frit failure during analysis.[61] These advancements have allowed for efficient high-pH nLC peptide separations.

1.1.3 Generation of Gas-phase Ions via Electrospray Ionization

Dr. John Fenn's implementation of electrospray ionization for generation of gas-phase ions, ushered in a new age of MS.[62] Electrospray ionization (ESI) allows for the "soft" generation of gas-phase biomolecular ions from solution by applying a 3–5 kV potential to a small aperture needle (~150 µm i.d.).[63-65] The ion source can be operated to generate positive or negative ions simply by flipping the polarity of the applied potential. More recent developments to reduce the size of the ion emitter needles (5–30µm i.d.) has resulted in optimal compatibility and sensitivity for proteomic nLC separations.[16, 66, 67] Nanoelectrospray ionization (nESI) typically employs lower potentials (1–2 kV) for the generation of analyte ions.

The generation of biomolecular gas-phase peptide ions via nESI is considered to occur through two main mechanisms. As the nESI-generated analyte droplets are undergoing solvent evaporation, Coulomb fission of the droplets occurs as the droplets approach the Rayleigh limit.[63, 64] Under the ion ejection model (IEM), as a desolvating analyte droplet is approaching the Rayleigh limit, an analyte ion is ejected as a charge carrier, generating a gas-phase ion.[68, 69] The charge residue model (CRM) suggests that, instead of an analyte being ejected from a droplet near the Rayleigh limit, charging of the analyte occurs upon complete desolvation of the droplet, resulting in more highly charged gas-phase ions.[70] It is widely considered that smaller tryptic peptides undergo IEM-type charging, while larger proteins and protein complexes undergo CRM type charging.[15, 71] Both IEM and CRM theoretical modeling agree well with experimental results in positive ion mode nESI, while in negative ion mode, ~20% less charging is observed.[72] This discrepancy suggests that the type of charge carrier affects ion charging and generation in a manner that is currently not well understood.

1.1.4 High Resolution Mass Spectrometry and Fragmentation for Proteomics

Modern proteomic experiments typically utilize high resolution MS to maximally annotate the gas-phase peptide ions eluting from an nLC separation.[6, 13] The use of high resolution MS has greatly increased the assignment of PTMs and improved bioinformatic processing. Incredible mass accuracy of <10 ppm is routinely achieved. Many modern proteomic software packages, such as MassMatrix, OMSSA, Proteome Discoverer, and MaxQuant, utilize high mass accuracy to increase the confidence and accuracy of peptide/protein identifications.[73-76] The increase in MS resolution and speed has opened the door for greatly improved analysis of complex proteomic peptide mixtures.

1.1.4.1 Time-of-Flight (TOF) Mass Spectrometer

TOF mass spectrometers operate under the relatively robust principle of conserved kinetic energy.[77-79] If a group of ions of differing mass but the same charge is accelerated to the same electric potential, the resulting kinetic energy of each ion is equivalent. Thus from Equation 1.2, the velocities of the ions with unique mass are different. This difference in ion velocity results in differing time-of-flights in a field-free drift region. A diagram of a Waters Micromass LCT Premier, utilized for work in this thesis, can be seen in Figure 1.2.

Equation 1.2: $E_k = \frac{mv^2}{2}$

Routine resolution of the Waters Micromass LCT TOF is >5,000 at 400 m/z (Waters).[78, 79] Modern TOF instruments can routinely achieve >40,000 resolution at 400 m/z. One major advantage of TOF instruments is their incredible scan speed. TOF analysis only takes hundreds of μs per scan, thus thousands of scans can be completed to deeply sample eluting peptides. TOF systems can undergo significant mass calibration deviations with ambient temperature fluctuations in a laboratory, thus the use of a lock-mass or internal calibration is often necessary during proteomic analysis to obtain >2ppm mass error.[79]
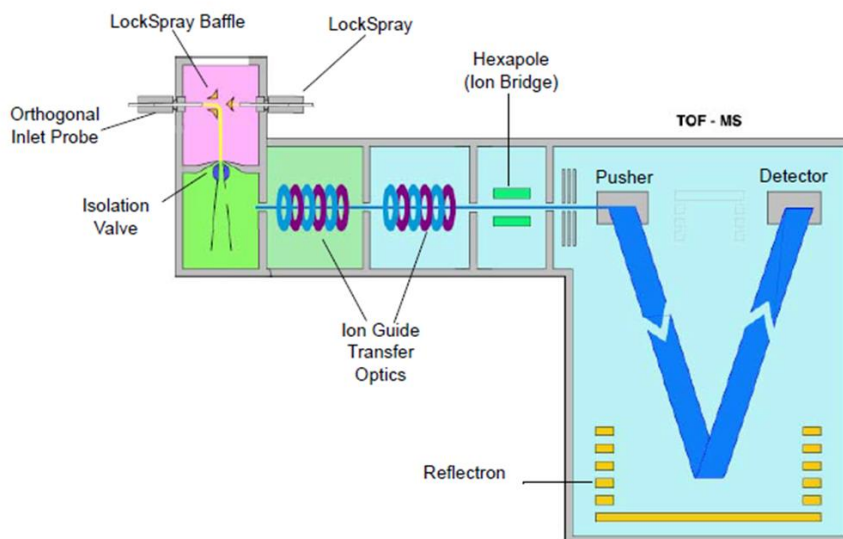
Figure 1.2: Schematic of a Waters Micromass LCT TOF mass spectrometer.

1.1.4.2 Fourier Transform-Ion Cyclotron Resonance (FT-ICR) Mass Spectrometers

The FT-ICR mass spectrometer is an incredibly flexible MS platform. It features >300,000 resolution at m/z 400 and can complete almost every form of available peptide activation/fragmentation (Bruker).[8, 80] The FT-ICR detects peptide ion frequencies as they undergo cyclotron orbit in a magnetic field (Equation 1.4).[81, 82] One unique feature of the FT-ICR MS is that the resolution of the instrument is directly related to the applied magnetic field strength.

Equation 1.4: $\omega_c = \dfrac{zB}{m}$

Recently, 21 T magnetic fields have been employed to baseline resolve entire antibody ions for top-down analysis.[83-85] FT-ICR instrumentation can complete ion-electron, ion-ion, ion-photon, and collisional based peptide fragmentation.[80] However, FT-ICR mass spectrometers pose significant challenges for use in proteomic experiments. Commercially available FT-ICRs, such as the Bruker SolariX seen in Figure 1.4, do not possess a method for dynamic ion population control. The lack of active gain control (AGC) can result in significant space charge effects and reduction of ion resolution and mass accuracy during the elution of highly concentrated peptides from an nLC column.[81, 82, 86] On the other hand, AGC can cause low abundance peptides to be missed. Also, commercial FT-ICRs can only complete a high resolution mass spectrum scan every 0.5-1 s, resulting in significantly lower proteomic coverage when compared to Orbitrap and TOF systems. Typically, commercial FT-ICRs only fragment the most abundant 4 peptides eluting with

7

on-line nLC, where an Orbitrap can fragment the most abundant 10-15 peptides in the same time frame.[17, 86] The FT-ICR excels at ion-electron fragmentation methods due to excellent confinement of electrons in the magnetic field. Unique negative ion-electron fragmentation techniques, such as electron detachment dissociation (EDD) and negative ion electron capture dissociation (niECD), can be readily employed without significant instrument modification.
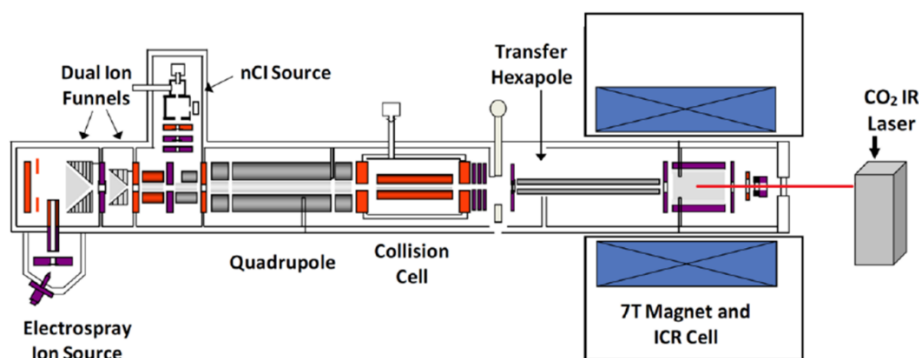
Figure 1.3: Schematic of a 7T Bruker SolariX FT-ICR mass spectrometer.

1.1.4.3 Peptide Fragmentation for Proteomics

MS based selection and fragmentation, i.e. tandem mass spectrometry (MS/MS) is the backbone of modern proteomics. In a typical experiment, a mass spectrum is first acquired of many co-eluting peptides. Three to 15 of the co-eluting peptides are then selected for collisional activation/fragmentation. Peptide fragmentation occurs due to inelastic collisions with an inert gas such as He or Ar.[78, 87] The fragmentation of peptide precursors ions occurs sequentially until all selected precursors are dissociated. This method of peptide selection and subsequent, sequential fragmentation is termed data-dependent acquisition (DDA).[88, 89] While DDA can routinely identify and reliably fragment thousands of eluting peptides in highly complex proteomic samples, it is currently not possible to sample all eluting peptides in a single experiment.

Data-independent acquisition (DIA) attempts to remedy the shortfalls of DDA by activating the entire population of co-eluting peptide ions at one time.[90] This approach can effectively sample the wide dynamic range of peptide abundances eluting from an nLC column. A major concern with DIA workflows is the reliance on high resolution MS to effectively resolve fragment ions and the subsequent bioinformatic tools ability to properly assign peptide fragments to the correct precursor ion.[42, 90-92] A popular DIA workflow to improve precursor/fragment assignments is sequential isolation window acquisition (SWATH), where a window of 25-50 m/z is fragmented

8

at once, and this window is scanned across the entire m/z region as peptides are eluting from the LC.[91, 93] Another common alternative to SWATH analysis is MS^E, where peptide ions are separated by shape, size, and charge via ion-mobility and then subsequently fragmented. In an MS^E experiment, peptide fragment ions are correlated to the precursor ion drift time, reducing the complexity of the fragment ion spectrum.[94, 95] SWATH and MS^E analysis requires fast MS scan speeds, e.g. TOF and ion mobility instrumentation, in order to complete a full m/z scan during the 15-30 second wide peptide peaks typically observed with nLC separations.

While peptides are typically activated/fragmented via ion-neutral collisions, ion-electron and ion-ion activation methods can provide improved residue specific PTM identification. Electron capture dissociation (ECD) and electron transfer dissociation (ETD) do not result in PTM neutral losses commonly observed in slow-heating techniques such as collision induced dissociation (CID).[96-98] Also, ECD and ETD fragmentation results in more peptide bond cleavages and less observed neutral losses with highly charged ($\geq$3+) peptide precursors when compared to CID.[99-101] These radical driven fragmentation methods require multiply charged precursors for subsequent detection of peptide fragments.

When examining negatively charged peptides, CID typically does not generate many sequence informative fragment ions.[102, 103] Ultraviolet photodissociation (UVPD) and negative ion electron transfer dissociation (NETD) have recently been developed as promising peptide anion fragmentation techniques for proteomic analysis.[61, 104-106] Unfortunately these fragmentation methods are known to involve abundant CO_2 neutral losses, complicating peptide residue assignments.[105, 107] While other peptide anion fragmentation methods such as electron detachment dissociation (EDD), electron induced dissociation (EID), and negative ion electron capture dissociation (niECD) exist, often their low fragmentation efficiency and long scan times are not amenable to nLC timescales.[108-110]

1.2 Protein Post-translational Modifications (PTMs)

It is estimated that approximately 20,000 unique protein transcripts are produced from the human genome and much more than ~80,000 related protein isoforms exist.[111, 112] While the number of unique protein sequences is large, the addition of PTMs to proteins results in an exponential increase of unique proteoforms.[111-113] A myriad of PTMs exist that significantly alter the properties and interactions of the protein, such as lipidation, ubiquitination, glycosylation, and oxidation.[114-

[117] It is estimated there are over 300 unique PTMs.[118] Many of these PTMs occur at low relative concentrations and may significantly affect peptide separation and detection. For instance, upon lipidation of a protein, the resulting tryptic peptide will be more hydrophobic than its unmodified counterpart, and often will get irreversibly trapped on standard C18 mobile phases.[119, 120] In this dissertation, the detection of the acidic PTMs phosphorylation, sulfation, and phosphopantetheinylation (Ppant) is explored extensively.

1.2.1 Phosphorylation

Protein phosphorylation is regarded to be one of the most common PTMs observed in the proteome.[118] It is estimated that up to one third of proteins are phosphorylated.[121, 122] Phosphorylation occurs mainly on Serine, Threonine, and Tyrosine residues (Figure 1.5). Histidine phosphorylation has also been discovered but is difficult to detect effectively due to its rapid hydrolysis.[123, 124] Protein kinases append a phosphate group to a protein from an adenosine triphosphate (ATP) substrate.[7] Phosphatases can than remove the added phosphate, resulting in a high degree of signaling control through the addition and subtraction of phosphate groups.[7] This PTM addition and subtraction can significantly alter the structure and function of a protein. Phosphorylation is responsible for many cellular signaling cascades, resulting in gene expression and protein synthesis.[113, 125, 126]
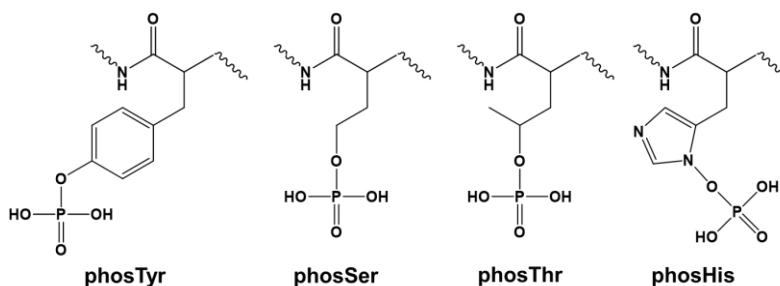
Figure 1.4: Phosphorylated residues examined in phosphoproteomic analyses.

MS studies of phosphopeptides/proteins often rely on affinity chromatography for purification of the modified peptides. Immobilized metal affinity chromatography (IMAC) with Fe^{3+} or Ga^{3+} and metal oxide affinity chromatography (MOAC) with TiO_2 or ZrO_2 can successfully bind phosphopeptides at low pH.[127-130] Unmodified peptides are then washed off of the material and phosphopeptides are eluted at high pH. The isolation and enrichment of phosphopeptides improves

the concentration of these peptides, while removing unmodified peptides from the analysis. These purification techniques have aided the explosion of recent phosphoproteome studies.[7, 131-133]

1.2.2 Sulfation

The PTM sulfation is rarely studied in the context of a proteomic workflow, resulting in a relative lack of understanding and knowledge of this PTM's effects.[134] Protein sulfation occurs on Tyrosine residues in the Golgi apparatus via tyrosylprotein sulfotransferases (TPSTs).[135] The TPSTs utilize adenosine 3'-phosphate 5'-phosphosulfate (PAPS) as the substrate for sulfonate addition to Tyr.[134, 135] Interestingly, sulfatases are usually expressed at very low cellular concentrations and activities, suggesting sulfation is rarely reversed at the cellular level.[134-136] Sulfation of Tyr has been shown to greatly increase protein-protein interactions and is integral for healthy murine development.[137-142]

Sulfation is a challenging PTM to study via common proteomic workflows. Upon positive ion mode ionization of a sulfopeptide/protein, significant proton mediated sulfonate elimination occurs.[143, 144] This PTM loss often occurs prior to detection in the mass spectrometer, resulting in a lack of sulfopeptide identifications.[144] Also, like phosphorylation, sulfation occurs at low stoichiometric levels. Recent developments of MOAC and weak-anion exchange (WAX) have shown promise as methods to enrich sulfopeptides.[145, 146] These enrichment techniques also can enrich phosphopeptides, which constitute a potential significant contaminant.[130, 147] Phosphorylation and sulfation only differ by 9.5 mDa, making routine differentiation only possible with long transient high resolution MS experiments. The resolving power needed to differentiate these two PTMs can result in long scan times, reducing nLC compatibility.[148]

1.2.3 Phosphopantetheinylation

Phosphopantetheine – Ser
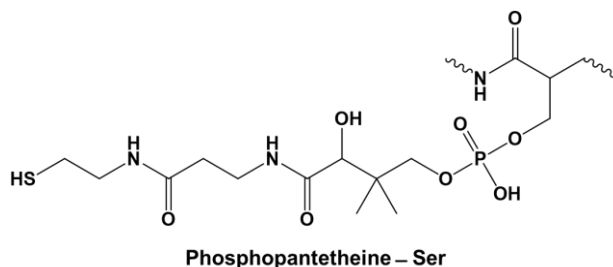
Figure 1.5: Phosphopantetheine (PPant) arm appended to an active site Serine residue.

11

Phosphopantetheine (PPant) modification of acyl carrier proteins (ACPs) and peptidyl carrier proteins (PCPs) is necessary for enzymatic production of fatty acids, polyketide, and non-ribosomal natural products (Figure 1.6).[149, 150] The addition PPant allows for covalent tethering of fatty acid and natural product intermediates throughout their respective enzymatic extension/modification. PPant is added to serine residues via 4′-phosphopantetheine transferases (PPTases) from a 4′-phosphopantetheine-CoA substrate.[149-151] The PPant modification is rather long (~2 nm) allowing for efficient shuttling of the enzyme substrate to various enzymatic domains. While purification and isolation of Ppant-containing peptides typically is not completed, several MS methods have been developed to study these unique peptides as discussed in section 1.3.1.

1.3 Natural Product Biosynthesis

Natural products or derivatives thereof are estimated to make up 40–50% of the current pharmaceuticals on the market today.[152-154] These drugs include penicillin, erythromycin, tetracycline, and vancomycin. These bioactive molecules are produced via polyketide synthases (PKSs) and non-ribosomal peptide synthetases (NRPSs). PKSs and NRPSs are typically large kDa to MDa protein complexes derived from many separate genes in an organism.[149, 150] Many natural products can be produced via total synthesis, but this approach often results in high costs and low yields. Frequently natural products are produced via semi-synthetic or chemoenzymatic approaches, where part of the entire natural product is produced by a PKS or NRPS enzyme.[155] If the biosynthetic mechanism of PKSs or NRPSs is well understood, large scale production of active pharmaceuticals can be accomplished, reducing the need for complex and tedious chemical manipulations.

Type I PKS enzymes operate under an assembly line like architecture. Each module in a type I PKS typically consists of at least an ACP, a ketosynthase (KS), and an acyl transferase (AT).[150] Many individual modules result in the overall elongation and tailoring of the growing natural product. The AT can be incorporated into each unique module (cis), or distinctly separate (trans) from each PKS module. The AT selects the acyl chain to be used for substrate elongation. The acyl units are usually small, such as methylmalonyl or malonyl.[150, 156] Upon ACP modification with PPant, the resulting Holo ACP is able to accept an activated acyl unit from the AT.[157, 158] The KS accepts the upstream substrate and catalyzes a Claisen-like condensation with the acyl-

extender unit tethered to the Holo ACP.[149, 150] The extended natural product intermediate can then be further modified by dehydratases, ketoreductases, or methylation domains, before being passed onto the next module for further elongation and tailoring.[150, 159] Thioesterase (TE) domains are typically included in the final module, catalyzing cyclization and release of the natural product.[150, 160]

1.3.1 Mass Spectrometry for the Characterization of Polyketide Synthases (PKSs) and Nonribosomal Peptide Synthetases (NRPSs)

MS is a powerful tool for the analysis of PKSs and NRPSs. With optimized conditions, the catalytic cycle of a PKS module can be examined via high resolution LC-MS with accurate mass detection of active site peptides, due to the covalent nature of PKS and NRPS enzymatic intermediates.[161-164] Upon CID activation of Holo ACP peptides/proteins, a characteristic PPant ejection ion is observed.[165] This ejection product can be used to identify new PKS and NRPS systems, and confirm the presence of active modules.[166, 167]

1.4 Dissertation Overview

This dissertation focuses on the use of positive and negative ion mode nESI for the detection of peptides carrying acidic PTMs. In Chapter 2, the discovery of trifluoroethanol (TFE) as a corona discharge suppressant led to improved negative ion nESI stability increases necessary for robust negative ion bottom-up workflows. Upon addition of TFE, pH dependent separations of tryptic peptides could be effectively completed in Chapter 3. Multiply phosphorylated and sulfated peptides were detected most effectively at pH 11 in negative ion mode. Chapter 4 examines sulfated peptides adducted with alkylamine bases under positive ion mode analysis. With slight collisional activation, a characteristic [SO_3+alkylamine] neutral loss is observed, and leveraged in online nLC-MS/MS DIA experiments. In Chapter 5, the PKS bryostatin module 3 (BryAM3) is examined via optimized tryptic digestion and separation. Successful detection of KS and ACP active site peptides was achieved with online nLC-MS/MS. Kirromycin C trans AT was observed to malonate non-active site cysteine containing peptides, an outcome that had not been previously reported. BryAM3 did not catalyze condensation of a surrogate triketide with malonyl, instead, unexpectedly, directly adding the triketide to the ACP. Chapter 6 summarizes these discoveries and discusses future research directions.

1.5 References

1. Bantscheff, M., Schirle, M., Sweetman, G., Rick, J., and Kuster, B. (2007) Quantitative mass spectrometry in proteomics: a critical review, *Anal. Bioanal. Chem. 389*, 1017-1031.
2. Gorg, A., Weiss, W., and Dunn, M. J. (2004) Current two-dimensional electrophoresis technology for proteomics, *Proteomics 4*, 3665-3685.
3. Domon, B., and Aebersold, R. (2006) Review - Mass spectrometry and protein analysis, *Science 312*, 212-217.
4. Altelaar, A. F. M., Munoz, J., and Heck, A. J. R. (2013) Next-generation proteomics: towards an integrative view of proteome dynamics, *Nat. Rev. Genet. 14*, 35-48.
5. Aebersold, R., and Mann, M. (2016) Mass-spectrometric exploration of proteome structure and function, *Nature 537*, 347-355.
6. Aebersold, R., and Mann, M. (2003) Mass spectrometry-based proteomics, *Nature 422*, 198-207.
7. Riley, N. M., and Coon, J. J. (2016) Phosphoproteomics in the Age of Rapid and Deep Proteome Profiling, *Anal. Chem. 88*, 74-94.
8. Brodbelt, J. S. (2016) Ion Activation Methods for Peptides and Proteins, *Anal. Chem. 88*, 30-51.
9. MacBeath, G. (2002) Protein microarrays and proteomics, *Nat. Genet. 32*, 526-532.
10. Melton, L. (2004) Protein arrays: Proteomics in multiplex, *Nature 429*, 101-107.
11. Rusmini, F., Zhong, Z. Y., and Feijen, J. (2007) Protein immobilization strategies for protein biochips, *Biomacromolecules 8*, 1775-1789.
12. Petricoin, E. F., Hackett, J. L., Lesko, L. J., Puri, R. K., Gutman, S. I., Chumakov, K., Woodcock, J., Feigal, D. W., Zoon, K. C., and Sistare, F. D. (2002) Medical applications of microarray technologies: a regulatory science perspective, *Nat. Genet. 32*, 474-479.
13. Domon, B., and Aebersold, R. (2006) Mass Spectrometry and Protein Analysis, *Science 312*, 212-217.
14. Marginean, I., Tang, K., Smith, R., and Kelly, R. (2014) Picoelectrospray Ionization Mass Spectrometry Using Narrow-Bore Chemically Etched Emitters, *J. Am. Soc. Mass Spectrom. 25*, 30-36.
15. Kebarle, P., and Verkerk, U. H. (2009) Electrospray: from ions in solution to ions in the gas phase, what we know now, *Mass. Spectrom. Rev. 28*, 898-917.
16. Wilm, M., and Mann, M. (1996) Analytical Properties of the Nanoelectrospray Ion Source, *Anal. Chem. 68*, 1-8.
17. Michalski, A., Damoc, E., Hauschild, J. P., Lange, O., Wieghaus, A., Makarov, A., Nagaraj, N., Cox, J., Mann, M., and Horning, S. (2011) Mass Spectrometry-based Proteomics Using Q Exactive, a High-performance Benchtop Quadrupole Orbitrap Mass Spectrometer, *Mol. Cell. Proteomics 10*, 11.
18. Easterling, M. L., Mize, T. H., and Amster, I. J. (1999) Routine part-per-million mass accuracy for high-mass ions: Space-charge effects in MALDI FT-ICR, *Anal. Chem. 71*, 624-632.
19. Tsybin, Y. O. (2014) From High- to Super-resolution Mass Spectrometry, *CHIMIA 68*, 168-174.
20. Switzar, L., Giera, M., and Niessen, W. M. A. (2013) Protein Digestion: An Overview of the Available Techniques and Recent Developments, *J. Proteome Res. 12*, 1067-1077.

21. Moradian, A., Kalli, A., Sweredoski, M. J., and Hess, S. (2014) The top-down, middle-down, and bottom-up mass spectrometry approaches for characterization of histone variants and their post-translational modifications, *Proteomics 14*, 489-497.
22. Vandermarliere, E., Mueller, M., and Martens, L. (2013) Getting intimate with trypsin, the leading protease in proteomics, *Mass Spectrom. Rev. 32*, 453-465.
23. Richards, A. L., Hebert, A. S., Ulbrich, A., Bailey, D. J., Coughlin, E. E., Westphall, M. S., and Coon, J. J. (2015) One-hour proteome analysis in yeast, *Nat. Protoc. 10*, 701-714.
24. Nagaraj, N., Alexander Kulak, N., Cox, J., Neuhauser, N., Mayr, K., Hoerning, O., Vorm, O., and Mann, M. (2012) System-wide Perturbation Analysis with Nearly Complete Coverage of the Yeast Proteome by Single-shot Ultra HPLC Runs on a Bench Top Orbitrap, *Mol. Cell. Proteomics 11*.
25. Compton, P. D., Zamdborg, L., Thomas, P. M., and Kelleher, N. L. (2011) On the Scalability and Requirements of Whole Protein Mass Spectrometry, *Anal. Chem. 83*, 6868-6874.
26. Kelleher, N. L. (2004) Peer Reviewed: Top-Down Proteomics, *Anal. Chem. 76*, 196 A-203 A.
27. Chait, B. T. (2006) Mass Spectrometry: Bottom-Up or Top-Down?, *Science 314*, 65-66.
28. Alves, P., Arnold, R. J., Clemmer, D. E., Li, Y., Reilly, J. P., Sheng, Q., Tang, H., Xun, Z., Zeng, R., and Radivojac, P. (2008) Fast and accurate identification of semi-tryptic peptides in shotgun proteomics, *Bioinformatics 24*, 102-109.
29. Siuti, N., and Kelleher, N. L. (2007) Decoding protein modifications using top-down mass spectrometry, *Nat. Meth. 4*, 817-821.
30. Meyer, B., Papasotiriou, D. G., and Karas, M. (2011) 100% protein sequence coverage: a modern form of surrealism in proteomics, *Amino Acids 41*, 291-310.
31. Catherman, A. D., Skinner, O. S., and Kelleher, N. L. (2014) Top Down proteomics: Facts and perspectives, *Biochem. Biophys. Res. Commun. 445*, 683-693.
32. DeHart, C. J., Fellers, R. T., Fornelli, L., Kelleher, N. L., and Thomas, P. M. (2017) Bioinformatics Analysis of Top-Down Mass Spectrometry Data with ProSight Lite, In *Protein Bioinformatics: From Protein Modifications and Networks to Proteomics* (Wu, C. H., Arighi, C. N., and Ross, K. E., Eds.), pp 381-394, Springer New York, New York, NY.
33. Zhao, Y., Sun, L., Zhu, G., and Dovichi, N. J. (2016) Coupling Capillary Zone Electrophoresis to a Q Exactive HF Mass Spectrometer for Top-down Proteomics: 580 Proteoform Identifications from Yeast, *J. Proteome Res. 15*, 3679-3685.
34. Tran, J. C., Zamdborg, L., Ahlf, D. R., Lee, J. E., Catherman, A. D., Durbin, K. R., Tipton, J. D., Vellaichamy, A., Kellie, J. F., Li, M., Wu, C., Sweet, S. M. M., Early, B. P., Siuti, N., LeDuc, R. D., Compton, P. D., Thomas, P. M., and Kelleher, N. L. (2011) Mapping intact protein isoforms in discovery mode using top-down proteomics, *Nature 480*, 254-258.
35. Catherman, A. D., Li, M., Tran, J. C., Durbin, K. R., Compton, P. D., Early, B. P., Thomas, P. M., and Kelleher, N. L. (2013) Top Down Proteomics of Human Membrane Proteins from Enriched Mitochondrial Fractions, *Anal. Chem. 85*, 1880-1888.
36. Mao, Y., Valeja, S. G., Rouse, J. C., Hendrickson, C. L., and Marshall, A. G. (2013) Top-Down Structural Analysis of an Intact Monoclonal Antibody by Electron Capture Dissociation-Fourier Transform Ion Cyclotron Resonance-Mass Spectrometry, *Anal. Chem. 85*, 4239-4246.

37. Tran, J. C., and Doucette, A. A. (2008) Rapid and Effective Focusing in a Carrier Ampholyte Solution Isoelectric Focusing System: A Proteome Prefractionation Tool, *J. Proteome Res. 7*, 1761-1766.

38. Shen, Y., Tolić, N., Zhao, R., Paša-Tolić, L., Li, L., Berger, S. J., Harkewicz, R., Anderson, G. A., Belov, M. E., and Smith, R. D. (2001) High-Throughput Proteomics Using High-Efficiency Multiple-Capillary Liquid Chromatography with On-Line High-Performance ESI FTICR Mass Spectrometry, *Anal. Chem. 73*, 3011-3021.

39. Tran, J. C., and Doucette, A. A. (2008) Gel-Eluted Liquid Fraction Entrapment Electrophoresis: An Electrophoretic Method for Broad Molecular Weight Range Proteome Separation, *Anal. Chem. 80*, 1568-1573.

40. Simpson, D. C., Ahn, S., Pasa-Tolic, L., Bogdanov, B., Mottaz, H. M., Vilkov, A. N., Anderson, G. A., Lipton, M. S., and Smith, R. D. (2006) Using size exclusion chromatography-RPLC and RPLC-CIEF as two-dimensional separation strategies for protein profiling, *Electrophoresis 27*, 2722-2733.

41. Capriotti, A. L., Cavaliere, C., Foglia, P., Samperi, R., and Laganà, A. (2011) Intact protein separation by chromatographic and/or electrophoretic techniques for top-down proteomics, *J. Chromatog. A 1218*, 8760-8776.

42. Fellers, R. T., Greer, J. B., Early, B. P., Yu, X., LeDuc, R. D., Kelleher, N. L., and Thomas, P. M. (2015) ProSight Lite: Graphical software to analyze top-down mass spectrometry data, *Proteomics 15*, 1235-1238.

43. Zhang, Z. Q., Pan, H., and Chen, X. Y. (2009) Mass Spectrometry for Structural Characterization fo Therapeutic Antibodies, *Mass Spectrom. Rev. 28*, 147-176.

44. Laskay, Ü. A., Lobas, A. A., Srzentić, K., Gorshkov, M. V., and Tsybin, Y. O. (2013) Proteome Digestion Specificity Analysis for Rational Design of Extended Bottom-up and Middle-down Proteomics Experiments, *Journal of Proteome Research 12*, 5558-5569.

45. Wu, C., Tran, J. C., Zamdborg, L., Durbin, K. R., Li, M., Ahlf, D. R., Early, B. P., Thomas, P. M., Sweedler, J. V., and Kelleher, N. L. (2012) A protease for 'middle-down' proteomics, *Nat. Methods 9*, 822-824.

46. Ryan, M. H., Petrone, D., Nemeth, J. F., Barnathan, E., Björck, L., and Jordan, R. E. (2008) Proteolysis of purified IgGs by human and bacterial enzymes in vitro and the detection of specific proteolytic fragments of endogenous IgG in rheumatoid synovial fluid, *Mol. Immunol. 45*, 1837-1846.

47. Tan, Y.-J., Wang, W.-H., Zheng, Y., Dong, J., Stefano, G., Brandizzi, F., Garavito, R. M., Reid, G. E., and Bruening, M. L. (2012) Limited Proteolysis via Millisecond Digestions in Protease-Modified Membranes, *Anal. Chem. 84*, 8357-8363.

48. Cannon, J., Lohnes, K., Wynne, C., Wang, Y., Edwards, N., and Fenselau, C. (2010) High-Throughput Middle-Down Analysis Using an Orbitrap, *J. Proteome Res. 9*, 3886-3890.

49. Kalli, A., and Hakansson, K. (2010) Electron capture dissociation of highly charged proteolytic peptides from Lys N, Lys C and Glu C digestion, *Mol. Biosyst. 6*, 1668-1681.

50. Boyne, M. T., Garcia, B. A., Li, M., Zamdborg, L., Wenger, C. D., Babai, S., and Kelleher, N. L. (2009) Tandem Mass Spectrometry with Ultrahigh Mass Accuracy Clarifies Peptide Identification by Database Retrieval, *J. Proteome Res. 8*, 374-379.

51. Fornelli, L., Ayoub, D., Aizikov, K., Beck, A., and Tsybin, Y. O. (2014) Middle-Down Analysis of Monoclonal Antibodies with Electron Transfer Dissociation Orbitrap Fourier Transform Mass Spectrometry, *Anal. Chem. 86*, 3005-3012.

52. Mellors, J. S., and Jorgenson, J. W. (2004) Use of 1.5-µm Porous Ethyl-Bridged Hybrid Particles as a Stationary-Phase Support for Reversed-Phase Ultrahigh-Pressure Liquid Chromatography, *Anal. Chem. 76*, 5441-5450.
53. Grinias, K. M., Godinho, J. M., Franklin, E. G., Stobaugh, J. T., and Jorgenson, J. W. (2016) Development of a 45kpsi ultrahigh pressure liquid chromatography instrument for gradient separations of peptides using long microcapillary columns and sub-2µm particles, *J. Chromatog. A 1469*, 60-67.
54. Kennedy, R. T., and Jorgenson, J. W. (1989) Preparation and evaluation of packed capillary liquid chromatography columns with inner diameters from 20 to 50 micrometers, *Anal. Chem. 61*, 1128-1135.
55. MacNair, J. E., Lewis, K. C., and Jorgenson, J. W. (1997) Ultrahigh-Pressure Reversed-Phase Liquid Chromatography in Packed Capillary Columns, *Anal. Chem. 69*, 983-989.
56. Skoog, D. A., Holler, F. J., and Crouch, S. R. (2006) *Principles of Instrumental Analysis*, Cengage Learning, Independence, KY.
57. Giddings, J. C., and Byring, H. (1955) A Molecular Dynamic Theory of Chromatography, *J. Phys. Chem. 59*, 416-421.
58. Jorgenson, J. W. (2010) Capillary Liquid Chromatography at Ultrahigh Pressures, In *Annual Rev. Anal. Chem.* (Yeung, E. S., and Zare, R. N., Eds.), pp 129-150, Annual Reviews, Palo Alto.
59. Cortes, H. J., Pfeiffer, C. D., Richter, B. E., and Stevens, T. S. (1987) Porous ceramic bed supports for fused silica packed capillary columns used in liquid chromatography, *J. High Res. Chromatog. 10*, 446-448.
60. Kirkland, J. J., van Straten, M. A., and Claessens, H. A. (1995) High pH mobile phase effects on silica-based reversed-phase high-performance liquid chromatographic columns, *Journal of Chromatography A 691*, 3-19.
61. McAlister, G. C., Russell, J. D., Rumachik, N. G., Hebert, A. S., Syka, J. E., Geer, L. Y., Westphall, M. S., Pagliarini, D. J., and Coon, J. J. (2012) Analysis of the acidic proteome with negative electron-transfer dissociation mass spectrometry, *Anal. Chem. 84*, 2875-2882.
62. Fenn, J. B., Mann, M., Meng, C. K., Wong, S. F., and Whitehouse, C. M. (1989) Electrospray Ionization for Mass Spectrometry of Large Biomolecules, *Science 246*, 64-71.
63. Kebarle, P., and Tang, L. (1993) From Ions in Solution to Ions in the Gas Phase, *Anal. Chem. 65*, 972A-986A.
64. Fenn, J. B., Mann, M., Meng, C. K., Wong, S. F., and Whitehouse, C. M. (1990) Electrospray ionization–principles and practice, *Mass Spectrom. Rev. 9*, 37-70.
65. Konermann, L., Ahadi, E., Rodriguez, A. D., and Vahidi, S. (2012) Unraveling the Mechanism of Electrospray Ionization, *Anal. Chem. 85*, 2-9.
66. Valaskovic, G. A., Kelleher, N. L., Little, D. P., Aaserud, D. J., and McLafferty, F. W. (1995) Attomole-Sensitivity Electrospray Source for Large-Molecule Mass Spectrometry, *Anal. Chem. 67*, 3802-3805.
67. Gale, D. C., and Smith, R. D. (1993) Small volume and low flow-rate electrospray Ionization mass spectrometry of aqueous samples, *Rapid Commun. Mass Spectrom. 7*, 1017-1021.
68. Thomson, B. A., and Iribarne, J. V. (1979) Field induced ion evaporation from liquid surfaces at atmospheric pressure, *J. Chem. Phys. 71*, 4451-4463.

69. Kebarle, P., and Peschke, M. (2000) On the mechanisms by which the charged droplets produced by electrospray lead to gas phase ions, *Anal. Chim. Acta 406*, 11-35.
70. Fernandez de la Mora, J. (2000) Electrospray ionization of large multiply charged species proceeds via Dole's charged residue mechanism, *Anal. Chim. Acta 406*, 93-104.
71. Dole, M., Mack, L. L., Hines, R. L., Mobley, R. C., Ferguson, L. D., and Alice, M. B. (1968) Molecular Beams of Macroions, *J. Chem. Phys. 49*, 2240-2249.
72. Allen, S. J., Schwartz, A. M., and Bush, M. F. (2013) Effects of Polarity on the Structures and Charge States of Native-Like Proteins and Protein Complexes in the Gas Phase, *Analytical Chemistry 85*, 12055-12061.
73. Xu, H., and Freitas, M. A. (2009) MassMatrix: A database search program for rapid characterization of proteins and peptides from tandem mass spectrometry data, *Proteomics 9*, 1548-1555.
74. Cox, J., and Mann, M. (2008) MaxQuant enables high peptide identification rates, individualized p.p.b.-range mass accuracies and proteome-wide protein quantification, *Nat. Biotech. 26*, 1367-1372.
75. Geer, L. Y., Markey, S. P., Kowalak, J. A., Wagner, L., Xu, M., Maynard, D. M., Yang, X., Shi, W., and Bryant, S. H. (2004) Open Mass Spectrometry Search Algorithm, *J. Proteome Res. 3*, 958-964.
76. Cox, J., Neuhauser, N., Michalski, A., Scheltema, R. A., Olsen, J. V., and Mann, M. (2011) Andromeda: A Peptide Search Engine Integrated into the MaxQuant Environment, *J. Proteome Res. 10*, 1794-1805.
77. Plass, W. R., Dickel, T., and Scheidenberger, C. (2013) Multiple-reflection time-of-flight mass spectrometry, *Int. J. Mass Spectrom. 349*, 134-144.
78. Hoffman, E. D., and Stroobant, V. (2001) *Mass Spectrometry - Principles & Applications* 2nd ed., Wiley.
79. Chernushevich, I. V., Loboda, A. V., and Thomson, B. A. (2001) An introduction to quadrupole–time-of-flight mass spectrometry, *J. Mass Spectrom. 36*, 849-865.
80. Sleno, L., and Volmer, D. A. (2004) Ion activation methods for tandem mass spectrometry, *J. Mass Spectrom. 39*, 1091-1112.
81. Marshall, A. G., Hendrickson, C. L., and Jackson, G. S. (1998) Fourier transform ion cyclotron resonance mass spectrometry: A primer, *Mass Spectrom. Rev. 17*, 1-35.
82. Amster, I. J. (1996) Fourier transform mass spectrometry, *J. Mass Spectrom. 31*, 1325-1337.
83. Hendrickson, C. L., Quinn, J. P., Kaiser, N. K., Smith, D. F., Blakney, G. T., Chen, T., Marshall, A. G., Weisbrod, C. R., and Beu, S. C. (2015) 21 Tesla Fourier Transform Ion Cyclotron Resonance Mass Spectrometer: A National Resource for Ultrahigh Resolution Mass Analysis, *J. Am. Soc. Mass Spectrom. 26*, 1626-1632.
84. Shaw, J. B., Lin, T. Y., Leach, F. E., Tolmachev, A. V., Tolic, N., Robinson, E. W., Koppenaal, D. W., and Pasa-Tolic, L. (2016) 21 Tesla Fourier Transform Ion Cyclotron Resonance Mass Spectrometer Greatly Expands Mass Spectrometry Toolbox, *J. Am. Soc. Mass Spectrom. 27*, 1929-1936.
85. He, L. D., Anderson, L. C., Barnidge, D. R., Murray, D. L., Hendrickson, C. L., and Marshall, A. G. (2017) Analysis of Monoclonal Antibodies in Human Serum as a Model for Clinical Monoclonal Gammopathy by Use of 21 Tesla FT-ICR Top-Down and Middle-Down MS/MS, *J. Am. Soc. Mass Spectrom. 28*, 827-838.
86. Bogdanov, B., and Smith, R. D. (2005) Proteomics by FTICR mass spectrometry: Top down and bottom up, *Mass Spectrom. Rev. 24*, 168-200.

87. Wysocki, V. H., Tsaprailis, G., Smith, L. L., and Breci, L. A. (2000) Special feature: Commentary - Mobile and localized protons: a framework for understanding peptide dissociation, *Journal of Mass Spectrometry 35*, 1399-1406.

88. Wang, N., and Li, L. (2008) Exploring the Precursor Ion Exclusion Feature of Liquid Chromatography−Electrospray Ionization Quadrupole Time-of-Flight Mass Spectrometry for Improving Protein Identification in Shotgun Proteome Analysis, *Anal. Chem. 80*, 4696-4710.

89. Courchesne, P. L., Jones, M. D., Robinson, J. H., Spahr, C. S., McCracken, S., Bentley, D. L., Luethy, R., and Patterson, S. D. (1998) Optimization of capillary chromatography ion trap-mass spectrometry for identification of gel-separated proteins, *Electrophoresis 19*, 956-967.

90. Chapman, J. D., Goodlett, D. R., and Masselon, C. D. (2014) Multiplexed and Data-independent Tandem Mass Spectrometry for Global Proteome Profiling, *Mass Spectrom. Rev. 33*, 452-470.

91. Gillet, L. C., Navarro, P., Tate, S., Röst, H., Selevsek, N., Reiter, L., Bonner, R., and Aebersold, R. (2012) Targeted Data Extraction of the MS/MS Spectra Generated by Data-independent Acquisition: A New Concept for Consistent and Accurate Proteome Analysis, *Mol. Cell. Proteomics 11*.

92. Masselon, C., Paša-Tolić, L., Lee, S.-W., Li, L., Anderson, G. A., Harkewicz, R., and Smith, R. D. (2003) Identification of tryptic peptides from large databases using multiplexed tandem mass spectrometry: simulations and experimental results, *Proteomics 3*, 1279-1286.

93. Selevsek, N., Chang, C.-Y., Gillet, L. C., Navarro, P., Bernhardt, O. M., Reiter, L., Cheng, L.-Y., Vitek, O., and Aebersold, R. (2015) Reproducible and Consistent Quantification of the Saccharomyces cerevisiae Proteome by SWATH-mass spectrometry, *Mol. Cell. Proteomics 14*, 739-749.

94. Lee, S., Li, Z., Valentine, S. J., Zucker, S. M., Webber, N., Reilly, J. P., and Clemmer, D. E. (2012) Extracted fragment ion mobility distributions: A new method for complex mixture analysis, *Int. J. Mass Spectrom. 309*, 154-160.

95. Distler, U., Kuharev, J., Navarro, P., Levin, Y., Schild, H., and Tenzer, S. (2014) Drift time-specific collision energies enable deep-coverage data-independent acquisition proteomics, *Nat. Meth. 11*, 167-+.

96. Håkansson, K., Cooper, H. J., Emmett, M. R., Costello, C. E., Marshall, A. G., and Nilsson, C. L. (2001) Electron Capture Dissociation and Infrared Multiphoton Dissociation MS/MS of an N-Glycosylated Tryptic Peptide To Yield Complementary Sequence Information, *Anal. Chem. 73*, 4530-4536.

97. Stensballe, A., Jensen, O. N., Olsen, J. V., Haselmann, K. F., and Zubarev, R. A. (2000) Electron capture dissociation of singly and multiply phosphorylated peptides, *Rapid Commun. Mass Spectrom. 14*, 1793-1800.

98. Mikesh, L. M., Ueberheide, B., Chi, A., Coon, J. J., Syka, J. E. P., Shabanowitz, J., and Hunt, D. F. (2006) The utility of ETD mass spectrometry in proteomic analysis, *Biochim. Biophys. Acta 1764*, 1811-1822.

99. Good, D. M., Wirtala, M., McAlister, G. C., and Coon, J. J. (2007) Performance Characteristics of Electron Transfer Dissociation Mass Spectrometry, *Mol. Cell. Proteomics 6*, 1942-1951.

100. Iavarone, A. T., Paech, K., and Williams, E. R. (2004) Effects of Charge State and Cationizing Agent on the Electron Capture Dissociation of a Peptide, *Anal. Chem. 76*, 2231-2238.

101. Zubarev, R. A., Horn, D. M., Fridriksson, E. K., Kelleher, N. L., Kruger, N. A., Lewis, M. A., Carpenter, B. K., and McLafferty, F. W. (2000) Electron Capture Dissociation for Structural Characterization of Multiply Charged Protein Cations, *Anal. Chem. 72*, 563-573.

102. Ewing, N. P., and Cassady, C. J. (2001) Dissociation of multiply charged negative ions for hirudin (54–65), fibrinopeptide B, and insulin A (oxidized), *J. Am. Soc. Mass Spectrom. 12*, 105-116.

103. Clipston, N. L., Jai-nhuknan, J., and Cassady, C. J. (2003) A comparison of negative and positive ion time-of-flight post-source decay mass spectrometry for peptides containing basic residues, *Int. J. Mass Spectrom. 222*, 363-381.

104. Riley, N. M., Rush, M. J. P., Rose, C. M., Richards, A. L., Kwiecien, N. W., Bailey, D. J., Hebert, A. S., Westphall, M. S., and Coon, J. J. (2015) The Negative Mode Proteome with Activated Ion Negative Electron Transfer Dissociation (AI-NETD), *Mol. Cell. Proteomics 14*, 2644-2660.

105. Madsen, J. A., Kaoud, T. S., Dalby, K. N., and Brodbelt, J. S. (2011) 193-nm photodissociation of singly and multiply charged peptide anions for acidic proteome characterization, *Proteomics 11*, 1329-1334.

106. Madsen, J. A., Xu, H., Robinson, M. R., Horton, A. P., Shaw, J. B., Giles, D. K., Kaoud, T. S., Dalby, K. N., Trent, M. S., and Brodbelt, J. S. (2013) High-throughput Database Search and Large-scale Negative Polarity Liquid Chromatography–Tandem Mass Spectrometry with Ultraviolet Photodissociation for Complex Proteomic Samples, *Mol. Cell. Proteomics 12*, 2604-2614.

107. Coon, J. J., Shabanowitz, J., Hunt, D. F., and Syka, J. E. P. (2005) Electron Transfer Dissociation of Peptide Anions, *J. Am. Soc. Mass Spectrom. 16*, 880-882.

108. Kjeldsen, F., Silivra, O. A., Ivonin, I. A., Haselmann, K. F., Gorshkov, M., and Zubarev, R. A. (2005) Ca-C Backbone Fragmentation Dominates in Electron Detachment Dissociation of Gas-Phase Polypeptide Polyanions, *Chem. Eur. J. 11*, 1803-1812.

109. Kalli, A., Grigorean, G., and Hakansson, K. (2011) Electron Induced Dissociation of Singly Deprotonated Peptides, *J. Am. Soc. Mass Spectrom. 22*, 2209-2221.

110. Yoo, H. J., Wang, N., Zhuang, S., Song, H., and Håkansson, K. (2011) Negative-Ion Electron Capture Dissociation: Radical-Driven Fragmentation of Charge-Increased Gaseous Peptide Anions, *J. Am. Chem. Soc. 133*, 16790-16793.

111. Muñoz, J., and Heck, A. J. R. (2014) From the Human Genome to the Human Proteome, *Angew. Chem. Int. Ed. 53*, 10864-10866.

112. Wilhelm, M., Schlegl, J., Hahne, H., Gholami, A. M., Lieberenz, M., Savitski, M. M., Ziegler, E., Butzmann, L., Gessulat, S., Marx, H., Mathieson, T., Lemeer, S., Schnatbaum, K., Reimer, U., Wenschuh, H., Mollenhauer, M., Slotta-Huspenina, J., Boese, J.-H., Bantscheff, M., Gerstmair, A., Faerber, F., and Kuster, B. (2014) Mass-spectrometry-based draft of the human proteome, *Nature 509*, 582-587.

113. Karve, T. M., and Cheema, A. K. (2011) Small Changes Huge Impact: The Role of Protein Posttranslational Modifications in Cellular Homeostasis and Disease, *J. Amino Acids 2011*, 207691.

114. Casey, P. J. (1995) Protein Lipidation in Cell Signaling, *Science 268*, 221-225.

115. Pickart, C. M. (2001) Mechanisms underlying ubiquitination, *Ann. Rev. Biochem. 70*, 503-533.
116. Dwek, R. A. (1996) Glycobiology: Toward understanding the function of sugars, *Chem. Rev. 96*, 683-720.
117. Valko, M., Leibfritz, D., Moncol, J., Cronin, M. T. D., Mazur, M., and Telser, J. (2007) Free radicals and antioxidants in normal physiological functions and human disease, *Int. J. Biochem. Cell Biol. 39*, 44-84.
118. Khoury, G. A., Baliban, R. C., and Floudas, C. A. (2011) Proteome-wide post-translational modification statistics: frequency analysis and curation of the swiss-prot database, *Sci. Rep. 1*, 90.
119. Martin, B. R., and Cravatt, B. F. (2009) Large-Scale Profiling of Protein Palmitoylation in Mammalian Cells, *Nat. Meth. 6*, 135-138.
120. Draper, J. M., Xia, Z., and Smith, C. D. (2007) Cellular palmitoylation and trafficking of lipidated peptides, *J. Lipid Res. 48*, 1873-1884.
121. Mann, M., Ong, S. E., Gronborg, M., Steen, H., Jensen, O. N., and Pandey, A. (2002) Analysis of protein phosphorylation using mass spectrometry: deciphering the phosphoproteome, *Trends Biotechnol. 20*, 261-268.
122. Chalmers, M. J., Quinn, J. P., Blakney, G. T., Emmett, M. R., Mischak, H., Gaskell, S. J., and Marshall, A. G. (2003) Liquid Chromatography−Fourier Transform Ion Cyclotron Resonance Mass Spectrometric Characterization of Protein Kinase C Phosphorylation, *J. Proteome Res. 2*, 373-382.
123. Klumpp, S., and Krieglstein, J. (2002) Phosphorylation and dephosphorylation of histidine residues in proteins, *Eur. J. Biochem. 269*, 1067-1071.
124. (2014) Proteomics: Phosphohistidine proteomics, *Nat. Meth. 11*, 1091-1091.
125. Wang, X., Pattison, J. S., and Su, H. (2013) Posttranslational Modification and Quality Control, *Circ. Res. 112*, 367-381.
126. Hitosugi, T., and Chen, J. (2014) Post-translational modifications and the Warburg effect, *Oncogene 33*, 4279-4285.
127. Neville, D. C. A., Townsend, R. R., Rozanas, C. R., Verkman, A. S., Price, E. M., and Gruis, D. B. (1997) Evidence for phosphorylation of serine 753 in CFTR using a novel metal-ion affinity resin and matrix-assisted laser desorption mass spectrometry, *Protein Sci. 6*, 2436-2445.
128. Nühse, T. S., Stensballe, A., Jensen, O. N., and Peck, S. C. (2003) Large-scale Analysis of in Vivo Phosphorylated Membrane Proteins by Immobilized Metal Ion Affinity Chromatography and Mass Spectrometry, *Mol. Cell. Proteomics 2*, 1234-1243.
129. Posewitz, M. C., and Tempst, P. (1999) Immobilized Gallium(III) Affinity Chromatography of Phosphopeptides, *Anal. Chem. 71*, 2883-2892.
130. Kweon, H. K., and Håkansson, K. (2006) Selective Zirconium Dioxide-Based Enrichment of Phosphorylated Peptides for Mass Spectrometric Analysis, *Anal. Chem. 78*, 1743-1749.
131. Thingholm, T. E., Jensen, O. N., and Larsen, M. R. (2009) Analytical strategies for phosphoproteomics, *Proteomics 9*, 1451-1468.
132. Yates, J. R., Ruse, C. I., and Nakorchevsky, A. (2009) Proteomics by Mass Spectrometry: Approaches, Advances, and Applications, In *Annu. Rev. Biomed. Eng.*, pp 49-79, Annual Reviews, Palo Alto.

133. Harsha, H. C., and Pandey, A. (2010) Phosphoproteomics in Cancer, *Mol. Oncolgy 4*, 482-495.
134. Seibert, C., and Sakmar, T. P. (2008) Toward a framework for sulfoproteomics: Synthesis and characterization of sulfotyrosine-containing peptides, *Biopolymers 90*, 459-477.
135. Moore, K. L. (2003) The biology and enzymology of protein tyrosine O-sulfation, *J. Biol. Chem. 278*, 24243-24246.
136. Hanson, S. R., Best, M. D., and Wong, C.-H. (2004) Sulfatases: Structure, Mechanism, Biological Activity, Inhibition, and Synthetic Utility, *Angew. Chem. Int. Ed. 43*, 5736-5763.
137. Kehoe, J. W., and Bertozzi, C. R. (2000) Tyrosine sulfation: a modulator of extracellular protein-protein interactions, *Chem. Biol. 7*, R57-R61.
138. Ouyang, Y. B., Crawley, J. T. B., Aston, C. E., and Moore, K. L. (2002) Reduced body weight and increased postimplantation fetal death in tyrosylprotein sulfotransferase-1-deficient mice, *J. Biol. Chem. 277*, 23781-23787.
139. Choe, H., Li, W. H., Wright, P. L., Vasilieva, N., Venturi, M., Huang, C. C., Grundner, C., Dorfman, T., Zwick, M. B., Wang, L. P., Rosenberg, E. S., Kwong, P. D., Burton, D. R., Robinson, J. E., Sodroski, J. G., and Farzan, M. (2003) Tyrosine sulfation of human antibodies contributes to recognition of the CCR5 binding region of HIV-1 gp120, *Cell 114*, 161-170.
140. Huang, C. C., Venturi, M., Majeed, S., Moore, M. J., Phogat, S., Zhang, M. Y., Dimitrov, D. S., Hendrickson, W. A., Robinson, J., Sodroski, J., Wyatt, R., Choe, H., Farzan, M., and Kwong, P. D. (2004) Structural basis of tyrosine sulfation and V-H-gene usage in antibodies that recognize the HIV type 1 coreceptor-binding site on gp120, *Proc. Natl. Acad. Sci. U.S.A. 101*, 2706-2711.
141. Leyte, A., Vanschijndel, H. B., Niehrs, C., Huttner, W. B., Verbeet, M. P., Mertens, K., and Vanmourik, J. A. (1991) Sulfation of Tyr1680 of Human Blood-Coagulation Factor-VIII is Essential for the Interaction of Factor-VIII with Von-Willebrand Factor, *J. Biol. Chem. 266*, 740-746.
142. Danan, L. M., Yu, Z., Ludden, P. J., Jia, W., Moore, K. L., and Leary, J. A. (2010) Catalytic Mechanism of Golgi-Resident Human Tyrosylprotein Sulfotransferase-2: A Mass Spectrometry Approach, *J Am Soc Mass Spectrom 21*, 1633-1642.
143. Yagami, T., Kitagawa, K., Aida, C., Fujiwara, H., and Futaki, S. (2000) Stabilization of a tyrosine O-sulfate residue by a cationic functional group: formation of a conjugate acid-base pair, *J. Peptide Res. 56*, 239-249.
144. Yu, Y. H., Hoffhines, A. J., Moore, K. L., and Leary, J. A. (2007) Determination of the sites of tyrosine O-sulfation in peptides and proteins, *Nat. Meth. 4*, 583-588.
145. Hersberger, K. E. (2012) Metal-Oxide Enrichment and Gas-Phase Characterization of Sulfopeptides using Fourier Transform Ion Cyclotron Resonance Mass Spectrometry., University of Michigan.
146. Robinson, M. R., and Brodbelt, J. S. (2016) Integrating Weak Anion Exchange and Ultraviolet Photodissociation Mass Spectrometry with Strategic Modulation of Peptide Basicity for the Enrichment of Sulfopeptides, *Anal. Chem. 88*, 11037-11045.
147. Hennrich, M. L., Groenewold, V., Kops, G. J. P. L., Heck, A. J. R., and Mohammed, S. (2011) Improving Depth in Phosphoproteomics by Using a Strong Cation Exchange-Weak Anion Exchange-Reversed Phase Multidimensional Separation Approach, *Anal. Chem. 83*, 7137-7143.

148. Bossio, R. E., and Marshall, A. G. (2002) Baseline Resolution of Isobaric Phosphorylated and Sulfated Peptides and Nucleotides by Electrospray Ionization FTICR MS: Another Step toward Mass Spectrometry-Based Proteomics, *Anal. Chem. 74*, 1674-1679.

149. Sieber, S. A., and Marahiel, M. A. (2005) Molecular Mechanisms Underlying Nonribosomal Peptide Synthesis: Approaches to New Antibiotics, *Chem. Rev. 105*, 715-738.

150. Fischbach, M. A., and Walsh, C. T. (2006) Assembly-Line Enzymology for Polyketide and Nonribosomal Peptide Antibiotics: Logic, Machinery, and Mechanisms, *Chem. Rev. 106*, 3468-3496.

151. Walsh, C. T., Gehring, A. M., Weinreb, P. H., Quadri, L. E. N., and Flugel, R. S. (1997) Post-translational modification of polyketide and nonribosomal peptide synthases, *Curr. Opin. Chem. Biol. 1*, 309-315.

152. Lahlou, M. (2013) The success of natural products in drug discovery, *Pharmacol. Pharm. 4*, 17-31.

153. Newman, D. J., and Cragg, G. M. (2007) Natural Products as Sources of New Drugs over the Last 25 Years, *J. Nat. Prod. 70*, 461-477.

154. Helfrich, E. J. N., and Piel, J. (2016) Biosynthesis of polyketides by trans-AT polyketide synthases, *Nat. Prod. Rep. 33*, 231-316.

155. Koehn, F. E., and Carter, G. T. (2005) The evolving role of natural products in drug discovery, *Nat. Rev. Drug. Discov. 4*, 206-220.

156. Bonnett, Shilah A., Rath, Christopher M., Shareef, A.-R., Joels, Joanna R., Chemler, Joseph A., Håkansson, K., Reynolds, K., and Sherman, David H. (2011) Acyl-CoA Subunit Selectivity in the Pikromycin Polyketide Synthase PikAIV: Steady-State Kinetics and Active-Site Occupancy Analysis by FTICR-MS, *Chem. Biol. 18*, 1075-1081.

157. Ye, Z., Musiol, Ewa M., Weber, T., and Williams, Gavin J. (2014) Reprogramming Acyl Carrier Protein Interactions of an Acyl-CoA Promiscuous trans-Acyltransferase, *Chem. Biol. 21*, 636-646.

158. Musiol, E. M., Greule, A., Hartner, T., Kulik, A., Wohlleben, W., and Weber, T. (2013) The AT(2) Domain of KirCI Loads Malonyl Extender Units to the ACPs of the Kirromycin PKS, *ChemBioChem 14*, 1343-1352.

159. Staunton, J., and Weissman, K. J. (2001) Polyketide biosynthesis: a millennium review, *Nat. Prod. Rep. 18*, 380-416.

160. Chen, S., Xue, Y. Q., Sherman, D. H., and Reynolds, K. A. (2000) Mechanisms of molecular recognition in the pikromycin polyketide synthase, *Chem. Biol. 7*, 907-918.

161. Ding, Y., Rath, C. M., Bolduc, K. L., Håkansson, K., and Sherman, D. H. (2011) Chemoenzymatic Synthesis of Cryptophycin Anticancer Agents by an Ester Bond-Forming Non-ribosomal Peptide Synthetase Module, *J. Am. Chem. Soc. 133*, 14492-14495.

162. Rath, C. M., Janto, B., Earl, J., Ahmed, A., Hu, F. Z., Hiller, L., Dahlgren, M., Kreft, R., Yu, F., Wolff, J. J., Kweon, H. K., Christiansen, M. A., Håkansson, K., Williams, R. M., Ehrlich, G. D., and Sherman, D. H. (2011) Meta-omic Characterization of the Marine Invertebrate Microbial Consortium That Produces the Chemotherapeutic Natural Product ET-743, *ACS Chem. Biol. 6*, 1244-1256.

163. Dutta, S., Whicher, J. R., Hansen, D. A., Hale, W. A., Chemler, J. A., Congdon, G. R., Narayan, A. R. H., Hakansson, K., Sherman, D. H., Smith, J. L., and Skiniotis, G. (2014) Structure of a modular polyketide synthase, *Nature 510*, 512-517.

164. Whicher, J. R., Dutta, S., Hansen, D. A., Hale, W. A., Chemler, J. A., Dosey, A. M., Narayan, A. R. H., Hakansson, K., Sherman, D. H., Smith, J. L., and Skiniotis, G. (2014) Structural rearrangements of a polyketide synthase module during its catalytic cycle, *Nature 510*, 560-564.
165. Dorrestein, P. C., Bumpus, S. B., Calderone, C. T., Garneau-Tsodikova, S., Aron, Z. D., Straight, P. D., Kolter, R., Walsh, C. T., and Kelleher, N. L. (2006) Facile Detection of Acyl and Peptidyl Intermediates on Thiotemplate Carrier Domains via Phosphopantetheinyl Elimination Reactions during Tandem Mass Spectrometry, *Biochemistry 45*, 12756-12766.
166. Bumpus, S. B., Evans, B. S., Thomas, P. M., Ntai, I., and Kelleher, N. L. (2009) A proteomics approach to discovering natural products and their biosynthetic pathways, *Nat. Biotech. 27*, 951-956.
167. Meier, J. L., Niessen, S., Hoover, H. S., Foley, T. L., Cravatt, B. F., and Burkart, M. D. (2009) An Orthogonal Active Site Identification System (OASIS) for Proteomic Profiling of Natural Product, *ACS Chem. Biol. 4*, 948-957.

Chapter 2

Corona Discharge Suppression in Negative Ion Mode Nanoelectrospray Ionization via Trifluoroethanol Addition

2.1 Introduction

Nanoelectrospray ionization (nESI) has gained popularity as a "soft" ionization source due to several advantages compared with conventional electrospray ionization (ESI). Due to the smaller capillary diameters employed in nESI, initially formed droplets have nanometer size, whereas ESI produces micrometer-sized droplets.[1-4] The reduction in initial droplet size lowers the deposition of ionization energy and increases the likelihood of gas-phase ions being generated from evaporating progeny droplets, resulting in higher ion counts and lower limits of detection.[3, 5-9] For example, consumption of only zeptomoles of peptides was recently reported with microfabricated nESI needles.[10] The lower deposition of ionization energy in nESI compared with ESI is often utilized to maintain native proteins and complexes into the gas phase, allowing for the examination of tertiary and quaternary structure with ion mobility and/or mass spectrometric measurements.[11-13] Nanoflow liquid chromatography (nLC) separations (nL/min) are ideally suited for coupling with nESI, resulting in robust and stable positive ion mode ionization and online detection with modern mass spectrometers.[14-17]

While positive ion mode nESI is suitable for the detection of basic and neutral compounds, typically acidic molecules are not ionized effectively.[18, 19] Many proteomes have been predicted to exhibit multimodular pI distributions with a minimum at pI 7.[20, 21] However, in conventional positive ion mode nLC/MS analysis, the majority of detected peptides have pIs greater than 5.[22, 23] By including a second dimension of peptide separation prior to reversed phase elution, such as strong cation exchange (SCX) or isoelectric focusing (IEF), acidic peptides can be identified with

positive polarity nESI.[24-26] However, Yates and co-workers reported an absence of peptides with pIs ≤4 in a combined protein fractionation/multidimensional protein identification technology (MudPIT) approach; still excluding a majority of the low pI region.[24] Several acidic post-translational modifications, such as sulfation, phosphorylation, and sialylation, greatly reduce overall analyte pI. Utilization of negative polarity nESI can improve the detection of acidic molecules due to the inherent tendency to form negative charges, which is often leveraged in the field of metabolomics.[27-31] Coon and co-workers demonstrated the use of alkaline separations and negative ion mode detection as an effective method to probe the acidic proteome.[23, 32] However, unfortunately, nESI does not typically perform robustly in negative ion mode.

Under negative polarity, corona discharge is often observed at the tip of nESI emitters.[23, 33] Corona discharge results in degradation of spray stability and needle tip geometry, ultimately leading to loss of signal. This phenomenon was observed as early as by Fenn and co-workers' first experiments with negative ion mode ESI.[18, 34] Several methods have been implemented to suppress the observed plasma. The introduction of high dielectric nebulizing gas, such as sulfur hexafluoride or dry oxygen, has been employed to increase the local dielectric environment at the ESI needle tip as well as promote stable generation of analyte droplets for negative ion generation.[34-36] Also, pressurization of the mass spectrometer's inlet region (2-6 bar) has been shown to afford an increased dielectric environment, reducing corona discharge.[37, 38] In addition, organic solvents, such as methanol (MeOH), isopropyl alcohol, and fluorosolvents can be added to samples to reduce the onset spray voltage below the dielectric breakdown of air.[39, 40] Chlorosolvents have previously been utilized as electron scavengers for the reduction of corona discharge events, but is immiscible with aqueous samples.[39, 41, 42] Fluorosolvent addition has also been utilized extensively as a method to retain and improve ionization of hydrophilic small molecules and oligonucleotides through ion-pairing on reversed-phase resins and improved ESI droplet desolvation.[43-46] Furthermore, small needle-tip geometry has been reported to decrease minimum spray voltage below ambient atmosphere dielectric limits.[47] While these approaches have been effective, instrumental modification, dilution of precious sample, and analyte solubility are still concerns, particularly with regards to online separations and "native" MS experiments.[48]

Herein we report the stabilization of negative ion mode nESI and suppression of corona discharge via trifluoroethanol (TFE) addition to aqueous sample matrices. A series of small molecules,

26

peptides, and proteins were examined with varying amounts of TFE modifier. The utility of TFE as a mobile phase additive was examined via nanoflow separation and detection of tryptic peptides at elevated pH in negative ion mode. With the addition of trace TFE, negative ion mode nESI analysis can be used to effectively characterize acidic molecules present in many complex aqueous matrices analyzed with MS.

2.2 Experimental

2.2.1 Chemicals

Water, MeOH, ethanol (EtOH), 2,2,2-trifluoroethanol, ammonium bicarbonate, ammonium acetate, 48% hydrofluoric acid (HF), and formic acid were purchased from Fisher Scientific (Pittsburgh, PA). Equine myoglobin (Myo), bovine ubiquitin, bovine serum albumin (BSA), bovine α-casein, bovine β-casein, 5 M ammonium hydroxide, triethylamine (TEA), dithiothreitol, maltohexanose (MH), tetrahydrocortisone-(3-β-D-glucuronide) (TC), paromomycin (PA), angiotensin I (AngI), and [Arg[8]]–vasopressin (Vas), were obtained from Sigma-Aldrich (St. Louis, MO). Phosphatidylserine 16:0-18:2 (PS) was purchased from Avanti Polar Lipids (Alabaster, Al). Tyrosine phosphopeptide (TSTEPQpYQPGEN) (pYpep) was purchased from EMD Millipore (Billerica, MA). Sulfated cholecystokinin (CCKS) was purchased from Abcam (Cambridge, MA). The synthetic peptide (YFYLIPLEYLK) (SynPep) was purchased from GenicBio (Shanghai, China). Modified sequencing grade trypsin was obtained from Promega (Madison, WI). Water, MeOH, and EtOH were HPLC grade. TFE was peptide synthesis grade. All compounds were used as purchased.

2.2.2 Direct Infusion nESI Mass Spectrometry

All direct infusion mass spectra were collected on a Waters Micromass LCT Premier equipped with a Z-Spray nESI source. Borosilicate nESI needles were pulled to approximately 3-8 µm tip i.d.'s on a Sutter Instruments P-97 micropipette puller and gold coated using a Quorum Technologies SC7620 sputter coater as previously described.[11] Each acquisition was performed with the emitter tip approximately 6 mm away from the sample cone. To each solution, unless otherwise noted, 0.2% ammonium hydroxide was added to promote analyte deprotonation. Sample flow rates were estimated to be 20-50 nl/min for direct infusion experiments.[11] Each protein was examined at 10 µM. Peptide and small molecule concentration in their respective solutions were

5 µM. Spray voltage was applied at – (1.25-1.35) kV and remained constant for each experiment performed. The source region was heated to 65°C for all experiments.

2.2.3 Nanoflow Liquid Chromatography/Mass Spectrometry

BSA, α-casein, and β-casein were mixed in a 1:1:1 ratio at 75 µM each. This mixture was subjected to reduction, alkylation, and tryptic digestion at a 1:50 protease:protein ratio. High pH tolerant trap and analytical columns were slurry packed with Waters Xbridge C18, 5 µm particles as previously described.[23, 49] Trap column and analytical column dimensions were 75 µm i.d. x 5 cm and 75 µm i.d. x 17 cm, respectively. Fused silica nESI emitters were pulled on a Sutter Instruments P-2000 laser micropipette puller and HF etched as previously described to approximately 4-6 µm tip i.d .[50] Mobile phase solvent A (95% H_2O, 5% MeOH) and B (5% H_2O, 95% MeOH) were buffered with 0.2% TEA to pH 11 with formic acid and ammonium hydroxide.[51] TFE was added to both mobile phases at 0.2% where noted. Sample loading was completed at 2 µL/min, placing a total of 500 fmol of each tryptically digested protein on column. Gradient elution was completed at 250 nL/min with the following gradient: 2–75% B; 0–85 min. Negative ion mode mass spectra were collected at 1M data points on a Bruker 7 T SolariX Fourier transform ion cyclotron resonance mass spectrometer with 0.1 s ion accumulation time. Nanospray voltage was held at 1.25 kV and the drying gas temperature was set to 150°C. Mass spectra were externally calibrated to < 2 ppm error. Following triplicate data collection, peptide matches were determined using an in-house Excel macro. Peptides were only assigned if error was < 10 ppm. Alkylation of cysteine was set as a fixed modification. Variable modifications were set at two missed tryptic cleavages, and methionine oxidation.

2.3 Results and Discussion

2.3.1 Negative Ion Nanoelectrospray Stability with Different Solvent Modifiers

A five peptide mixture of angiotensin I, sulfated cholecystokinin, [Arg[8]]–vasopressin, synthetic peptide (YFYLIPLEYLK), and tyrosine phosphopeptide was subjected to direct infusion MS analysis for a total of 30 min to assess negative ion mode nESI stability. Stability was assessed as ± σ of the sample's total ion counts for the duration of the experiment. Figure 2.1 shows the corresponding results from experiments with three different solvent modifiers. A completely aqueous solution resulted in an average of $0.78 \pm 0.14 \times 10^6$ counts. By adding 0.2% MeOH, the

observed average counts approximately doubled to $1.54 \pm 0.09 \times 10^6$ with the signal variability decreasing as indicated. However, at approximately 12 min, corona discharge occurred, degrading the needle's conductive coating and resulting in lower ion counts with increased fluctuation.
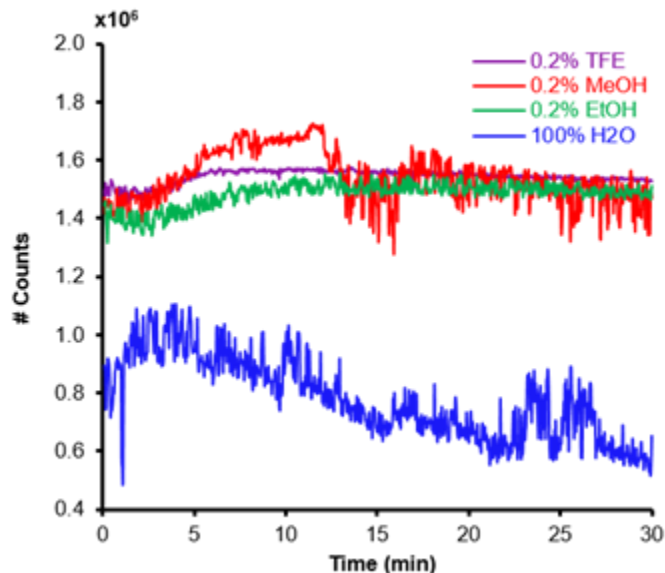
Figure 2.1: Negative ion nESI stability observed with a five peptide mixture and various solvent modifiers at -1.25 kV.

Sporadic corona discharge reoccurred for the remainder of the experiment. Example images of emitters before and after corona discharge can be seen in the supporting information. (Figure 2.2). With 0.2% EtOH or 0.2% TFE solutions, average ion counts of $1.48 \pm 0.04 \times 10^6$ and $1.54 \pm 0.02 \times 10^6$ were observed, respectively, both corresponding to lower signal variability than for MeOH addition. However, upon trace addition of TFE, spray stability is approximately twice as stable as with EtOH addition and four times more stable than with MeOH addition under identical conditions. Overall, the addition of TFE resulted in similar ion counts as for EtOH and MeOH, but resulted in suppression of corona discharge events for more robust anion generation. The plasma at the nESI needle tip, visible to the naked eye at -1.25 kV, also was absent following TFE addition.
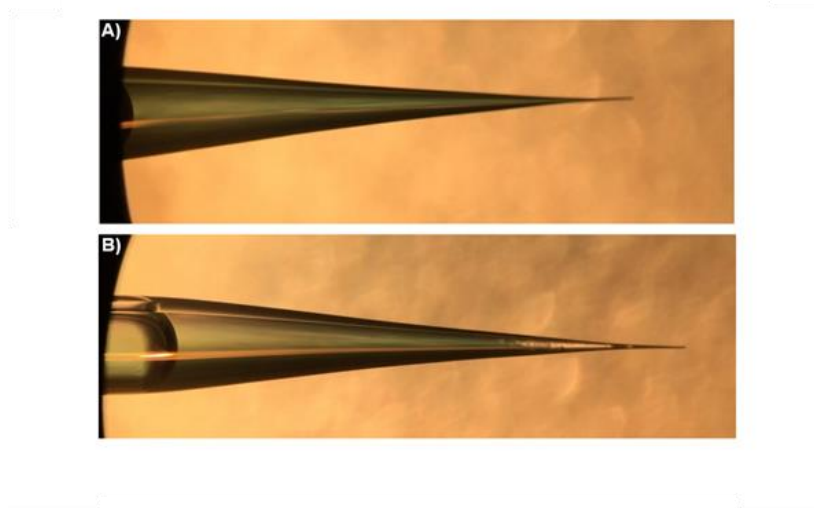
Figure 2.2: Example images of nESI emitters **A)** prior to corona discharge (-1.20 kV) and **B)** after corona discharge (-1.30 kV).

We hypothesize the mechanism of corona discharge suppression in negative ion mode via TFE addition is due to the unique electronic properties of the gaseous TFE molecule. As modified aqueous solvent undergoes nanoelectrospray, the higher vapor pressure of TFE compared with water implies preferential TFE evaporation from desolvating analyte droplets.[52] The gas phase TFE can act as electron scavenger due to the highly electronegative fluorine atoms, suppressing plasma formation in a manner similar to SF_6 gas.[36] These properties result in a higher local dielectric constant at the tip of the nESI emitter, thus decreasing corona discharge events. When the nESI voltage of a TFE laden solution is steadily increased, the onset of corona discharge is ~100 V higher when compared to other organic modifiers, indicating the local dielectric
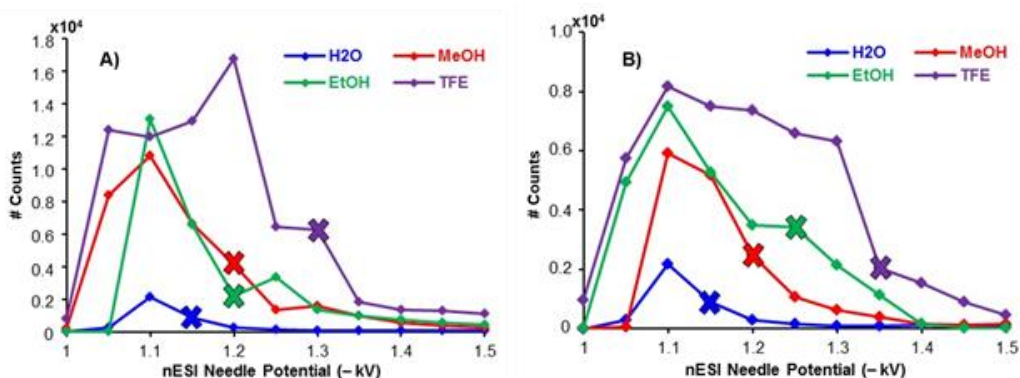
Figure 2.3: Plots examining myoglobin total ion current as a function of negative ion mode emitter potential with organic modifier concentrations of **A)** 0.2% and **B)** 1.0%. The potential when visible corona discharge occurs is denoted by ✖.

30

environment at the needle tip has been increased (Figure 2.3). To further confirm whether the observed corona discharge suppression is a gas-phase phenomenon, TFE in MeOH was orthogonally nanoelectrosprayed via a separate lockspray emitter at a ~6 mm offset when compared to the analyte nESI emitter. As seen in Figure 2.4, the total ion current for the protein myoglobin nanoelectrosprayed in negative ion mode from an aqueous solution with 0.2% NH_4OH is both increased and stabilized when TFE is present in the orthogonal lockspray solution as compared to MeOH alone and is most effective when included in the sample solution. These result support the hypothesis that TFE corona discharge suppression is likely linked to an increase in the gas-phase dielectric environment at emitter tips (Figure 2.5).
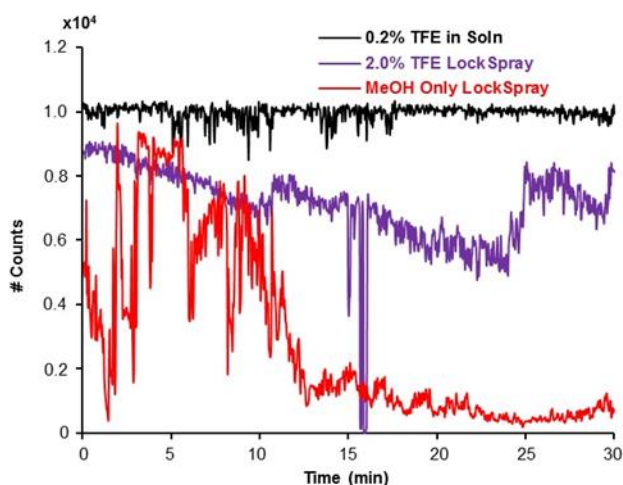
Figure 2.4: Negative ion nESI stability for 10 µM myoglobin in 99.8% H2O and 0.2% NH4OH solution examined with an ~6 mm offset lockspray concomitantly spraying 100% MeOH (red) or 2% TFE in MeOH (purple). When 0.2% TFE is only included in the analyte solution (black) stability is maximized.

2.3.2 Negative Ion Charge State Effects with Solvent Modifiers

While the addition of TFE increases nESI stability in negative ion mode, it is possible that the presence of TFE may alter observed analyte charge states, similar to the supercharging reagents m-nitrobenzyl alcohol and sulfolane.[53] By altering analyte charging, the mechanisms of tandem mass spectrometry activation techniques such as electron detachment dissociation (EDD), negative ion electron capture dissociation (niECD), negative electron transfer dissociation (NETD) and negative ultraviolet photodissociation (NUVPD) can be altered, resulting in either increased or reduced information content.[32, 54-56] Furthermore, shifts in analyte charge can place a compound
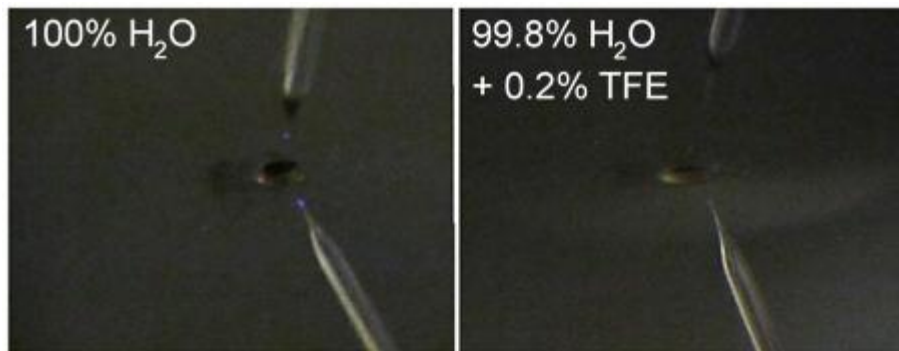
Figure 2.5: Example images of nESI needles in 100% aqueous solvent (Left) and the sample with 0.2% TFE added (Right). Corona discharge is not observed at 1.25 kV upon addition of 0.2% TFE.

outside the optimal detection range of some mass analyzers, including quadrupoles. Finally, the maintenance of native protein structure into the gas phase is dependent on the charge state of the protein, thus alterations in the overall protein charge can cause Coulomb-induced unfolding events.[53]
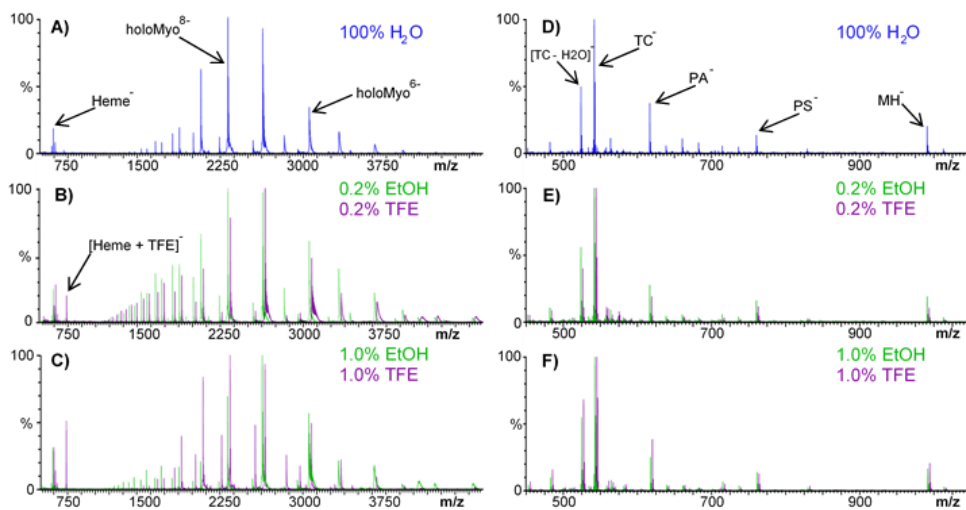
Figure 2.6: Negative ion nESI spectra of myoglobin and small molecule mix [TC = tetrahydrocortisone-(3-β-D-glucuronide), PA = paromomycin, PS = phosphatidylserine 16:0-18:2, MH = maltohexanose] in **A & D)** 100% H2O, **B & E)** 0.2% modifier, and **C & F)** 1.0% modifier, respectively. Spectra are offset by 15 m/z for clarity.

We examined the average charge states (Z_{avg}) and ionization behaviors of three proteins upon negative ion nESI as a function of organic modifier percentage. As seen in Figure 2.6 (left), neither EtOH nor TFE resulted in significantly altered myoglobin charge states although a [Heme + TFE]$^-$ adduct was observed for TFE laden solutions. At TFE concentrations greater than 1.0% (139 mM), TFE appears to disrupt Heme hydrogen bonding, resulting in slightly higher Apo to Holo

32

myoglobin ratios as compared with the EtOH laden solvent. For BSA and ubiquitin, no significant charge state alteration was observed up to 1.0% TFE (Figure 2.7). Z_{avg} was determined following
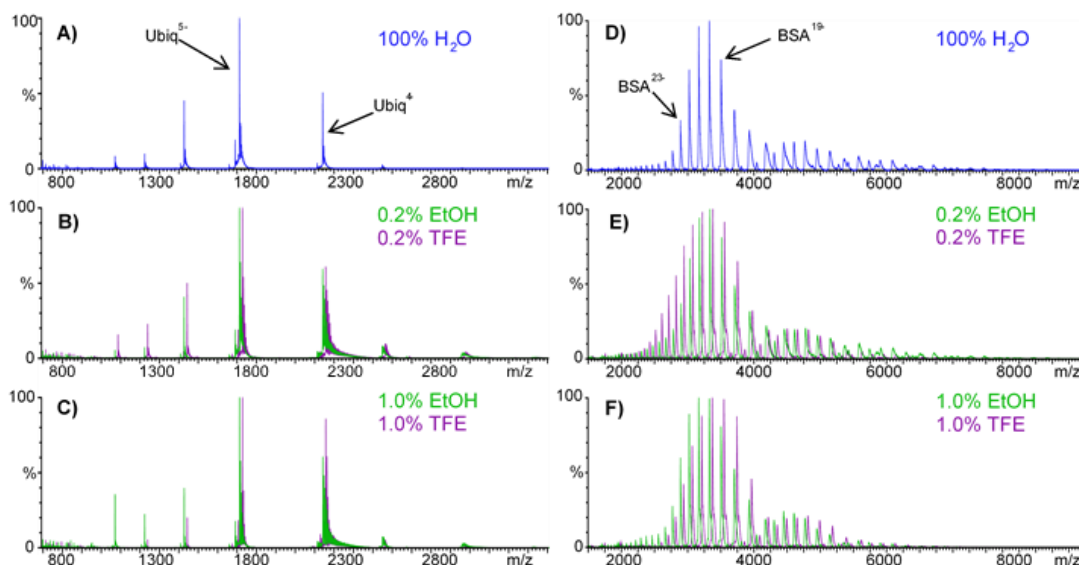
Figure 2.7: Negative ion mode nESI spectra of ubiquitin and BSA in **A & D)** 100% H2O, **B & E)** 0.2% organic modifier, and **C & F)** 1.0% modifier, respectively. Spectra are offset by 15 m/z for clarity.

triplicate analysis of ubiquitin, myoglobin, and BSA with and without solvent modifier. For these three proteins, observed charge states for equivalent organic modifier percentages were within error of each modifier type (Figure 2.8). Thus, the relatively low concentration of organic modifier in each solution does not affect Z_{avg} observed under primarily aqueous conditions. We further examined the addition of TFE to "native" buffers to improve negative ion mode spray stability: identical myoglobin charge state distributions were observed in 100 mM ammonium acetate solution at pH 7.2 with and without 1.0% TFE addition (Figure 2.9). The charge states observed under these conditions have been previously reported as indicative of the native gas phase confirmation of myoglobin.[53]

Mixtures of five peptides and four small molecules, respectively, were also examined as a function of organic modifier percentage. As seen in Figure 2.6 (right) and Figure 2.10, increasing the percentage of EtOH or TFE did not significantly alter observed charge states (within ±σ) of the peptides or small molecules studied. In both model systems, as organic modifier percentage is increased, the signal observed for all molecules is slightly improved. These results indicate that

33

with trace addition of TFE to negative ion mode nESI analysis, corona discharge can be mitigated while not altering charging of proteins, peptides, and small molecules.
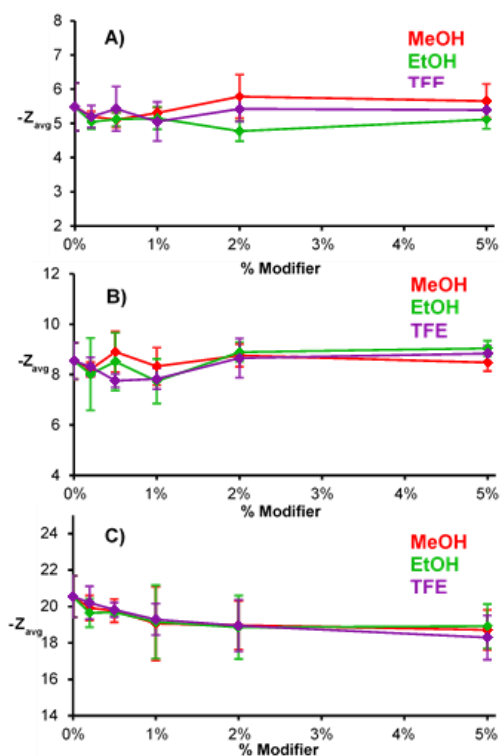
Figure 2.8: Average charge states observed (normalized intensity to charge) for **A)** ubiquitin, **B)** myoglobin, **C)** BSA as a function of organic modifier percentage. Error bars are one standard deviation from the mean.
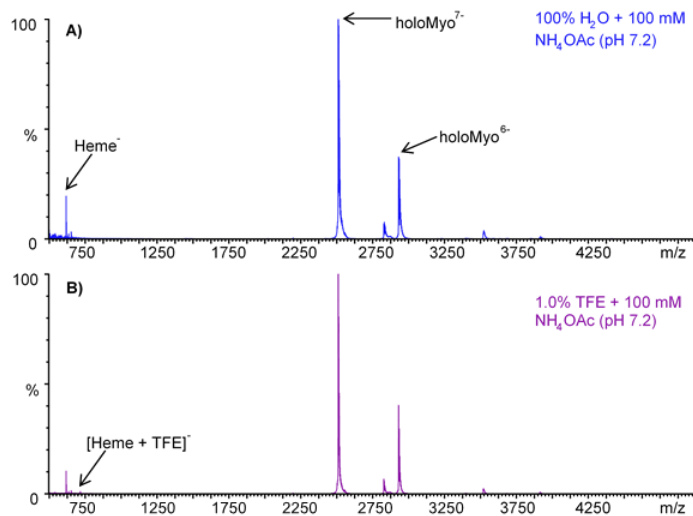
Figure 2.9: Negative ion mode nESI spectra of "native" myoglobin in **A)** 100 mM ammonium acetate and **B)** 100 mM ammonium acetate with 1.0% TFE.
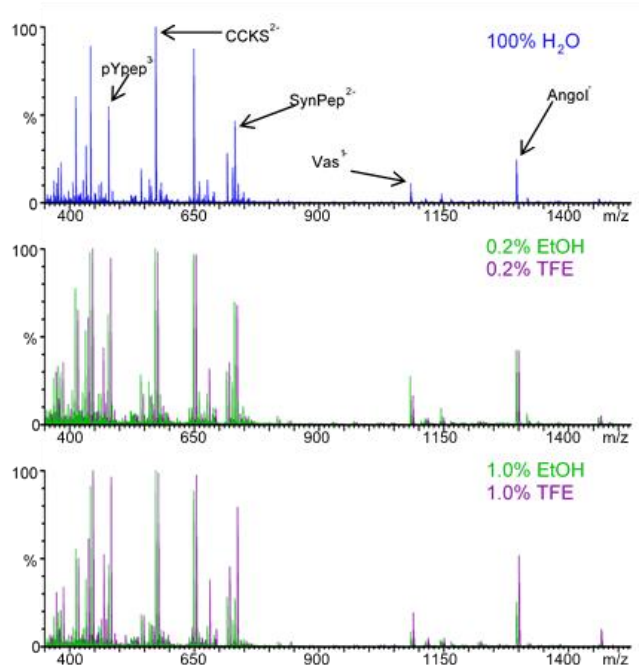
Figure 2.10: Observed negative ion mode nESI spectra of a five peptide mixture as a function of organic modifier. Spectra are offset by 15 m/z for clarity.

2.3.3 Negative Ion nLC-MS of Tryptic Peptides

The addition of TFE to mobile phase solvents was also examined as a method of stabilizing nESI at high aqueous percentages commonly encountered at the beginning of liquid chromatography gradients. Figure 2.11A shows base peak chromatograms, demonstrating the effect of adding 0.2% TFE to a negative ion mode nLC/MS experiment. From 7–27 min, increased peptide signal is clearly observed upon TFE addition. In Figure 2.11B, sample extracted ion chromatograms demonstrate how commonly identified peptides are altered by TFE addition in the early elution region of analysis. Sequence coverage observed for α-casein, β-casein, and BSA without TFE present was $53 \pm 8\%$, $24 \pm 7\%$, and $70 \pm 7\%$, respectively. When 0.2% TFE was included in the mobile phases, the sequence coverage for α-casein, β-casein, and BSA increased to $80 \pm 3\%$, $38 \pm 7\%$, and $81 \pm 3\%$, respectively. A total of 111 unique peptides were detected when TFE was added, compared with 93 unique peptides without TFE.

Detected peptides were classified into three categories based on mobile phase composition; early eluting (2–26% B), moderate eluting (27–51% B), and late eluting (≥52% B). Based on this classification, without TFE 17 peptides are classified as early eluting, 55 as moderate eluting, and 21 as late eluting. Upon addition of 0.2% TFE to the mobile phase, 61 peptides are classified as

35
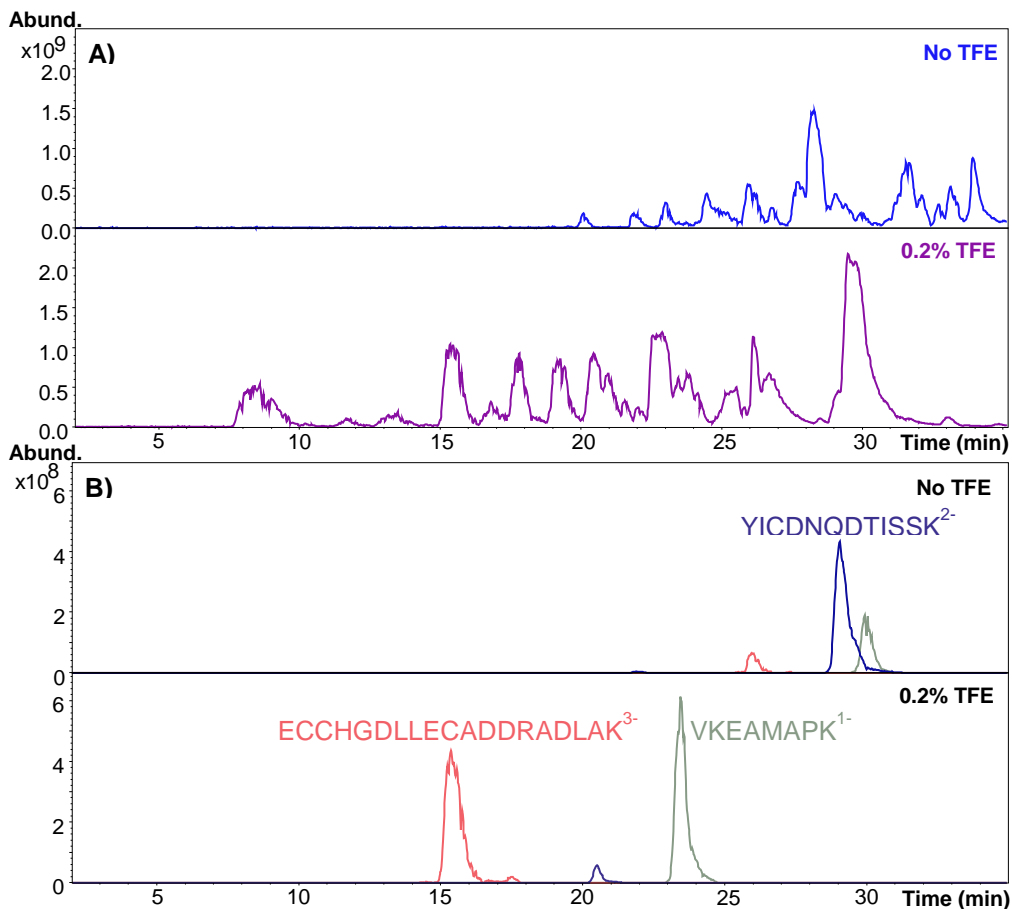
Figure 2.11: **A**) Base peak chromatograms of early elution region from negative ion mode nLC/MS analysis of tryptic peptides without (top) and with (bottom) TFE present in the mobile phase. **B**) Example extracted ion chromatograms of early eluting tryptic peptides observed in both experiments.

early eluting, 34 as moderate eluting, and 16 as late eluting. Peptides that were found in both nLC/MS experiments were examined for retention time shifts upon the addition of 0.2% TFE. Without TFE addition, the average peptide elution time was 42.0 min, whereas after TFE addition the average retention time was 34.7 min. The addition of TFE to mobile phase A caused a reduction in stationary phase retention due to the increased hydrophobicity of the eluent. Despite an approximately 7 min shift in peptide retention, TFE addition and subsequent corona discharge suppression allows for robust detection of peptides eluting in a mostly aqueous solvent and an overall increase in total ion current and peptide identification by 30% and 18% respectively.

36

2.4 Conclusions

Trace addition of TFE to aqueous samples for negative ion mode nESI analysis results in significant suppression of corona discharge at nESI emitter tips. This suppression, in turn, results in stabilized signal and increased longevity of nESI needles under negative polarity. All samples examined in this study benefited in signal abundance and stability without altering observed analyte charge states upon TFE addition. Furthermore, TFE addition to negative ion nLC/MS experiments improved sequence coverage and only slightly altered chromatography. To further improve separations in the future, mobile phase A composition of 97.8% H_2O, 2% MeOH, and 0.2% TFE will be used to reduce peptide elution shifts. Additional experiments to elucidate the mechanism of TFE corona discharge suppression are currently in progress.

2.5 References

1. Wilm, M., and Mann, M. (1996) Analytical Properties of the Nanoelectrospray Ion Source, *Anal. Chem. 68*, 1-8.
2. Gomez, A., and Tang, K. (1994) Charge and fission of droplets in electrostatic sprays, *Phys. Fluids 6*, 404-414.
3. Kebarle, P., and Verkerk, U. H. (2009) Electrospray: from ions in solution to ions in the gas phase, what we know now, *Mass. Spectrom. Rev. 28*, 898-917.
4. Hogan, C. J., Biswas, P., and Chen, D.-r. (2009) Charged Droplet Dynamics in the Submicrometer Size Range, *J. Phys. Chem. B 113*, 970-976.
5. Körner, R., Wilm, M., Morand, K., Schubert, M., and Mann, M. (1996) Nano electrospray combined with a quadrupole ion trap for the analysis of peptides and protein digests, *J. Am. Soc. Mass Spectrom. 7*, 150-156.
6. Covey, T. R., and Pinto, D. (2002) *Nanospray Electrospray Ionization Development*.
7. Covey, T. R., Thomson, B. A., and Schneider, B. B. (2009) Atmospheric pressure ion sources, *Mass Spectrom. Rev. 28*, 870-897.
8. Juraschek, R., Dülcks, T., and Karas, M. (1999) Nanoelectrospray—more than just a minimized-flow electrospray ionization source, *J. Am. Soc. Mass Spectrom. 10*, 300-308.
9. Schmidt, A., Karas, M., and Dülcks, T. (2003) Effect of different solution flow rates on analyte ion signals in nano-ESI MS, or: when does ESI turn into nano-ESI?, *J. Am. Soc. Mass Spectrom. 14*, 492-500.
10. Marginean, I., Tang, K., Smith, R., and Kelly, R. (2014) Picoelectrospray Ionization Mass Spectrometry Using Narrow-Bore Chemically Etched Emitters, *J. Am. Soc. Mass Spectrom. 25*, 30-36.
11. Hernandez, H., and Robinson, C. V. (2007) Determining the stoichiometry and interactions of macromolecular assemblies from mass spectrometry, *Nat. Protoc. 2*, 715-726.
12. Ruotolo, B. T., Benesch, J. L. P., Sandercock, A. M., Hyung, S. J., and Robinson, C. V. (2008) Ion mobility-mass spectrometry analysis of large protein complexes, *Nat. Protoc. 3*, 1139-1152.

13. Heck, A. J. R. (2008) Native mass spectrometry: a bridge between interactomics and structural biology, *Nat. Methods 5*, 927-933.

14. Wu, N., Collins, D. C., Lippert, J. A., Xiang, Y., and Lee, M. L. (2000) Ultrahigh pressure liquid chromatography/time-of-flight mass spectrometry for fast separations, *J. Microcolumn Sep. 12*, 462-469.

15. Aebersold, R., and Mann, M. (2003) Mass spectrometry-based proteomics, *Nature 422*, 198-207.

16. Thingholm, T. E., Jensen, O. N., and Larsen, M. R. (2009) Analytical strategies for phosphoproteomics, *Proteomics 9*, 1451-1468.

17. Lee, J. H., Hyung, S. W., Mun, D. G., Jung, H. J., Kim, H., Lee, H., Kim, S. J., Park, K. S., Moore, R. J., Smith, R. D., and Lee, S. W. (2012) Fully Automated Multifunctional Ultrahigh Pressure Liquid Chromatography System for Advanced Proteome Analyses, *J. Proteome Res. 11*, 4373-4381.

18. Yamashita, M., and Fenn, J. B. (1984) Negative ion production with the electrospray ion source, *J. Phys. Chem. 88*, 4671-4675.

19. Janek, K., Wenschuh, H., Bienert, M., and Krause, E. (2001) Phosphopeptide analysis by positive and negative ion matrix-assisted laser desorption/ionization mass spectrometry, *Rapid Commun. Mass Spectrom. 15*, 1593-1599.

20. Knight, C. G., Kassen, R., Hebestreit, H., and Rainey, P. B. (2004) Global analysis of predicted proteomes: Functional adaptation of physical properties, *Proc. Natl. Acad. Sci. U.S.A. 101*, 8390-8395.

21. Wu, S., Wan, P., Li, J., Li, D., Zhu, Y., and He, F. (2006) Multi-modality of pI distribution in whole proteome, *Proteomics 6*, 449-455.

22. Chen, E. I., Hewel, J., Felding-Habermann, B., and Yates, J. R. (2006) Large Scale Protein Profiling by Combination of Protein Fractionation and Multidimensional Protein Identification Technology (MudPIT), *Mol. Cell. Proteomics 5*, 53-56.

23. McAlister, G. C., Russell, J. D., Rumachik, N. G., Hebert, A. S., Syka, J. E., Geer, L. Y., Westphall, M. S., Pagliarini, D. J., and Coon, J. J. (2012) Analysis of the acidic proteome with negative electron-transfer dissociation mass spectrometry, *Anal. Chem. 84*, 2875-2882.

24. Washburn, M. P., Wolters, D., and Yates, J. R. (2001) Large-scale analysis of the yeast proteome by multidimensional protein identification technology, *Nat. Biotech. 19*, 242-247.

25. Essader, A. S., Cargile, B. J., Bundy, J. L., and Stephenson, J. L. (2005) A comparison of immobilized pH gradient isoelectric focusing and strong-cation-exchange chromatography as a first dimension in shotgun proteomics, *Proteomics 5*, 24-34.

26. Cargile, B. J., Bundy, J. L., Freeman, T. W., and Stephenson, J. L. (2004) Gel Based Isoelectric Focusing of Peptides and the Utility of Isoelectric Point in Protein Identification, *J. Proteome Res. 3*, 112-119.

27. Lu, W. Y., Clasquin, M. F., Melamud, E., Amador-Noguez, D., Caudy, A. A., and Rabinowitz, J. D. (2010) Metabolomic Analysis via Reversed-Phase Ion-Pairing Liquid Chromatography Coupled to a Stand Alone Orbitrap Mass Spectrometer, *Anal. Chem. 82*, 3212-3221.

28. Yuan, M., Breitkopf, S. B., Yang, X., and Asara, J. M. (2012) A positive/negative ion-switching, targeted mass spectrometry-based metabolomics platform for bodily fluids, cells, and fresh and fixed tissue, *Nat. Protoc. 7*, 872-881.

29. Robotham, S. A., Horton, A. P., Cannon, J. R., Cotham, V. C., Marcotte, E. M., and Brodbelt, J. S. (2016) UVnovo: A de Novo Sequencing Algorithm Using Single Series of Fragment Ions via Chromophore Tagging and 351 nm Ultraviolet Photodissociation Mass Spectrometry, *Anal. Chem. 88*, 3990-3997.
30. Robinson, M. R., and Brodbelt, J. S. (2016) Integrating Weak Anion Exchange and Ultraviolet Photodissociation Mass Spectrometry with Strategic Modulation of Peptide Basicity for the Enrichment of Sulfopeptides, *Anal. Chem. 88*, 11037-11045.
31. Robinson, M. R., Taliaferro, J. M., Dalby, K. N., and Brodbelt, J. S. (2016) 193 nm Ultraviolet Photodissociation Mass Spectrometry for Phosphopeptide Characterization in the Positive and Negative Ion Modes, *J. Proteome Res. 15*, 2739-2748.
32. Riley, N. M., Rush, M. J. P., Rose, C. M., Richards, A. L., Kwiecien, N. W., Bailey, D. J., Hebert, A. S., Westphall, M. S., and Coon, J. J. (2015) The Negative Mode Proteome with Activated Ion Negative Electron Transfer Dissociation (AI-NETD), *Mol. Cell. Proteomics 14*, 2644-2660.
33. Greer, S. M., Cannon, J. R., and Brodbelt, J. S. (2014) Improvement of Shotgun Proteomics in the Negative Mode by Carbamylation of Peptides and Ultraviolet Photodissociation Mass Spectrometry, *Anal. Chem. 86*, 12285-12290.
34. Fenn, J. B., Mann, M., Meng, C. K., Wong, S. F., and Whitehouse, C. M. (1989) Electrospray Ionization for Mass Spectrometry of Large Biomolecules, *Science 246*, 64-71.
35. Ikonomou, M., Blades, A., and Kebarle, P. (1991) Electrospray mass spectrometry of methanol and water solutions suppression of electric discharge with SF6 gas, *J. Am. Soc. Mass Spectrom. 2*, 497-505.
36. Wampler, F., Blades, A., and Kebarle, P. (1993) Negative ion electrospray mass spectrometry of nucleotides: ionization from water solution with SF6 discharge suppression, *J. Am. Soc. Mass Spectrom. 4*, 289-295.
37. Chen, L. C., Mandal, M. K., and Hiraoka, K. (2011) Super-Atmospheric Pressure Electrospray Ion Source: Applied to Aqueous Solution, *J. Am. Soc. Mass Spectrom. 22*, 2108-2114.
38. Rahman, M. M., Mandal, M. K., Hiraoka, K., and Chen, L. C. (2013) High pressure nanoelectrospray ionization mass spectrometry for analysis of aqueous solutions, *Analyst 138*, 6316-6322.
39. Zhu, J., and Cole, R. B. (2000) Formation and decompositions of chloride adduct ions, [M + Cl]−, in negative ion electrospray ionization mass spectrometry, *J. Am. Soc. Mass Spectrom. 11*, 932-941.
40. Wu, Z., Gao, W., Phelps, M. A., Wu, D., Miller, D. D., and Dalton, J. T. (2004) Favorable Effects of Weak Acids on Negative-Ion Electrospray Ionization Mass Spectrometry, *Anal. Chem. 76*, 839-847.
41. Cole, R. B., and Harrata, A. K. (1993) Solvent effect on analyte charge state, signal intensity, and stability in negative ion electrospray mass spectrometry; implications for the mechanism of negative ion formation, *J. Am. Soc. Mass Spectrom. 4*, 546-556.
42. Cole, R. B., and Harrata, A. K. (1992) Charge-state distributuion and electric-discharge suppression in negative-ion electrospray mass spectrometry using/chlorinated solvents, *Rapid Commun. Mass Spectrom. 6*, 536-539.
43. Apffel, A., Chakel, J. A., Fischer, S., Lichtenwalter, K., and Hancock, W. S. (1997) New procedure for the use of high-performance liquid chromatography-electrospray ionization

mass spectrometry for the analysis of nucleotides and oligonucleotides, *J. Chromatog. A 777*, 3-21.

44. Dai, G., Wei, X., Liu, Z., Liu, S., Marcucci, G., and Chan, K. K. (2005) Characterization and quantification of Bcl-2 antisense G3139 and metabolites in plasma and urine by ion-pair reversed phase HPLC coupled with electrospray ion-trap mass spectrometry, *J. Chromatog. B 825*, 201-213.

45. Kipper, K., Herodes, K., and Leito, I. (2011) Fluoroalcohols as novel buffer components for basic buffer solutions for liquid chromatography electrospray ionization mass spectrometry: Retention mechanisms, *J. Chromatog. A 1218*, 8175-8180.

46. Erb, R., and Oberacher, H. (2014) Comparison of mobile-phase systems commonly applied in liquid chromatography-mass spectrometry of nucleic acids, *Electrophoresis 35*, 1226-1235.

47. Chowdhury, S. K., and Chait, B. T. (1991) Method for the electrospray ionization of highly conductive aqueous solutions, *Anal. Chem. 63*, 1660-1664.

48. Konermann, L., and Douglas, D. J. (1998) Unfolding of proteins monitored by electrospray ionization mass spectrometry: a comparison of positive and negative ion modes, *J. Am. Soc. Mass Spectrom. 9*, 1248-1254.

49. Mellors, J. S., and Jorgenson, J. W. (2004) Use of 1.5-μm Porous Ethyl-Bridged Hybrid Particles as a Stationary-Phase Support for Reversed-Phase Ultrahigh-Pressure Liquid Chromatography, *Anal. Chem. 76*, 5441-5450.

50. Valaskovic, G. A., Kelleher, N. L., Little, D. P., Aaserud, D. J., and McLafferty, F. W. (1995) Attomole-Sensitivity Electrospray Source for Large-Molecule Mass Spectrometry, *Anal. Chem. 67*, 3802-3805.

51. Huffman, B. A., Poltash, M. L., and Hughey, C. A. (2012) Effect of Polar Protic and Polar Aprotic Solvents on Negative-Ion Electrospray Ionization and Chromatographic Separation of Small Acidic Molecules, *Anal. Chem. 84*, 9942-9950.

52. Iavarone, A. T., and Williams*, E. R. (2003) Mechanism of Charging and Supercharging Molecules in Electrospray Ionization, *J. Am. Chem. Soc. 125*, 2319-2327.

53. Sterling, H. J., Daly, M. P., Feld, G. K., Thoren, K. L., Kintzer, A. F., Krantz, B. A., and Williams, E. R. (2010) Effects of Supercharging Reagents on Noncovalent Complex Structure in Electrospray Ionization from Aqueous Solutions, *J. Am. Soc. Mass Spectrom. 21*, 1762-1774.

54. Wolff, J. J., Laremore, T. N., Busch, A. M., Linhardt, R. J., and Amster, I. J. (2008) Influence of Charge State and Sodium Cationization on the Electron Detachment Dissociation and Infrared Multiphoton Dissociation of Glycosaminoglycan Oligosaccharides, *J. Am. Soc. Mass Spectrom. 19*, 790-798.

55. Yoo, H. J., Wang, N., Zhuang, S., Song, H., and Håkansson, K. (2011) Negative-Ion Electron Capture Dissociation: Radical-Driven Fragmentation of Charge-Increased Gaseous Peptide Anions, *J. Am. Chem. Soc. 133*, 16790-16793.

56. Madsen, J. A., Kaoud, T. S., Dalby, K. N., and Brodbelt, J. S. (2011) 193-nm photodissociation of singly and multiply charged peptide anions for acidic proteome characterization, *Proteomics 11*, 1329-1334.

Improved Detection of Sulfated and Phosphorylated Peptides with Negative Ion Nanoelectrospray Ionization and Alkaline Reversed-phase Chromatography

3.1 Introduction

Proteomic experiments are a vital tool for the analysis of total cellular protein content[1, 2], protein expression[3-5], and post-translational modifications (PTMs).[6-10] Owing to continuing improvements in liquid chromatography mass spectrometry (LC-MS), thousands of proteins can be routinely interrogated.[11-13] Coon et al. have recently demonstrated the ability to examine 4002 proteins in the yeast proteome in a 1 hr bottom-up analysis.[11] While this feat is impressive, an organism's proteome is exponentially more complex if post-translational modifications and the resulting proteoforms are to be interrogated.[14-16] Kelleher et al. have demonstrated the ability to use multidimensional chromatography and top-down analysis to discover more than 5,000 human mitochondrial proteoforms.[17]

While there are a myriad of PTMs that contribute to proteoform complexity, acidic PTMs such as phosphorylation and sulfation are of particular importance. Phosphorylation contributes to disease states[18], enzyme activity[19], and cellular signaling cascades.[20, 21] Protein sulfation influences, e.g. thrombin clotting inhibition[22, 23] and the viral recognition and injection of HIV.[24] The addition of these acidic PTMs decreases the pI of the peptide/protein due to the highly acidic nature of the added sulfonate or phosphate group. In a typical proteomic workflow, low pH mobile phases and positive ion mode ionization are utilized to generate gas-phase analyte. While this approach has been effective for the analysis of phosphopeptides, laborious enrichment of the phosphorylated peptides is typically needed in order to increase effective phosphopeptide concentration and to

decrease ion suppression from higher pI, more hydrophobic unmodified peptides.[10, 25] The analysis of sulfated peptides in positive ion mode is exceedingly difficult due to the facile elimination of the SO_3 modification in a proton rich environment.[26-29] Thus, for the analysis of the sulfoproteome, the use of negative ion mode nanoelectrospray (nESI) is necessary to couple with high resolution nanoflow liquid chromatography (nLC) peptide separations.

The use of negative ion nLC-MS for proteomic analysis has been examined in a handful of studies. Brodbelt et al. and Coon et al. demonstrated the utility of negative ion mode to discover unique peptides not found in positive ion mode.[30-32] It is predicted that the human proteome pI is bimodially distributed.[33] By examining the proteome in negative ion mode, deeper proteomic profiling of the acidic proteome can occur.[31, 32, 34] In order to improve analyte deprotonation and negative ion generation, mobile phase pHs are often increased anywhere from 8-11.5.[27, 31, 34] While the increase in pH is intuitive to promote analyte deprotonation, previous studies have suggested that addition of acidic mobile phase modifiers can also improve anion generation.[35] Notably, previous anion proteomic studies have not included acidic PTMs in the proteome wide searches.[31, 34] Due to the acidic nature of phosphorylation and sulfation, we hypothesize that would peptides carrying such modifications are more abundant and efficiently discovered in negative ion mode LC-MS analysis compared with conventional positive ion mode LC-MS.

Here, we determine the optimal mobile phase pH and nESI polarity for the detection of phospho- and sulfopeptides in a complex mixture of tryptically digested proteins. A complex mixture of tryptic peptides were examined as a function of mobile phase pH and detection polarity. Phosphorylated and sulfated acidic peptides are examined to optimize detection efficiency for these modified peptides. This study systematically demonstrates the utility of high pH negative ion mode nLC-MS proteomics for large-scale acidic PTM analysis.

3.2 Experimental

3.2.1 Chemicals

Water, methanol, 2,2,2-trifluoroethanol (TFE), ammonium bicarbonate, 48% hydrofluoric acid (HF), and formic acid (FA) were purchased from Fisher Scientific (Pittsburgh, PA). Bovine serum albumin (BSA), α-S1-casein (70%), β-casein, cytochrome C (CytC), lactotransferrin (LactoT), 5 M ammonium hydroxide, triethylamine (TEA), triethanolamine (TEOA), and dithiothreitol

obtained from Sigma-Aldrich (St. Louis, MO). Sulfated cholecystokinin [DsYMGWMDF] (CCKS) caerulein [pEQDsYTGWMDF] were purchased from Bachem (Bubendorf, Switzerland). Modified sequencing grade trypsin was obtained from Promega (Madison, WI). Water and MeOH were HPLC grade. All compounds were used as purchased.

3.2.2 Nanoflow Liquid Chromatography/Mass Spectrometry

BSA, α-s1-casein, β-casein, LactoT, and CytC were mixed at 75 µM each. This mixture was subjected to reduction, alkylation, and tryptic digestion at a 1:100 protease:protein ratio. Sulfopeptides were spiked into the resulting tryptic peptides at a 1:5 sulfopeptide:tryptic peptide ratio. High pH tolerant trap and analytical columns were slurry packed with Waters Xbridge C18, 5 µm particles as previously described.[30, 36] Trap column and analytical column dimensions were 75 µm i.d. x 5 cm and 75 µm i.d. x 20 cm, respectively. Fused silica nESI emitters were pulled on a Sutter Instruments P-2000 laser micropipette puller and HF etched as previously described to approximately 4-6 µm tip i.d.[37] Mobile phase solvent A (97.0% H_2O, 2.8% MeOH, 0.2% TFE) and B (2.8% H_2O, 97.0% MeOH, 0.2%TFE) were buffered with 0.2% TEA for pH 11 and 9, 0.2% TEOA for pH 7 and 5, and 0.1% FA for pH 3 solutions.[38] FA and NH_4OH were used to modify mobile phase pHs. Sample loading was completed at 2 µL/min, placing a total of 200 fmol of each tryptically digested protein and 40 fmol of each sulfopeptide on column. Gradient elution was completed at 250 nL/min with the following gradient: 2–75% B; 0–85 min: 75–95% B; 85–105 min. All mass spectra were collected at 1M data points on a Bruker 7 T SolariX Fourier transform ion cyclotron resonance mass spectrometer with 0.1 s ion accumulation time. Nanospray voltage was held at ± 1.25 kV and the drying gas temperature was set to 150˚C. Mass spectra were externally calibrated to < 2 ppm error in both positive and negative ion mode. Following triplicate data collection, observed peptides were assigned using Bruker DataAnalysis 4.4 and BioTools 3.2. Peptides were only assigned if error was < 10 ppm. Alkylation of cysteine was set as a fixed modification. Variable modifications were set at two missed tryptic cleavages, and methionine oxidation. Peptide pIs were calculated via ExPASy's "Compute pI/MW" tool (www.expasy.org). Grand average of hydropathy (GRAVY) peptide scores were calculated via an on-line tool (www.gravy-calculator.de).[39] Only peptides that were found in at least 2 out of 3 replicates were utilized for pI and GRAVY analysis.

3.3 Results and Discussion

3.3.1 Total Protein Sequence Coverages as a Function of pH and nESI Polarity

A total of six proteins were tryptically digested and analyzed under a variety of mobile phase pHs and with both polarities. Figure 3.1 summarizes the protein sequence coverages observed. In general, sequence coverage is similar for each protein regardless of the mobile phase pH and detection polarity with some notable exceptions for the phosphorylated and acidic proteins α-S1-casein, β-casein, and BSA. α-S1-casein and β-casein exhibit sequence coverage increases of 18% and 16%, respectfully, at pH 11 in negative ion mode. The increase for α-S1-casein is due to the detection of the following peptides at pH 11 in negative ion mode; QFYQLDAYPSGAWYYVPLGTQYTDAPSFSDIPNPIGSENSEK (pI = 3.77) and DIGpSEpSTEDQAMEDIK (pI < 3.71). β-casein's coverage increase at pH 11 in negative ion mode is due to the highly phosphorylated peptide ELEELNVPGEIVEpSLpSpSpSEESITR (pI << 3.83). All of these peptides are highly acidic in nature and two are multiply phosphorylated. The increased mobile phase pH of coupled with negative ion mode detection promotes detection of these acidic peptides in a complex sample.
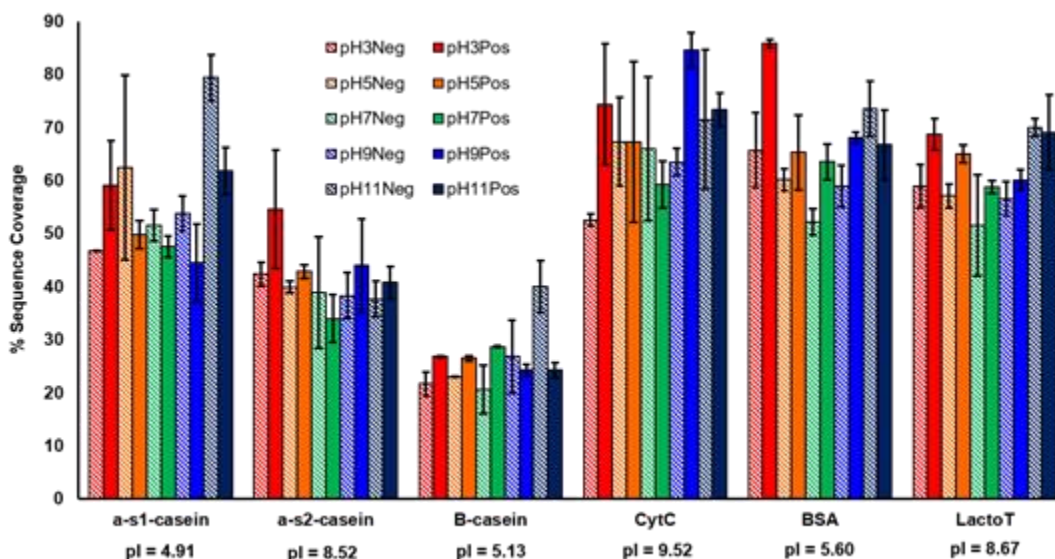
Figure 3.1: Summarized protein sequence coverages for triplicate LC-MS analysis of a 6 protein tryptic digest. Sequence coverage observed for the proteins examined are widely similar regardless of detection polarity and mobile phase pH.

Interestingly BSA, an acidic protein, shows the highest sequenced (~85%) at pH 3 in positive ion mode. This observation is likely due to more effective separation of peptides at low pH versus high

pH. As seen in Figure 3.2, the majority of peptides in the pH 3 base peak chromatogram (BPC) elute in an 80 min window, whereas at pH 11, they elute in a 65 min window. By increasing the separation efficiency at low pH, even acidic peptides can be effectively ionized, as previously demonstrated with multidimensional protein identification technology (MudPIT).[40] The decreased separation efficiency at pH 11 is likely due to the utilization of the nESI MS friendly mobile phase buffering agent, TEA. At pH 3, the FA carboxylate group acts as a weak ion-pairing agent whereas, at pH 11, the relatively hydrophobic protonated TEA can act as a peptide ion paring agent, resulting in an increase of peptide retention times on the reversed phase nLC column.
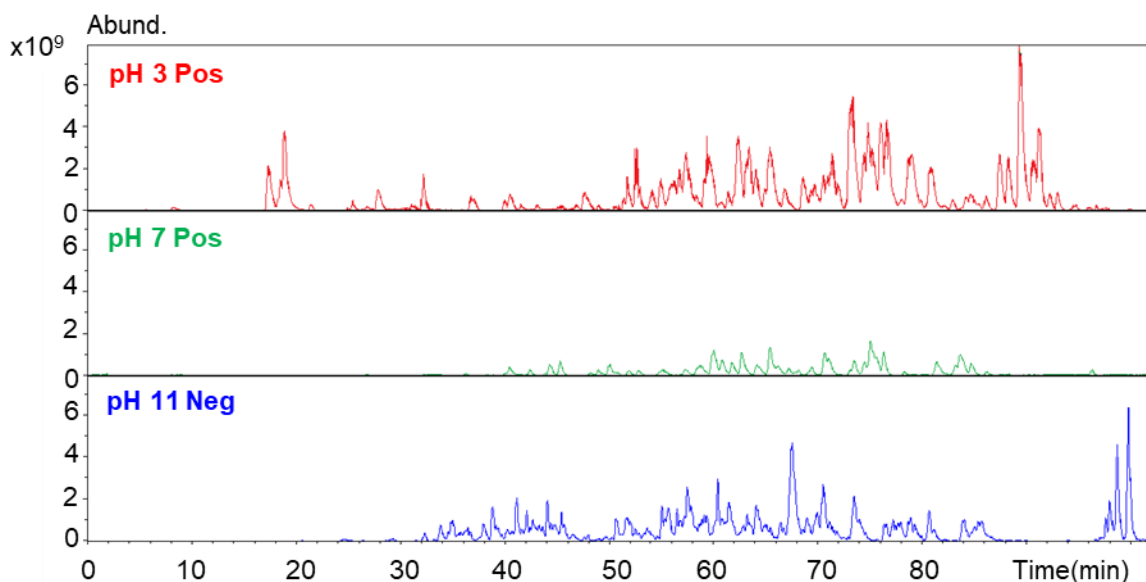
Figure 3.2: Example BPCs of pH 3 (Top), pH 7 (Middle), and pH 11 (Bottom) peptide elutions. Peptides are most effectively separated and detected at the pH extremes. The pH 7 elution exhibits ~70% lower abundance due to ineffective peptide charging in positive or negative ion mode.

For all proteins in this study, regardless of polarity utilized, minimum sequence coverage is observed at pH 7. This decrease is likely associated with the reduction of peptide elution window to 50 min (Figure 3.2). Also the BPC ion abundance is approximately 70% lower at pH 7 compared with both pH 3 and pH 11. These results are likely due to the lack of overall peptide charge at pH 7. At pH 7, both positive and negative charges will be present on the majority of peptides at various residues and N-/C-termini, resulting in a low negative or positive effective charge. This results in more hydrophobic peptides and later elution times due to a lack of charging.[41] The lack of overall solution peptide charging and reduction of the peptide elution window makes the generation of peptide ions without significant ion suppression challenging when utilizing nESI.

3.3.2 Comparison of Unmodified Peptides Detected at Different pH Values and Polarities

In order to examine any potential peptide sampling bias, the retention time (Rt) observed for unmodified peptides was plotted as a function of peptide pI and GRAVY score (Figure 3.3). Upon examination of the Rt vs pI plots, no apparent pI bias/correlation was observed. Overall, the average pI of detected unmodified peptides at pH 3 in positive ion mode was 6.34 while, in negative ion mode at pH 11, the average pI of the detected peptides was 6.29. Also the GRAVY score correlation is almost identical for these two contrasting analyses.
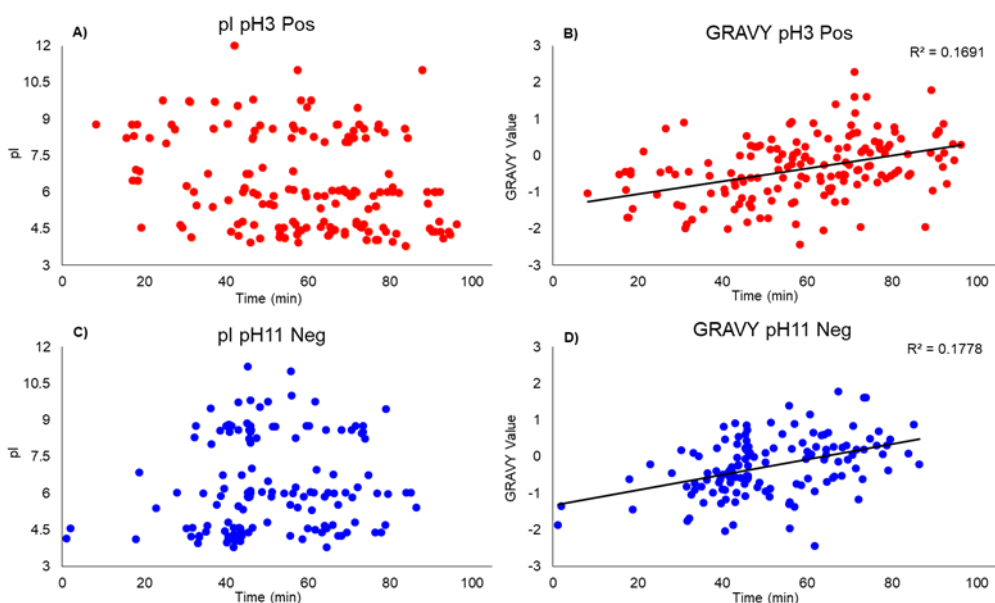
Figure 3.3: Summary peptide pI (A and C) and GRAVY scores (B and D) correlated with peptide retention time for unmodified peptides. Average peptide pI values and GRAVY correlations for contrasting detection modes and elution mobile phases were almost identical.

Next, we examined the impact of nESI polarity on the amount of peptides found at identical mobile phase pH (Figure 3.4). At pH 3, only five unique peptides out of 189 peptides were found in negative ion mode. At pH 7 the number of unique peptides observed in negative ion mode slightly increased to 11 and, at pH 11, an impressive 51 peptides were unique to negative ion mode. When comparing pH 3 positive ion mode analysis to pH 11 negative ion mode analysis, a 12% increase in peptide IDs was noted with negative ion mode detection at pH 11. However, surprisingly, the unique unmodified peptides identified from the negative ion mode pH 11 analysis had an average pI of 6.32 with the average pI of unique identified peptides from the positive ion mode pH 3
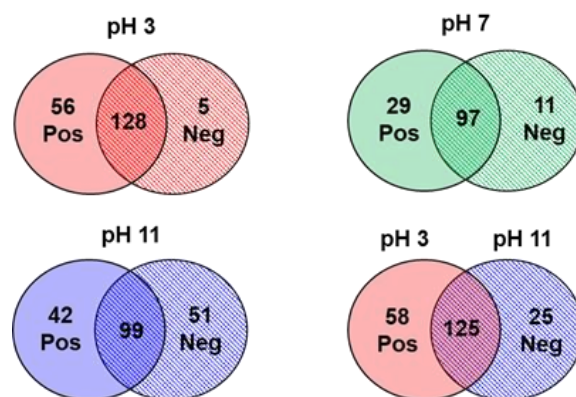
Figure 3.4: Summary of unmodified peptides detected with various nESI polarities and mobile phase pHs. Comparing pH 3 positive ion mode to pH 11 negative ion mode, ~12% of unique peptide IDs are due to negative ion mode analysis.

experiments being 6.46. The lack of peptide pI bias suggests the separation at high and low pH was sufficient for the sampling of most peptides in the six protein digest. The unique peptides identified were likely identified due to the semi-orthogonal nature of high- and low-pH C18 separations, allowing for separation and subsequent effective negative ion mode ionization at pH 11 of previously suppressed peptides.[42] Due to effective separation of peptides with greatly varying pI values, nESI, regardless of polarity could ionize a majority of eluting peptides without significant ion suppression of high or low pI peptides in this moderately complex sample. While trypsin fixes a positively charged amino acid to every cleaved peptide other proteases, i.e. Asp-N and Glu-C, may reduce overall peptide pI. Previous studies have determined trypsin, due to its high specificity and activity are ideal for large negative ion mode proteomic analysis despite the fixed positive charge.[31] Peptide pI values were not reported for unique negative ion mode identifications in this previous study, necessitating further study for comparison.

3.3.3 Optimized Detection of Acidic, Modified Peptides

While the identified unmodified peptides do not appear to exhibit any bias for detection polarity, acidically modified peptides are detected most efficiently at pH 11 in negative ion mode. The singly phosphorylated peptide VPQLEIVPNpSAEER is detected most efficiently with pH 3 and pH 11 negative ion mode ionization (Figure 3.5A). As seen in Figure 3.5B, the multiply phosphorylated peptide ELEELNVPGEIVEpSLpSpSpSEESITR is only detected in negative ion mode at pH 11. The addition of a single phosphorylation event to a peptide lowers the sidechain pKa of S,T,and Y by approximately 9, effectively adding a negative charge to the modified

residues.[43] As more phosphorylation events occur on a single peptide, the average pI of the peptide greatly decreases and the probability of the peptide to be deprotonated in solution increases accordingly, even at low pH. By switching from the standard pH 3 positive ion nESI approach to pH 11 negative ion mode analysis, the inherent negative charge of a highly phosphorylated peptide can be leveraged for efficient detection.
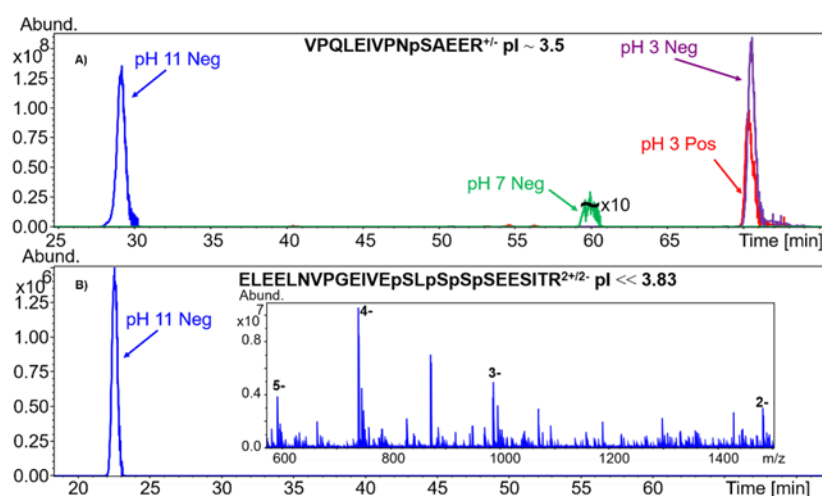
Figure 3.5: Example extracted ion chromatograms of a singly (**A**) and multiply (**B**) phosphorylated peptide. The singly phosphorylated peptide is efficiently detected at both pH extremes. The multiply phosphorylated peptide is only detected at pH 11 with negative ion mode ionization. The inset spectrum demonstrates the high charge states observed for the highly modified peptide.
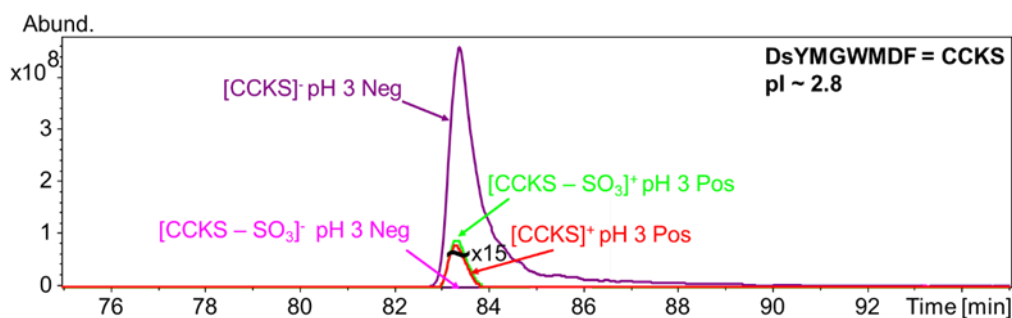
Figure 3.6: Example extracted ion chromatogram of the sulfopeptide CCKS from positive ion and negative ion mode analysis at pH 3. Approximately 55% of the sulfonate modification is lost in positive ion mode. By simply switching the detection polarity, CCKS is detected at 55x higher abundance.

Sulfated peptides undergo proton mediated elimination of the sulfonate in positive ion mode analysis. The degree of sulfonate loss depends on the ion source and ion transport conditions, for our relatively "soft" ion source amounting to ~55% sulfonate loss (Figure 3.6). Negative ion mode

48

nESI inherently reduces the proton mobility of the gas-phase peptides, eliminating the loss of the sulfate PTM. By increasing the pH of the mobile phase and employing negative ion mode detection, the highly acidic sulfate moiety can be leveraged. At pH 11 detection of CCKS and caerulein is 3x and 8x more sensitive, respectively, as compared to detection at pH 3 (Figure 3.7). Overall, utilization of negative ion mode nESI coupled with high pH separations, allows highly acidic, modified peptides to be detected most effectively in a complex mixture of tryptic peptides.
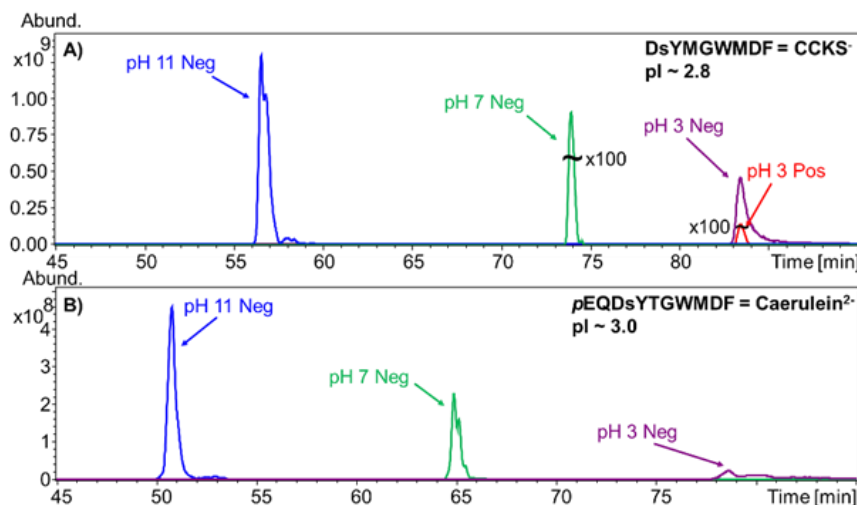
Figure 3.7: Extracted ion chromatograms of the sulfopeptides CCKS (A) and caerulein (B) at three elution pHs in both positive and negative mode. The sulfopeptides CCKS and caerulein are detected at 3x and 8x higher ion abundance respectfully in negative ion mode at high pH. Caerulein is not detected at all in positive ion mode.

3.4 Conclusions

Protein sequence coverage for tryptically digested proteins was mostly consistent across all detection polarities and mobile phases used. Peptides were separated most efficiently at the pH 3 and pH 11 extremes examined. By increasing mobile phase pH to 11 and altering nESI polarity to negative ion mode, highly phosphorylated and sulfated peptides can be detected most effectively without modification loss. Future work includes the analysis of phospho- and sulfoproteomes from standard HeLa cells in both low pH positive ion mode and high pH negative ion mode, as well as implementation of negative ion tandem mass spectrometry strategies, such as ultraviolet photodissociation, activated ion negative electron transfer dissociation, or negative ion electron capture dissociation..

3.5 References

1. Picotti, P., Bodenmiller, B., Mueller, L. N., Domon, B., and Aebersold, R. (2009) Full Dynamic Range Proteome Analysis of S. cerevisiae by Targeted Proteomics, *Cell 138*, 795-806.
2. Kim, M. S., Pinto, S. M., Getnet, D., Nirujogi, R. S., Manda, S. S., Chaerkady, R., Madugundu, A. K., Kelkar, D. S., Isserlin, R., Jain, S., Thomas, J. K., Muthusamy, B., Leal-Rojas, P., Kumar, P., Sahasrabuddhe, N. A., Balakrishnan, L., Advani, J., George, B., Renuse, S., Selvan, L. D., Patil, A. H., Nanjappa, V., Radhakrishnan, A., Prasad, S., Subbannayya, T., Raju, R., Kumar, M., Sreenivasamurthy, S. K., Marimuthu, A., Sathe, G. J., Chavan, S., Datta, K. K., Subbannayya, Y., Sahu, A., Yelamanchi, S. D., Jayaram, S., Rajagopalan, P., Sharma, J., Murthy, K. R., Syed, N., Goel, R., Khan, A. A., Ahmad, S., Dey, G., Mudgal, K., Chatterjee, A., Huang, T. C., Zhong, J., Wu, X., Shaw, P. G., Freed, D., Zahari, M. S., Mukherjee, K. K., Shankar, S., Mahadevan, A., Lam, H., Mitchell, C. J., Shankar, S. K., Satishchandra, P., Schroeder, J. T., Sirdeshmukh, R., Maitra, A., Leach, S. D., Drake, C. G., Halushka, M. K., Prasad, T. S., Hruban, R. H., Kerr, C. L., Bader, G. D., Iacobuzio-Donahue, C. A., Gowda, H., and Pandey, A. (2014) A draft map of the human proteome, *Nature 509*, 575-581.
3. Altelaar, A. F. M., Munoz, J., and Heck, A. J. R. (2013) Next-generation proteomics: towards an integrative view of proteome dynamics, *Nat. Rev. Genet. 14*, 35-48.
4. Breker, M., and Schuldiner, M. (2014) The emergence of proteome-wide technologies: systematic analysis of proteins comes of age, *Nat. Rev. Mol. Cell Biol. 15*, 453-464.
5. Aebersold, R., and Mann, M. (2016) Mass-spectrometric exploration of proteome structure and function, *Nature 537*, 347-355.
6. Liu, T., Qian, W. J., Gritsenko, M. A., Camp, D. G., Monroe, M. E., Moore, R. J., and Smith, R. D. (2005) Human plasma N-glycoproteome analysis by immunoaffinity subtraction, hydrazide chemistry, and mass spectrometry, *J. Proteome Res. 4*, 2070-2080.
7. Meinnel, T., and Giglione, C. (2008) Protein lipidation meets proteomics, *Front. Biosci. 13*, 6326-6340.
8. Witze, E. S., Old, W. M., Resing, K. A., and Ahn, N. G. (2007) Mapping protein post-translational modifications with mass spectrometry, *Nat. Methods 4*, 798-806.
9. Choudhary, C., Weinert, B. T., Nishida, Y., Verdin, E., and Mann, M. (2014) The growing landscape of lysine acetylation links metabolism and cell signalling, *Nat. Rev. Mol. Cell Biol. 15*, 536-550.
10. Riley, N. M., and Coon, J. J. (2016) Phosphoproteomics in the Age of Rapid and Deep Proteome Profiling, *Anal. Chem. 88*, 74-94.
11. Richards, A. L., Hebert, A. S., Ulbrich, A., Bailey, D. J., Coughlin, E. E., Westphall, M. S., and Coon, J. J. (2015) One-hour proteome analysis in yeast, *Nat. Protoc. 10*, 701-714.
12. Nagaraj, N., Alexander Kulak, N., Cox, J., Neuhauser, N., Mayr, K., Hoerning, O., Vorm, O., and Mann, M. (2012) System-wide Perturbation Analysis with Nearly Complete Coverage of the Yeast Proteome by Single-shot Ultra HPLC Runs on a Bench Top Orbitrap, *Mol. Cell. Proteomics 11*.
13. Aebersold, R., and Mann, M. (2003) Mass spectrometry-based proteomics, *Nature 422*, 198-207.
14. Chait, B. T. (2006) Mass Spectrometry: Bottom-Up or Top-Down?, *Science 314*, 65-66.

15. Zhao, Y., Sun, L., Zhu, G., and Dovichi, N. J. (2016) Coupling Capillary Zone Electrophoresis to a Q Exactive HF Mass Spectrometer for Top-down Proteomics: 580 Proteoform Identifications from Yeast, *J. Proteome Res. 15*, 3679-3685.

16. Tran, J. C., Zamdborg, L., Ahlf, D. R., Lee, J. E., Catherman, A. D., Durbin, K. R., Tipton, J. D., Vellaichamy, A., Kellie, J. F., Li, M., Wu, C., Sweet, S. M. M., Early, B. P., Siuti, N., LeDuc, R. D., Compton, P. D., Thomas, P. M., and Kelleher, N. L. (2011) Mapping intact protein isoforms in discovery mode using top-down proteomics, *Nature 480*, 254-258.

17. Catherman, A. D., Li, M., Tran, J. C., Durbin, K. R., Compton, P. D., Early, B. P., Thomas, P. M., and Kelleher, N. L. (2013) Top Down Proteomics of Human Membrane Proteins from Enriched Mitochondrial Fractions, *Anal. Chem. 85*, 1880-1888.

18. Thorner, J., Hunter, T., Cantley, L. C., and Sever, R. (2014) Signal Transduction: From the Atomic Age to the Post-Genomic Era, *Cold Spring Harbor Perspect. Biol. 6*.

19. Moorhead, Greg B. G., De Wever, V., Templeton, G., and Kerk, D. (2009) Evolution of protein phosphatases in plants and animals, *Biochem. J. 417*, 401-409.

20. Turjanski, A. G., Vaque, J. P., and Gutkind, J. S. (2007) MAP kinases and the control of nuclear events, *Oncogene 26*, 3240-3253.

21. Cohen, P. (2002) Protein kinases - the major drug targets of the twenty-first century?, *Nat. Rev. Drug Discov. 1*, 309-315.

22. Michnick, D. A., Pittman, D. D., Wise, R. J., and Kaufman, R. J. (1994) Identification of individual tyrosine sulfation sites within factor VIII required for optimal activity and efficient thrombin cleavage, *J. Biol. Chem. 269*, 20095-20102.

23. Hortin, G. (1990) Sulfation of tyrosine residues in coagulation factor V, *Blood 76*, 946-952.

24. Farzan, M., Mirzabekov, T., Kolchinsky, P., Wyatt, R., Cayabyab, M., Gerard, N. P., Gerard, C., Sodroski, J., and Choe, H. (1999) Tyrosine Sulfation of the Amino Terminus of CCR5 Facilitates HIV-1 Entry, *Cell 96*, 667-676.

25. Kweon, H. K., and Håkansson, K. (2006) Selective Zirconium Dioxide-Based Enrichment of Phosphorylated Peptides for Mass Spectrometric Analysis, *Anal. Chem. 78*, 1743-1749.

26. Hersberger, K. E., and Håkansson, K. (2012) Characterization of O-Sulfopeptides by Negative Ion Mode Tandem Mass Spectrometry: Superior Performance of Negative Ion Electron Capture Dissociation, *Anal. Chem. 84*, 6370-6377.

27. Robinson, M. R., and Brodbelt, J. S. (2016) Integrating Weak Anion Exchange and Ultraviolet Photodissociation Mass Spectrometry with Strategic Modulation of Peptide Basicity for the Enrichment of Sulfopeptides, *Anal. Chem. 88*, 11037-11045.

28. Seibert, C., and Sakmar, T. P. (2008) Toward a framework for sulfoproteomics: Synthesis and characterization of sulfotyrosine-containing peptides, *Biopolymers 90*, 459-477.

29. Yagami, T., Kitagawa, K., Aida, C., Fujiwara, H., and Futaki, S. (2000) Stabilization of a tyrosine O-sulfate residue by a cationic functional group: formation of a conjugate acid-base pair, *J. Peptide Res. 56*, 239-249.

30. McAlister, G. C., Russell, J. D., Rumachik, N. G., Hebert, A. S., Syka, J. E., Geer, L. Y., Westphall, M. S., Pagliarini, D. J., and Coon, J. J. (2012) Analysis of the acidic proteome with negative electron-transfer dissociation mass spectrometry, *Anal. Chem. 84*, 2875-2882.

31. Riley, N. M., Rush, M. J. P., Rose, C. M., Richards, A. L., Kwiecien, N. W., Bailey, D. J., Hebert, A. S., Westphall, M. S., and Coon, J. J. (2015) The Negative Mode Proteome with Activated Ion Negative Electron Transfer Dissociation (AI-NETD), *Mol. Cell. Proteomics 14*, 2644-2660.

32. Madsen, J. A., Xu, H., Robinson, M. R., Horton, A. P., Shaw, J. B., Giles, D. K., Kaoud, T. S., Dalby, K. N., Trent, M. S., and Brodbelt, J. S. (2013) High-throughput Database Search and Large-scale Negative Polarity Liquid Chromatography–Tandem Mass Spectrometry with Ultraviolet Photodissociation for Complex Proteomic Samples, *Mol. Cell. Proteomics 12*, 2604-2614.

33. Wu, S., Wan, P., Li, J., Li, D., Zhu, Y., and He, F. (2006) Multi-modality of pI distribution in whole proteome, *Proteomics 6*, 449-455.

34. Robinson, M. R., Taliaferro, J. M., Dalby, K. N., and Brodbelt, J. S. (2016) 193 nm Ultraviolet Photodissociation Mass Spectrometry for Phosphopeptide Characterization in the Positive and Negative Ion Modes, *J. Proteome Res. 15*, 2739-2748.

35. Wu, Z., Gao, W., Phelps, M. A., Wu, D., Miller, D. D., and Dalton, J. T. (2004) Favorable Effects of Weak Acids on Negative-Ion Electrospray Ionization Mass Spectrometry, *Anal. Chem. 76*, 839-847.

36. Mellors, J. S., and Jorgenson, J. W. (2004) Use of 1.5-μm Porous Ethyl-Bridged Hybrid Particles as a Stationary-Phase Support for Reversed-Phase Ultrahigh-Pressure Liquid Chromatography, *Anal. Chem. 76*, 5441-5450.

37. Valaskovic, G. A., Kelleher, N. L., Little, D. P., Aaserud, D. J., and McLafferty, F. W. (1995) Attomole-Sensitivity Electrospray Source for Large-Molecule Mass Spectrometry, *Anal. Chem. 67*, 3802-3805.

38. McClory, P. J., and Hakansson, K. (2017) Corona Discharge Suppression in Negative Ion Mode Nanoelectrospray Ionization via Trifluoroethanol Addition, *Anal. Chem. Submitted*.

39. Kyte, J., and Doolittle, R. F. (1982) A simple method for displaying the hydropathic character of a protein, *J. Mol. Biol. 157*, 105-132.

40. Washburn, M. P., Wolters, D., and Yates, J. R. (2001) Large-scale analysis of the yeast proteome by multidimensional protein identification technology, *Nat. Biotech. 19*, 242-247.

41. Gilar, M., Olivova, P., Daly, A. E., and Gebler, J. C. (2005) Two-dimensional separation of peptides using RP-RP-HPLC system with different pH in first and second separation dimensions, *J. Sep. Sci. 28*, 1694-1703.

42. Gilar, M., Olivova, P., Daly, A. E., and Gebler, J. C. (2005) Orthogonality of Separation in Two-Dimensional Liquid Chromatography, *Anal. Chem. 77*, 6426-6434.

43. Erb, R., and Oberacher, H. (2014) Comparison of mobile-phase systems commonly applied in liquid chromatography-mass spectrometry of nucleic acids, *Electrophoresis 35*, 1226-1235.

<center>**Chapter 4**</center>

<center>**Alkylamine Ion Pairing Agents for Positive Ion Mode Data-Independent Liquid
Chromatography/Mass Spectrometry Analysis of Sulfated Peptides**</center>

4.1 Introduction

Sulfated peptides and proteins are involved in several important biological processes from viral recognition and infection to thrombin clotting responses.[1, 2] Tyrosine sulfation is significant for protein-protein interactions. Upon sulfation of the chemokine receptor 5 (CCR5), the HIV coat protein gp120 optimally binds to T-cells, allowing for injection of viral material.[3-7] Sulfation is particularly important for blood coagulation. The secreted leech sulfoprotein hirudin binds thrombin, preventing a host's blood from clotting.[8] If hirudin Tyr63 is desulfated, thrombin is bound 10x less effectively and host clotting can prevent the leech from feeding.[8] Also, sulfation at Tyr1680 of the blood coagulation Factor VIII is integral for clotting responses. Mutation of Tyr1680 to Phe results in a moderate form of hemophilia.[9] Previous studies of tyrosylprotein sulfotransferase (TPST) knockout mice indicate developmental abnormalities, reproductive sterility, and death can occur in the absence of protein sulfation.[10-12]

While sulfation is an integral PTM, proteome-wide discovery and detection of sulfopeptides and proteins are difficult even with modern mass spectrometry platforms.[13] In standard proteomics experiments, positive ion mode nanoelectrospray ionization (nESI) is employed, resulting in proton mediated loss of the sulfate PTM.[14, 15] In negative ion mode the sulfate modification is retained, but exotic tandem mass spectrometry (MS/MS) activation techniques such as electron detachment dissociation (EDD), ultraviolet photodissociation (UVPD), negative electron transfer dissociation (NETD), or negative ion electron capture dissociation (niECD) are needed to

<center>53</center>

successfully sequence the peptides without sulfonate loss.[16-18] The discovery of sulfated residues has been examined with negative ion mode collision induced dissociation (CID), but site specific PTM identification and peptide sequencing could not be efficiently completed.[19-21] To further complicate detection and analysis, a phosphorylation event is only 9.5 mDa heavier than a sulfonation event. Only high resolution instruments have been able to unambiguously differentiate sulfonation and phosphorylation events via mass measurement without chemical tagging or purification.[22]

Leary et al. developed a method for the detection of sulfopeptides in positive ion mode utilizing a chemical tagging approach in which all tyrosine residues in a sample proteome are acetylated.[23] Because sulfonate moieties will be lost upon ionization/ion transport or collision induced dissociation (CID), any observed unmodified tyrosine residues were sulfated in the original organism. While this method can successfully discover sulfation events, it involves tedious and incomplete chemical modification, potentially leading to erroneous sulfation event identifications. Sulfotyrosine-specific antibodies have been developed and are highly discriminating against phoshotyrosine residues.[24, 25] However, currently, no large scale sulfoproteome immunoprecipitation analysis has been completed with these antibodies, most likely owing to cost. Brodbelt et al. have recently developed a method for the enrichment of sulfopeptides via weak anion exchange (WAX) separation.[17] By utilizing negative ion UVPD, the first direct evidence of sulfation of Tyr1513 in bovine coagulation factor V was discovered. However, acidic phosphorylated peptides were not explicitly examined as potential contaminants this WAX enrichment and analysis.

Stabilization of the sulfate PTM has been previously achieved using adduction strategies. The addition of mono- and divalent metal cations stabilizes the sulfate moiety in positive ion mode.[18, 26] Metal adducted sulfopeptides can then be successful sequenced with ECD or ETD for site specific sulfate identification.[18, 26] While these approaches can successfully be employed for single peptide sequencing, the metal adduction event is non-specific and would greatly complicate mass spectrometric analysis of complex samples, as most peptides would adduct various stoichiometries of metal ions. The tripeptide KKK has been successfully applied for the retention of sulfation events on glycans.[27, 28] The addition of a lysine containing peptide has been shown to stabilize peptide sulfation events as well, but application of a peptide ion pairing agent

to an on-line chromatographic separation of a complex proteome sample would be challenging and costly.[29] Also, the constant addition of KKK would result in potentially ion suppression in positive ion mode owing to its highly basic nature. Previously, simple alkylamines, e.g. diethylamine (DEA), have been shown to selectively adduct to polysulfonated azodyes, allowing for facile degree of sulfonation determination.[30, 31] These results suggest that small alkylamines should adduct peptide sulfation events selectively. Also, the use of small alkylamines is amenable to commonly used reversed-phase separation and nESI of peptides, potentially providing a rapid method for sulfoproteome analysis without the need for significant instrumental modifications.

Herein, we present a method for selective detection of sulfopeptides utilizing alkylamine adducts. Optimal binding conditions for the abduction of alkylamines to sulfopeptides are examined. A series of standard peptides are examined with seven different, readily available alkylamines. The CID characteristics of adducted sulfopeptides are examined and employed for on-line discovery of sulfopeptides in data-independent (DIA) nanoliquid chromatography tandem mass spectrometry experiments (nLC-MS/MS).

4.2 Experimental

4.2.1 Chemicals

Water, methanol (MeOH), acetonitrile (MeCN), ammonium bicarbonate, 48% hydrofluoric acid (HF), and formic acid (FA) were purchased from Fisher Scientific (Pittsburgh, PA). α-S1-casein (70%), β-casein, 5 M ammonium hydroxide, piperidine (Pipe), diethylamine (DEA), triethylamine (TEA), dipropylamine (DPA), tripropylamine (TPA), dibutylamine (DBA), tributylamine (TBA), dithiothreitol, angiotensin I [DRVYIHPFHL], leucine enkephalin [YGGFL], and cionin [NsYsYGWMDF] were obtained from Sigma-Aldrich (St. Louis, MO). Tyrosine phosphopeptide [TSTEPQpYQPGEN] (pYpep) was purchased from EMD Millipore (Billerica, MA). Insulin receptor 1 [TRDIYETDpYYRK], insulin receptor 3 [TRDIpYETDpYpYRK], and substance P [RPKPQQFFGLM] were purchased from Anaspec Inc. (Fremont, CA). Sulfated cholecystokinin [DsYMGWMDF], caerulein [pEQDsYTGWMDF], and gastrin I [EGPWLEEEEEAsYGWMDF] were purchased from Bachem (Bubendorf, Switzerland). Hirudin [DFEEIPEEsYLQ] was purchased from Advanced ChemTech (Louisville, KY). Modified sequencing grade trypsin was

obtained from Promega (Madison, WI).   Water, MeOH, and MeCN were HPLC grade. All compounds were used as purchased.

4.2.2 Direct Infusion Experiments

All direct infusion experiments were performed using an Advion Triversa Nanomate equipped with a 96 well plate and a chip with 4 µm nozzle i.d. Spray voltage was set at 1.25–1.35 kV in both positive and negative ion mode. All mass spectra were collected at 1M data points on a Bruker 7 T SolariX Fourier transform ion cyclotron resonance mass spectrometer with 0.1 s ion accumulation time. Drying gas was set to 150˚C. Mass spectra were externally calibrated to <2 ppm error in both positive and negative ion mode. The collision cell pressure (as read by an external gauge) was maintained at 6.5×10^{-6} mbar Argon for all experiments. All peptide solutions were made a 0.2 µM concentration in 1:1 water/MeOH.

4.2.3 Nanoflow Liquid Chromatography/Mass Spectrometry

α-casein and β-casein were mixed at 50 µM each. This mixture was subjected to reduction, alkylation, and tryptic digestion at a 1:100 protease:protein ratio. Sulfopeptides were spiked into the resulting tryptic peptides at various sulfopeptide:tryptic peptide ratios. High pH tolerant trap and analytical columns were slurry packed with Waters Xbridge C18, 5 µm particles as previously described.[32, 33] Trap column and analytical column dimensions were 75 µm i.d. x 5 cm and 75 µm i.d. x 20 cm, respectively. Fused silica nESI emitters were pulled on a Sutter Instruments P-2000 laser micropipette puller and HF etched as previously described to approximately 4-6 µm tip i.d.[34] Mobile phase solvents A (95.0% H_2O, 4.8% MeCN, 0.2% TEA) and B (4.8% H_2O, 95.0% MeCN, 0.2% TEA) were buffered to pH 11 and pH 3 with FA and NH_4OH. Sample loading was completed at 2 µL/min on a Proxeon EASY-nLC, placing a total of 250 fmol of each tryptically digested protein on column. Gradient elution was completed at 250 nL/min with the following gradient: 0–42% B; 0–60 min: 42–100% B; 60–65 min. Nanospray voltage was held at - 1.25 kV and the drying gas temperature was set to 150˚C. All chromatographic data were analyzed manually.

4.3 Results and Discussion

4.3.1 Alkylamine Adduct Selectivity and Sensitivity

A series of 11 peptides and eight bases was directly infused via positive ion mode nESI to determine the selectivity of alkylamine adduction to sulfopeptides. As seen in Figure 4.1A, sulfated hirudin [DFEEIPEEsYLQ] is stable at low pH in negative ion mode nESI. However, when the polarity is switched to positive ion mode, ~65% of the sulfate PTM is lost without any added collisional activation (Fig. 4.1B). Upon 4 V of collisional activation ~95% of the sulfate PTM is liberated (data not shown), demonstrating that, as expected in standard positive ion mode analysis, sulfation is highly labile. The addition of ammonium hydroxide to increase solution pH does not significantly alter the
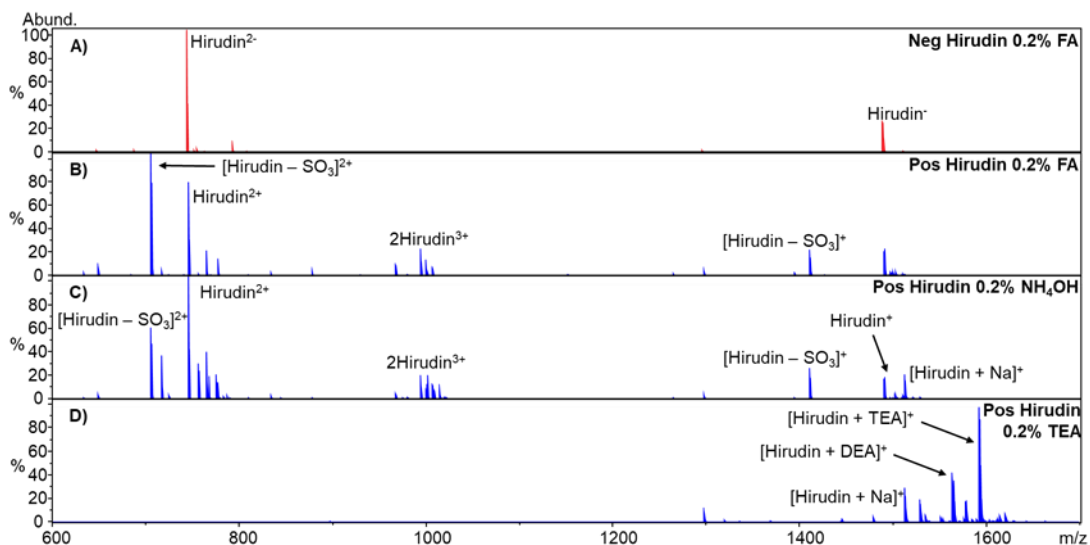
Figure 4.1: Negative ion mode nESI spectrum of sulfated hirudin [DFEEIPEEsYLQ] at low pH (**A**). Positive ion mode nESI spectra of hirudin with formic acid (**B**), ammonium hydroxide (**C**), and TEA (**D**). Successful retention of the sulfate moiety in positive ion mode was only observed with the addition of TEA.

observed positive ion mode mass spectrum (Fig. 4.1C). By contrast, when the triethylamine (TEA) base is added to the peptide solution, a clear sulfopeptide mass shift of 101.120 Da occurs, consistent with a TEA adduct in positive ion mode (Fig. 4.1D). This adduction is highly selective for sulfopeptides (Fig. 4.2). Dipropylamine (DPA) does not adduct to unmodified or phosphotyrosine-containing peptides, but successfully adducts to all sulfopeptides tested. Interestingly, caerulein [pEQDsYTGWMDF] and gastrin I [EGPWLEEEEEAsYGWMDF]

57

adduct multiple alkylamine bases despite only containing one sulfate group. Example spectra of cholecystokinin [DsYMGWMDF] (CCKS) adducted with all alkylamine bases examined are
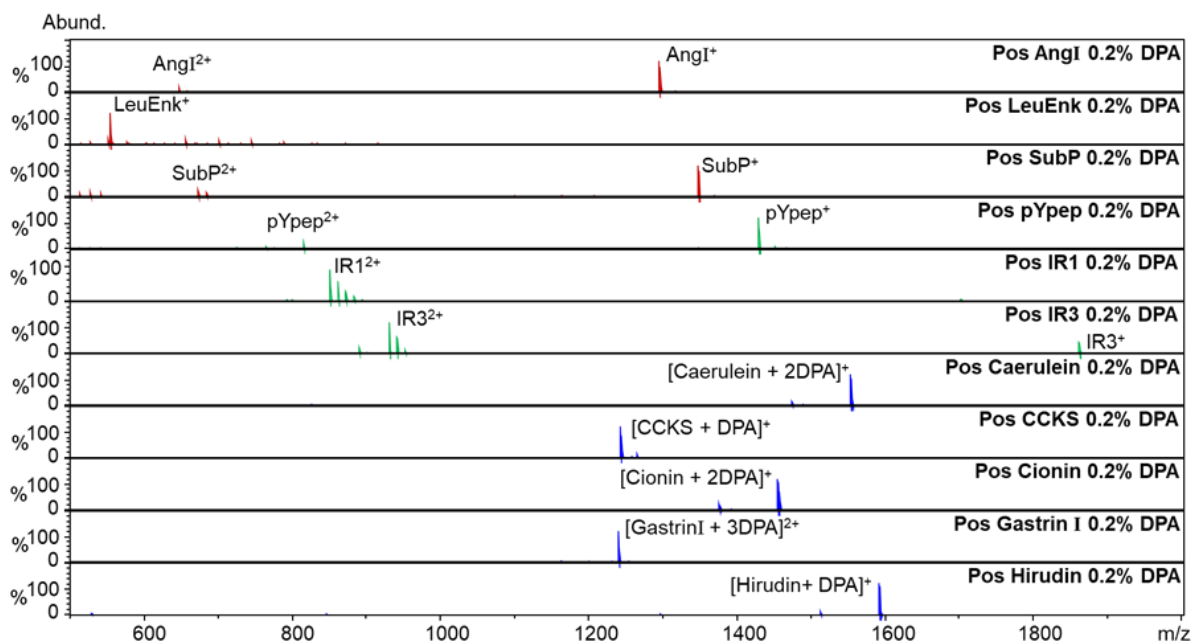
Figure 4.2: Example positive ion mode mass spectra of 11 standard peptides from nESI solvent with 0.2% DPA. Only sulfated peptides successfully adduct the alkylamine.
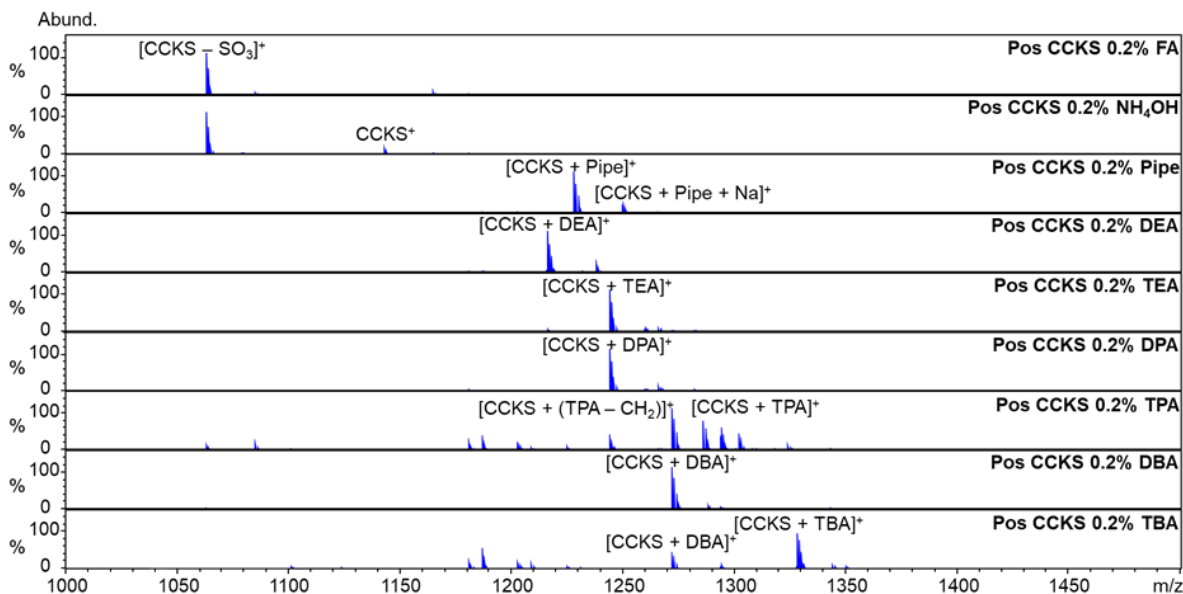
Figure 4.3: Positive ion mode nESI spectra of CCKS [DsYMGWMDF] from solutions at low pH (top) and high pH, resulting from addition of ammonium hydroxide and seven alkylamine bases, respectively. TPA and TBA showed alkylamine contamination, likely due to their only 98% purity compared with the other bases' purity of 99%+.

shown in Figure 4.3. CCKS alkylamine adduction successfully occurs regardless of the acyl chain length and gas-phase basicity of the tested bases. These results suggest a myriad of alkylamine bases can be utilized for future sulfopeptide studies via this adduction approach.
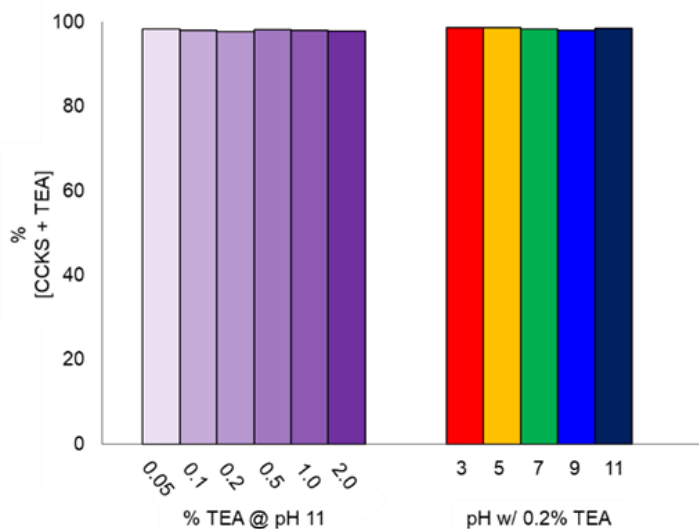
Figure 4.4: Efficiency of TEA adduction to the sulfopeptide (CCKS). Regardless of the TEA concentration or solution pH, 98–99% of CCKS is present in its alkylamine adducted state.

Concentration and pH dependent binding experiments were completed with the alkylamine TEA and the sulfopeptide CCKS (Figure 4.4). From 0.05% (3.6 mM) TEA to 2.0% (143.4 mM) TEA at pH 11–11.5, 98–99% of all CCKS signal is due to alkylamine adducts. With 0.2% TEA, CCKS is adducted at 98–99% efficiency regardless of solution pH. The sensitivity and pH independence of the adducts suggests this phenomenon can be coupled with existing proteomic preparation and separation platforms.

Upon slight (10–15 V collision energy) broadband collisional activation of observed alkylamine-adducted sulfopeptides, a characteristic [SO_3 + alkylamine] neutral loss is observed (see Figure 4.5 for the doubly sulfated peptide cionin). This neutral loss occurs for all sulfopeptide-alkylamine complexes studied and can be used as a diagnostic transition for sulfopeptide flagging. As seen in Figure 5, upon slight collisional activation, the doubly sulfated and TEA adducted cionin [NsYsYGWMDF] undergoes two characteristic neutral losses equivalent to the number of sulfate groups in this peptide. The strict selectivity of alkylamine adduction for strictly the sulfate PTM allows for the facile differentiation of tyrosine phosphorylation and sulfation without chemical or

enzymatic treatment on lower resolution quadrupole, time-of-flight, or ion-trap mass spectrometers.
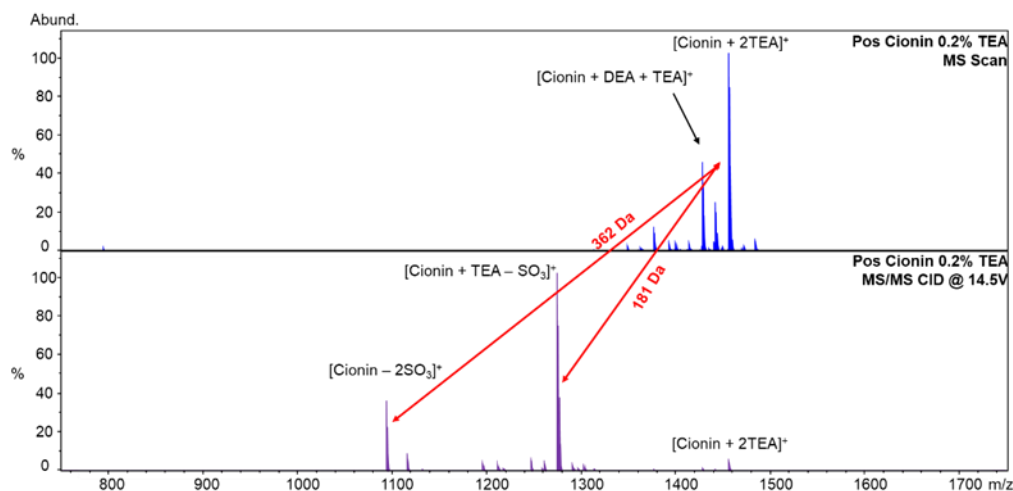
Figure 4.5: Example data-independent collisional activation (15 V) of the TEA-adducted, doubly sulfated peptide cionin [NsYsYGWMDF]. Two dominant neutral losses of [SO_3 + TEA] are observed.

We hypothesize that the alkylamines are interacting directly with the sulfate moiety, preventing proton rearrangement and accompanying facile elimination of the SO_3 group. Under standard positive ion mode nESI conditions, protons are in excess due to the addition of formic or acetic acid.[35, 36] Addition of an alkylamine base to the same solution allows for proton sequestration and ion pair formation with the sulfate group. Thus the alkylamine prevents, proton-mediated elimination of the SO_3 group by limiting the local proton mobility near the PTM (Figure 4.6). As seen in Figure 4.7, as alkylamine gas-phase basicity increases, the collisional energy needed to displace 95% of the adduct increases minimally, indicating that the proton mobility and subsequent SO_3 elimination is being reduced by all bases examined in this study. Similar sulfate stabilization has been reported with alternative charge carriers such as mono- and divalent metals, which are used to displace mobile protons, preventing SO_3 loss.[14, 18, 26] Alkylamines are likely selective for sulfated peptides (pK_a=1.85) compared with phosphorylated peptides (pK_{a1}=2.16, pK_{a2}=7.21) due to decreased proton affinity of the sulfate group.[37] This allows for effective gas-phase proton donation to the alkylamine (pK_a~11), whereas the phosphate group does not as effectively donate its ionizable proton to the base, resulting in weak alkylamine adduction and ion pairing.

60
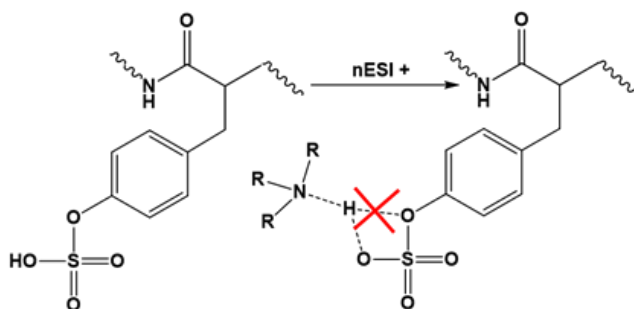
Figure 4.6: Proposed mechanism of alkylamine adduction. Alkylamine ion pairing results in a less mobile proton, thus limiting proton mediated elimination of the sulfate PTM.
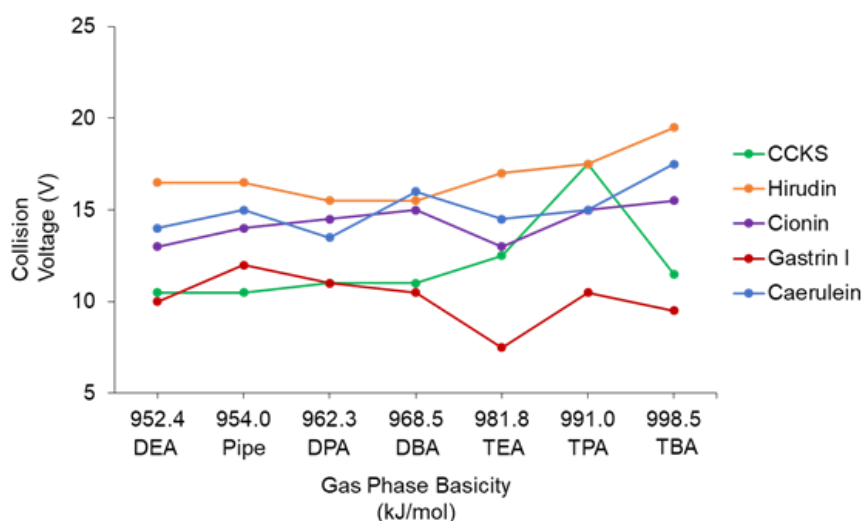
Figure 4.7: Gas-phase basicities as a function of collision voltage needed to dissociate 95% of the alkylamine-sulfopeptide complex.[38] For an increase in gas-phase basicity of 50 kJ/mol across the tested alkylamines, only ~ 1 V increase in required collisional energy is observed.

4.3.2 Positive Ion Mode Online Data-Independent nLC-MS/MS of Peptide Mixtures in the Presence of Alkylamines

A total of four sulfopeptides, were spiked into a phosphoprotein digest at various sulfopeptide:digest ratios. Upon positive ion mode DIA nLC-CID MS/MS of this moderately complex mixture, all four sulfopeptides were successfully discovered based on the [SO_3 + TEA] (181.077 Da) neutral loss transition observed at both pH 3 and pH 11. Example mass spectra from these pH 3 and pH 11 experiments can be seen in Figure 4.8. The phosphopeptide VPQLEIVPNpSAEER is not alkylamine adducted, nor significantly fragmented at 15 V of collision energy. The majority of other 1+ and 2+ peptide ions do not carry TEA adducts, nor fragment significantly at 15 V of activation. Peptide ions with charge greater than 3+ do dissociate

following 15 V DIA activation, but the characteristic [SO₃ + TEA] neutral loss is not observed. The latter mass spectral peaks are not annotated as sulfopeptides due to the lack of this characteristic neutral loss.
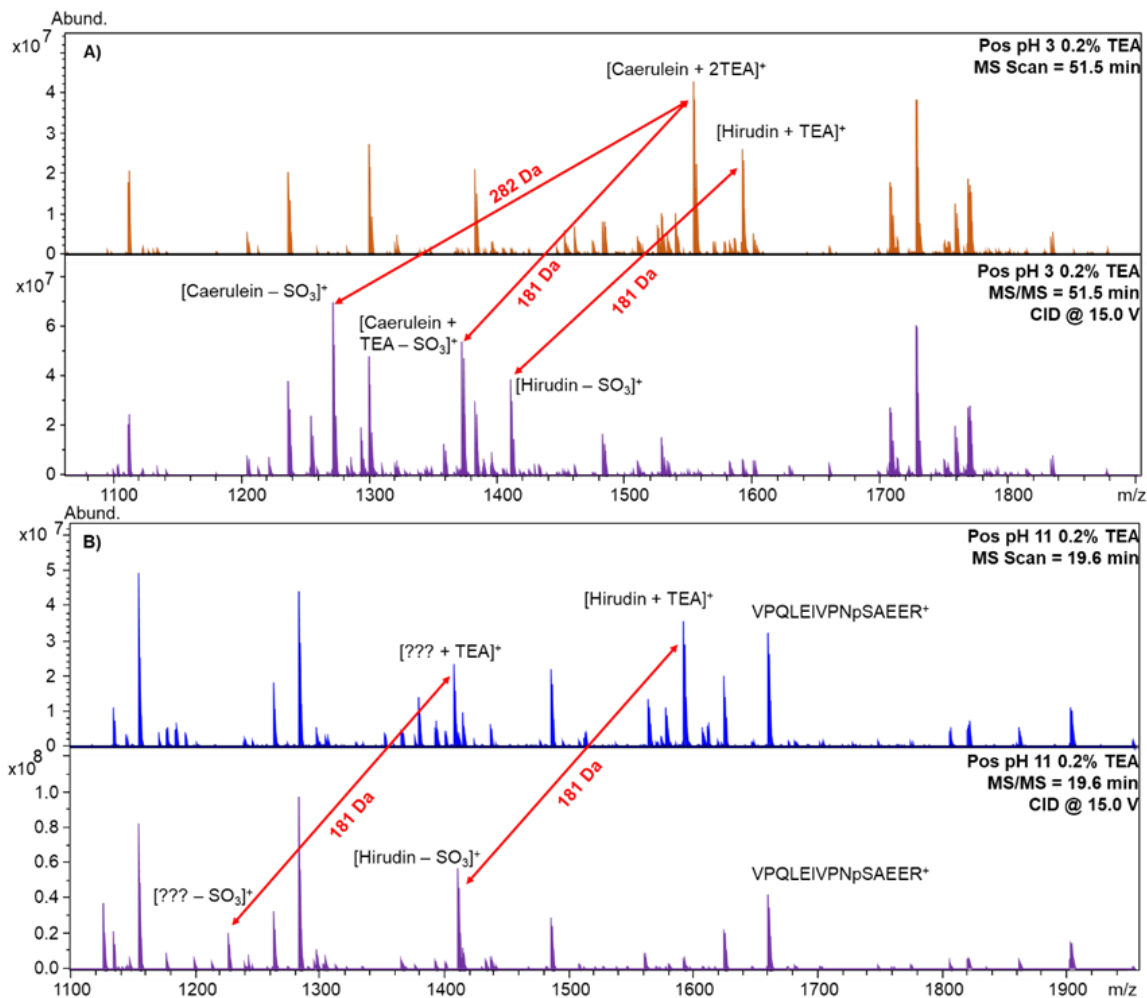
Figure 4.8: Example DIA positive ion mode nLC-MS/MS spectra at pH 3 (**A**) and pH 11 (**B**) separations. In both analyses, sulfopeptides are preferentially fragmented, while unmodified and phosphorylated peptides remain mostly intact upon collisional activation. In the sample pH 11 spectra (**B**), an unidentified peptide has undergone a [SO₃ + TEA] neutral loss, indicating it is a sulfopeptide.

Interestingly, a total of 17 unknown sulfate-containing peptides were discovered across all analyses. These unknown peptides do not match with any [tryptic peptide + TEA] complex or any common degradation products (oxidation, deamidation, desulfation, truncation, etc.) of the standard sulfopeptides. Further experiments are currently being designed for the determination of these unknowns.

The sensitivity of sulfopeptide discovery utilizing alkylamine adducts with DIA nLC-CID MS/MS was examined (Figure 4.9). Under pH 3 elution, all sulfopeptides could be discovered at a 50 fold sulfopeptide dilution factor (500 fmol tryptic peptides: 10 fmol sulfopeptide). With pH 11 mobile phases, all sulfopeptides were found at a 25 fold dilution factor (500 fmol tryptic peptides: 20 fmol sulfopeptide). In both studies, hirudin exhibited unexpected sensitivity at seemingly random dilution ratios. This observation is due to run-to-run carryover artificially inflating the amount of hirudin on column, as confirmed via blank injection (data not shown). Also, under pH 11 conditions, non-linear sensitivity was observed and is likely due to unstable nESI current for some experiments. This initial sensitivity study will be repeated in the future and combined with sulfopeptide enrichment technologies currently under investigation for further improved sensitivity.
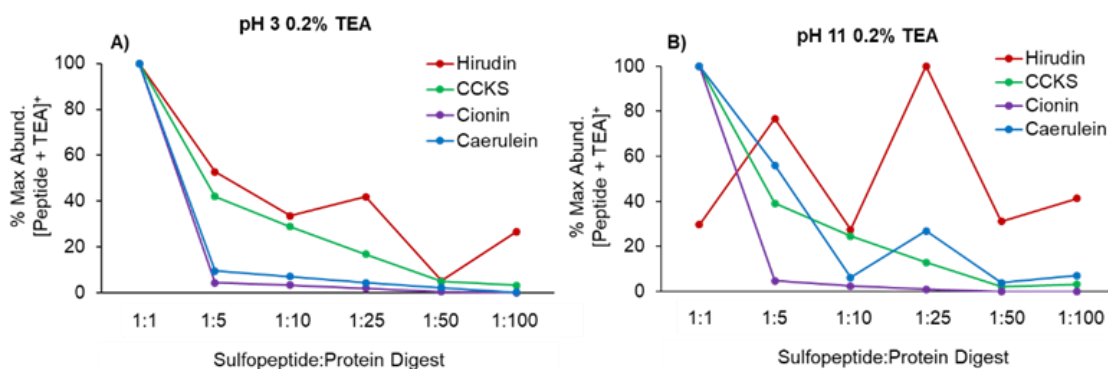
Figure 4.9: Sulfopeptide detection sensitivity observed in a background of tryptic peptides. At both pH 3 and 11 all four sulfopeptides could be discovered at a 50 fold and 25 fold lower amount than background tryptic peptides, respectfully. Hirudin run-to-run carryover is apparent as hirduin was detected most effectively under more dilute conditions. Carryover was confirmed via a blank injection.

4.4 Conclusions

Addition of alkylamine bases to positive ion mode nESI analysis of sulfopeptides results in dramatically increased retention of the sulfate PTM through ion pairing. All seven alkylamine bases examined here successfully formed adducts only with sulfopeptides from 0.05%-2% alkylamine concentration, regardless of solution pH. Upon 15 V collisional activation, a characteristic $[SO_3 + alkylamine]$ neutral loss is observed, and can be utilized for the discovery of sulfated peptides in positive ion mode proteomic workflows. Also, alkylamine adduction is highly selective, allowing for direct differentiation of sulfation and phosphorylation events on low-

resolution mass spectrometers without exotic peptide fragmentation techniques or challenging negative ion mode analysis. Future work includes mechanistic modeling of the gas-phase alkylamine-peptide complexes and direct alkylamine binding location measurement via, e.g. electron capture dissociation (ECD).

4.5 References

1. Moore, K. L. (2003) The biology and enzymology of protein tyrosine O-sulfation, *J. Biol. Chem. 278*, 24243-24246.
2. Kehoe, J. W., and Bertozzi, C. R. (2000) Tyrosine sulfation: a modulator of extracellular protein-protein interactions, *Chem. Biol. 7*, R57-R61.
3. Farzan, M., Mirzabekov, T., Kolchinsky, P., Wyatt, R., Cayabyab, M., Gerard, N. P., Gerard, C., Sodroski, J., and Choe, H. (1999) Tyrosine sulfation of the amino terminus of CCR5 facilitates HIV-1 entry, *Cell 96*, 667-676.
4. Farzan, M., Vasilieva, N., Schnitzler, C. E., Chung, S., Robinson, J., Gerard, N. P., Gerard, C., Choe, H., and Sodroski, J. (2000) A tyrosine-sulfated peptide based on the N terminus of CCR5 interacts with a CD4-enhanced epitope of the HIV-1 gp120 envelope glycoprotein and inhibits HIV-1 entry, *J. Biol. Chem. 275*, 33516-33521.
5. Cormier, E. G., Persuh, M., Thompson, D. A. D., Lin, S. W., Sakmar, T. P., Olson, W. C., and Dragic, T. (2000) Specific interaction of CCR5 amino-terminal domain peptides containing sulfotyrosines with HIV-1 envelope glycoprotein gp120, *Proc. Natl. Acad. Sci. U.S.A. 97*, 5762-5767.
6. Choe, H., Li, W. H., Wright, P. L., Vasilieva, N., Venturi, M., Huang, C. C., Grundner, C., Dorfman, T., Zwick, M. B., Wang, L. P., Rosenberg, E. S., Kwong, P. D., Burton, D. R., Robinson, J. E., Sodroski, J. G., and Farzan, M. (2003) Tyrosine sulfation of human antibodies contributes to recognition of the CCR5 binding region of HIV-1 gp120, *Cell 114*, 161-170.
7. Huang, C. C., Venturi, M., Majeed, S., Moore, M. J., Phogat, S., Zhang, M. Y., Dimitrov, D. S., Hendrickson, W. A., Robinson, J., Sodroski, J., Wyatt, R., Choe, H., Farzan, M., and Kwong, P. D. (2004) Structural basis of tyrosine sulfation and V-H-gene usage in antibodies that recognize the HIV type 1 coreceptor-binding site on gp120, *Proc. Natl. Acad. Sci. U.S.A. 101*, 2706-2711.
8. Stone, S. R., and Hofsteenge, J. (1986) Kinetics of the Inihibition of Thrombin by Hirudin, *Biochemistry 25*, 4622-4628.
9. Leyte, A., Vanschijndel, H. B., Niehrs, C., Huttner, W. B., Verbeet, M. P., Mertens, K., and Vanmourik, J. A. (1991) Sulfation of Tyr1680 of Human Blood-Coagulation Factor-VIII is Essential for the Interaction of Factor-VIII with Von-Willebrand Factor, *J. Biol. Chem. 266*, 740-746.
10. Borghei, A., Ouyang, Y. B., Westmuckett, A. D., Marcello, M. R., Landel, C. P., Evans, J. P., and Moore, K. L. (2006) Targeted disruption of tyrosylprotein sulfotransferase-2, an enzyme that catalyzes post-translational protein tyrosine O-sulfation, causes male infertility, *J. Biol. Chem. 281*, 9423-9431.

11. Ouyang, Y. B., Crawley, J. T. B., Aston, C. E., and Moore, K. L. (2002) Reduced body weight and increased postimplantation fetal death in tyrosylprotein sulfotransferase-1-deficient mice, *J. Biol. Chem. 277*, 23781-23787.

12. Westmuckett, A. D., Hoffhines, A. J., Borghei, A., and Moore, K. L. (2008) Early postnatal pulmonary failure and primary hypothyroidism in mice with combined TPST-1 and TPST-2 deficiency, *Gen. Comp. Endocrinol. 156*, 145-153.

13. Seibert, C., and Sakmar, T. P. (2008) Toward a framework for sulfoproteomics: Synthesis and characterization of sulfotyrosine-containing peptides, *Biopolymers 90*, 459-477.

14. Yagami, T., Kitagawa, K., Aida, C., Fujiwara, H., and Futaki, S. (2000) Stabilization of a tyrosine O-sulfate residue by a cationic functional group: formation of a conjugate acid-base pair, *J. Peptide Res. 56*, 239-249.

15. Škulj, S., and Rožman, M. (2015) Study of the gas-phase fragmentation behaviour of sulfonated peptides, *International Journal of Mass Spectrometry 391*, 11-16.

16. Hersberger, K. E., and Håkansson, K. (2012) Characterization of O-Sulfopeptides by Negative Ion Mode Tandem Mass Spectrometry: Superior Performance of Negative Ion Electron Capture Dissociation, *Anal. Chem. 84*, 6370-6377.

17. Robinson, M. R., and Brodbelt, J. S. (2016) Integrating Weak Anion Exchange and Ultraviolet Photodissociation Mass Spectrometry with Strategic Modulation of Peptide Basicity for the Enrichment of Sulfopeptides, *Anal. Chem. 88*, 11037-11045.

18. Medzihradszky, K. F., Guan, S., Maltby, D. A., and Burlingame, A. L. (2007) Sulfopeptide Fragmentation in Electron-Capture and Electron-Transfer Dissociation, *J. Am. Soc. Mass Spectrom. 18*, 1617-1624.

19. Ewing, N. P., and Cassady, C. J. (2001) Dissociation of multiply charged negative ions for hirudin (54–65), fibrinopeptide B, and insulin A (oxidized), *J. Am. Soc. Mass Spectrom. 12*, 105-116.

20. Edelson-Averbukh, M., Shevchenko, A., Pipkorn, R., and Lehmann, W. D. (2011) Discrimination Between Peptide O-Sulfo- and O-Phosphotyrosine Residues by Negative Ion Mode Electrospray Tandem Mass Spectrometry, *J. Am. Soc. Mass Spectrom. 22*, 2256-2268.

21. Rappsilber, J., Steen, H., and Mann, M. (2001) Labile sulfogroup allows differentiation of sulfotyrosine and phosphotyrosine in peptides, *J. Mass Spectrom. 36*, 832-833.

22. Bossio, R. E., and Marshall, A. G. (2002) Baseline Resolution of Isobaric Phosphorylated and Sulfated Peptides and Nucleotides by Electrospray Ionization FTICR MS: Another Step toward Mass Spectrometry-Based Proteomics, *Anal. Chem. 74*, 1674-1679.

23. Yu, Y. H., Hoffhines, A. J., Moore, K. L., and Leary, J. A. (2007) Determination of the sites of tyrosine O-sulfation in peptides and proteins, *Nat. Meth. 4*, 583-588.

24. Kehoe, J. W., Velappan, N., Walbolt, M., Rasmussen, J., King, D., Lou, J. L., Knopp, K., Pavlik, P., Marks, J. D., Bertozzi, C. R., and Bradbury, A. R. M. (2006) Using phage display to select antibodies recognizing post-translational modifications independently of sequence context, *Mol. Cell. Proteomics 5*, 2350-2363.

25. Hoffhines, A. J., Damoc, E., Bridges, K. G., Leary, J. A., and Moore, K. L. (2006) Detection and Purification of Tyrosine-sulfated Proteins Using a Novel Anti-sulfotyrosine Monoclonal Antibody, *J. Biol. Chem. 281*, 37877-37887.

26. Liu, H., and Håkansson, K. (2006) Electron Capture Dissociation of Tyrosine O-Sulfated Peptides Complexed with Divalent Metal Cations, *Anal. Chem. 78*, 7570-7576.

27. Zhang, Y., Go, E. P., Jiang, H., and Desaire, H. (2005) A Novel Mass Spectrometric Method to Distinguish Isobaric Monosaccharides that are Phosphorylated or Sulfated Using Ion-Pairing Reagents, *J. Am. Soc. Mass Spectrom. 16*, 1827-1839.

28. Irungu, J., Dalpathado, D. S., Go, E. P., Jiang, H., Ha, H.-V., Bousfield, G. R., and Desaire, H. (2006) Method for Characterizing Sulfated Glycoproteins in a Glycosylation Site-Specific Fashion, Using Ion Pairing and Tandem Mass Spectrometry, *Anal. Chem. 78*, 1181-1190.

29. Patrick, A. L., and Polfer, N. C. (2015) H2SO4 and SO3 Transfer Reactions in a Sulfopeptide-Basic Peptide Complex, *Anal. Chem. 87*, 9551-9554.

30. Ballantine, J. A., Slater, P. S., and Games, D. E. (1995) The Use of Amine Base to Enhance the Sensitivity of Electrospray Mass Spectrometry Towards Complex Polysulphonated Azo Dyes, *Rapid Commun. Mass Spectrom. 9*, 1403-1410.

31. Ballantine, J. A., Games, D. E., and Slater, P. S. (1997) The Use of Diethylamine to Determine the Number of Sulphonate Groups Present Within Polysulphonated Alkali Metal Salts by Electrospray Mass Spectrometry, *Rapid Commun. Mass Spectrom. 11*, 630-637.

32. McAlister, G. C., Russell, J. D., Rumachik, N. G., Hebert, A. S., Syka, J. E., Geer, L. Y., Westphall, M. S., Pagliarini, D. J., and Coon, J. J. (2012) Analysis of the acidic proteome with negative electron-transfer dissociation mass spectrometry, *Anal. Chem. 84*, 2875-2882.

33. Mellors, J. S., and Jorgenson, J. W. (2004) Use of 1.5-μm Porous Ethyl-Bridged Hybrid Particles as a Stationary-Phase Support for Reversed-Phase Ultrahigh-Pressure Liquid Chromatography, *Anal. Chem. 76*, 5441-5450.

34. Valaskovic, G. A., Kelleher, N. L., Little, D. P., Aaserud, D. J., and McLafferty, F. W. (1995) Attomole-Sensitivity Electrospray Source for Large-Molecule Mass Spectrometry, *Anal. Chem. 67*, 3802-3805.

35. Riley, N. M., and Coon, J. J. (2016) Phosphoproteomics in the Age of Rapid and Deep Proteome Profiling, *Anal. Chem. 88*, 74-94.

36. Aebersold, R., and Mann, M. (2016) Mass-spectrometric exploration of proteome structure and function, *Nature 537*, 347-355.

37. Haynes, W. M. (2016) *CRC Handbook of Chemistry and Physics, 97th Edition*, CRC Press.

38. Hunter, E. P. L., and Lias, S. G. (1998) Evaluated gas phase basicities and proton affinities of molecules: An update, *J. Phys. Chem. Ref. Data 27*, 413-656.

Observation of the Polyketide Synthase Bryostatin "in action" via Optimized Digestion and nLC-MS/MS Detection

5.1 Introduction

Many organisms in nature produce bioactive secondary metabolites that can be leveraged as antibiotics, and other pharmaceuticals.[1] A major portion of these natural products, e.g., the antibiotics tetracycline and erythromycin, are polyketides, generated by large, modular polyketide synthases (PKSs).[2, 3] Bryostatin-1, initially isolated from the marine bryozoan *Bugula neritina*, has proven to be a potent inhibitor of protein kinase C, causing sensitization of cancer cells to chemotherapy.[4-8] Bryostatin-1 has also exhibited promising activity in the treatment of Alzheimer's disease, stroke, and diabetes.[9-12] Current production of bryostatin-1 via total synthesis is inefficient and involves a total of 27 steps to complete.[13] The difficultly of brute force synthesis has resulted in exorbitantly high prices ($16.6 Million/g) and scarce supply (Sigma).

While total synthesis is not currently an effective method for the production of bryostatin-1, the discovery of the bryostatin (Bry) PKS gene cluster in the uncultured bacterial symbiont *Endobugula sertula* has opened the door for potential biosynthetic production[14] Studies of several individual Bry modules have provided insight into enzymatic selectivity and activity. The Bry enzymatic architecture can be seen in Figure 5.1. BryP has been discovered to be a mainly malonyl specific trans didomain acyltransferase (AT) subunit.[15] Also the 3-hydroxy-3-methylglutaryl (HMG) cassette BryR, has been examined for catalyzing of the unique β-branching event observed in bryostatin-1 biosynthesis.[16]

In this study we examine the catalytic process of BryA module 3 (BryAM3) and the resulting β-branching and *O*-methylation of the growing natural product (Figure 5.1) via high resolution tandem mass spectrometry. Through observation of BryAM3 "in action", we hope to gain insights into the catalytic mechanisms employed by this enzyme, and apply these findings to future studies with unnatural acyl substrate condensation and introduction of BryAM3 into other PKS pathways. BryAM3 is approximately 122 kDa necessitating digestion for on-line detection of covalently bound enzymatic intermediates. Fast BryAM3 tryptic digestion was modified from previous studies on the pikromycin module 5 PKS, to retain labile natural product intermediates and maximize active-site peptide detection.[17, 18]
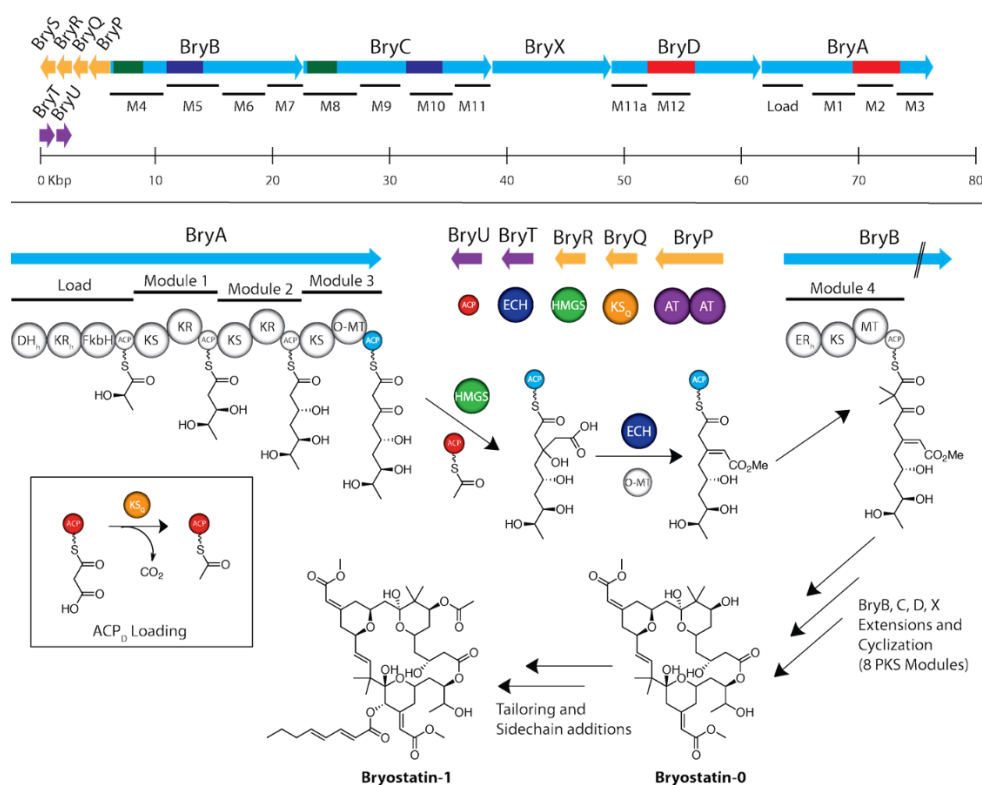
Figure 5.1: Architecture of the bryostatin gene cluster (Top) and proposed organization of the initial PKS domains (Bottom).[14] The BryA module 3 (BryAM3) ketosynthase (KS) accepts an upstream triketide and completes a Claisen condensation with the malonyl extender unit loaded on the BryM3 acyl carrier protein (ACP). The resulting tetraketide is then further tailored by the HMG cassette, resulting in a unique β-branching event. The β-branched tetraketide is dehydrated, *O*-methylated, and passed upstream for further extension and modification of the natural product scaffold. Figure produced by Samuel T. Slocum.

Loading of the malonyl extender unit onto the acyl carrier protein (ACP) via Kirromycin trans AT (KirCAT) was monitored and quantified. Introduction of a thiophenol surrogate triketide was

examined for loading onto the ketosynthase (KS) and for condensation with the malonyl loaded on the phosphopantetheinylated (Holo) ACP.

5.2 Experimental

5.2.1 BryAM3 and KirCAT Expression and Purification

All protein expression optimization and purification was performed by Samuel T. Slocum in Prof. David Sherman's Laboratory. Overexpression plasmids were generate by amplifying the genes from the linear DNA and inserting into pMCSG7 through ligation independent cloning (LIC).[19] BryAM3 was amplified from a cosmid containing a fragment of the *Endobugula sertula* genome.[14] KirCAT was amplified from a plasmid generously provided by the lab of Professor Gavin Williams.[20] KirCAT and BryAM3 were expressed in *E. coli* BL21 (DE3) and in *E. coli* Bap1 (which contains a genomic integration of the sfp phosphopantetheinyl transferase), respectfully.[21] Transformed cells were grown at 37°C in 1L of Terrific Broth (TB) in 2L, baffled Fernbach flasks until OD600 reached ~ 1. Cells were cooled to 20°C and overexpression of proteins of interest were induced by addition of 0.2 mM isopropyl b-D-thiogalactopyranoside (GoldBio). Cells were grown for an additional 12-16 hours with shaking before harvesting by centrifugation and freezing at -80°C. Cell pellets were subsequently thawed at 4°C and resuspended in 7 mL/g buffer A [300 mM NaCl, 10% glycerol, 50 mM HEPES pH 8.0] with 0.8 mg/mL lysozyme and 5mM $MgCl_2$ added. Cells were lysed by sonication and clarified by centrifugation. Clarified lysates were passed over a 0.45 µm filter and 50 mM imidazole (pH 7.5) was added before loading onto a 5 mL HiPrep FF NiNTA (GE Healthcare) column. The column was washed with 100 mL buffer A with added 50 mM imidazole and proteins were eluted with 20 mL buffer A containing 200 mM imidazole. Eluted fractions were exchanged into storage buffer [100 mM NaCl, 20 mM HEPES 7.8, 10% glycerol] using PD10 columns (GE Healthcare), flash frozen in liquid nitrogen and stored at -80°C until needed.

5.2.2 Optimization of Malonyl and Surrogate Triketide Addition

Frozen BryAM3 enzyme fractions (~60 µM) and KirCAT (~150 µM) were first thawed on ice. 1.2 nmol of BryAM3 and 0.3 nmol of KirCAT were mixed with 1 µmol of Mg_2Cl. Molar ratios from 1 to 200 of malonyl- and methylmalonyl-*N*-acetylcysteamine (SNAC) were added and allowed to react at 25°C for 60 min. Molar ratios from 1 to 10 of thiophenol (TP)0linked substrates were

added to the mixtures and incubated for 30 min at 25°C. All samples were immediately subjected to tryptic digestion.

5.2.3 Improved Tryptic Digestion for BryAM3

Tryptic digestion was completed with significant modification to previous protocols.[17, 18] The protein mixture was first exposed to 2.5 M urea denaturation with vigorous mixing for 10 min. Denatured BryAM3 was then diluted to <1 M urea and subjected to 30 min of digestion at 37°C. A protein to trypsin ratio of 1:10 was utilized for all digestions. The tryptic digestion was then quenched with 10% formic acid to pH 4 to limit acid catalyzed hydrolysis of ketosynthase (KS) intermediates.

5.2.4 Nanoflow Liquid Chromatography/Mass Spectrometry

All digests were diluted to ~500 nM. Trap and analytical columns were slurry packed in 75 µm i.d. capillaries with Phenomenex Luna C18(2) material as previously described.[22] Trap and analytical columns were 5 and 25 cm long, respectively. Mobile phases A (95.0% H_2O, 4.9% MeCN, 0.1% FA) and B (4.9% H_2O, 95.0% MeCN, 0.1% FA) were degassed with sonication and He purging. Approximately 2.5 pmol of digest was loaded and desalted with 17 µl of mobile phase A at 2 µl/min. Sample elution and wash conditions are described in Figure 5.2 and 5.4. Mass spectra were collected on a 7T Bruker SolariX Fourier transform ion-cyclotron resonance (FT-ICR) instrument at 100 ms ion accumulation time. Nanoelectrospray ionization voltage was set at – 1.25-1.35 kV for all experiments. Mass spectra were externally calibrated to <2 ppm error before each day's analyses. Accumulate during detect was utilized to improve mass spectrum scans speeds by ~20%. For collision induced fragmentation (CID) of the active site peptides, a separate analysis was completed using a preferred mass list. A MS/MS ion accumulation boost of 300 ms was applied for increased fragment ion sensitivity. The peptides.cef CID energy file was selected for charge sensitive ion fragmentation. All peptides and fragments were assigned at < 5ppm mass error.

5.3 Results and Discussion

5.3.1 Optimization of BryAM3 Active Site Peptide Identification and Separation

Previous studies of the PKS PikAIII via LC-MS demonstrated the need for efficient and fast protein digestion and separation.[17, 18] Initial attempts to examine BryAM3 utilizing identical digestion protocols did not result in the discovery of active site peptides, which carry the natural product intermediates. Modifications to the existing digestion protocol were necessary to observe BryAM3 active site peptides. Alterations included the addition of a denaturant and doubling the digestion time (Figure 5.2). Optimization of the nLC gradient was also necessary to successfully detect the large BryAM3 active site peptides (3rd and 4th largest tryptic peptides) (Figure 5.2). After these method modifications, the KS active site peptide [VSYFLGLQGPSLSIDTM*C*SSSLTAIHEACEHLHR] and the ACP active site peptide [ESLELELDIEPGMLDESKPFTDLGLD*S*INGVTWIR] could be routinely detected at ~40 min and ~42.5 min, respectively. Example mass spectra of KS Apo and ACP Holo active site peptides are shown in Figure 5.3. Peptide identities were confirmed via online tandem mass spectrometry (Figure 5.3).
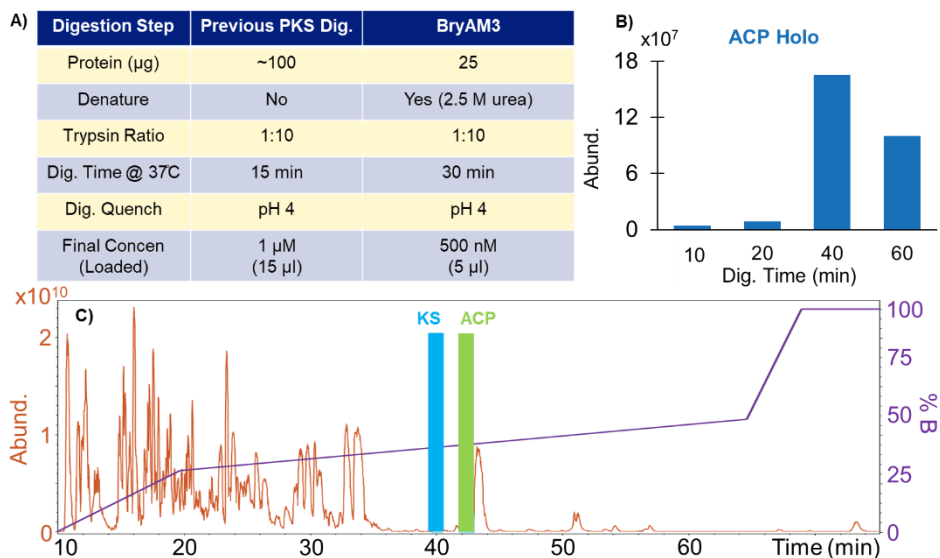

Figure 5.2: Alterations to previous PKS digestion protocols include the addition of a denaturant (**A**) and longer tryptic digestion (Dig) time (**B**). An example base peak chromatogram (BPC) of the optimized BryAM3 digestion and nLC gradient (**C**). The larger >30 mer active site peptides elute at rather high mobile phase strength (> 40% MeCN).

Due to the fast and inefficient tryptic digestion required to retain covalently tethered intermediates, significant run-to-run carryover was observed. BryAM3 peptides could be detected at high abundance for more than seven blank injections after a single BryAM3 injection (data not shown). Thus the implementation of an aggressive column wash cycle was imperative for accurate active site occupancy quantitation. The use of trifluoroethanol as an effective solvent to remove proteinaceous material from C18 has been previously described by Mechtler et al.[23] With the implementation of a 5 μl wash injection (99% trifluoroethanol, 1% trifluoroacetic acid) and three mobile phase cycles, peptide carryover is nearly eliminated (Figure 5.4). After all BryAM3 injections, these washing steps were included to improve overall peptide quantitation.
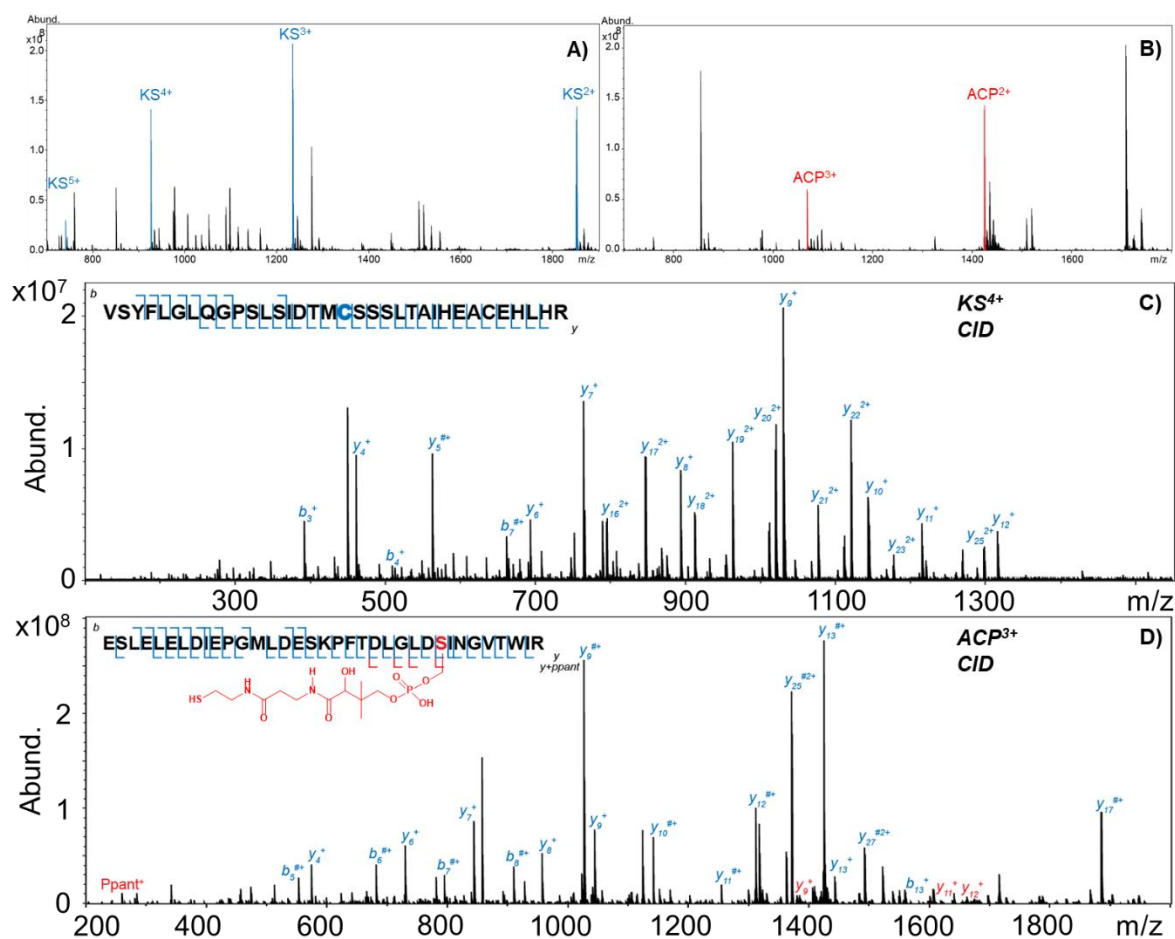

Figure 5.3: Example mass spectra of KS (**A**) and ACP (**B**) active site peptides, eluting at Rt = 39.5 and 41.8 min, respectively. MS/MS confirmation of both KS^{4+} (**C**) and ACP^{3+} (**D**) active site peptides with high (>90%) sequence coverage. # denotes H$_2$O loss. The phosphopantetheine (Ppant) ejection ion was also observed upon ACP active site peptide activation.

Upon establishing routine active site peptide detection, relative quantitation of ACP active site peptide states could be completed. As seen in Figure 5.5, the use of BAP1 *E. coli* cells for the expression BryAM3 was highly efficient as 98% of detected ACP active site peptide was successfully phosphopantetheinylated (i.e. in its Holo form). These results suggest that the purified Holo BryAM3 is should readily accept malonyl for enzymatic condensation, β-branching, and *O*-methylation events.
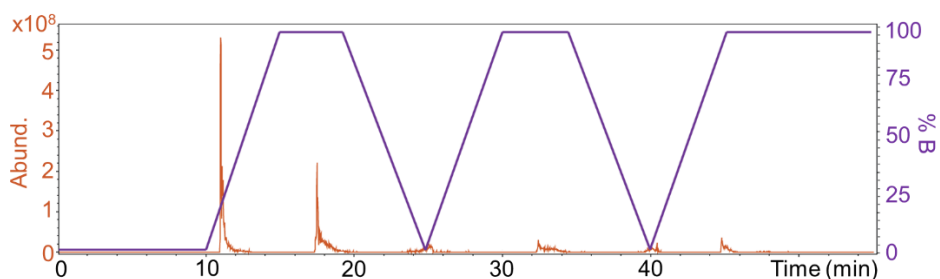
Figure 5.4: Extracted ion chromatogram (orange), showing significant carry-over of a 3+ peptide during a column wash. Following a 5 µl injection of acidified trifluoroethanol and three mobile phase cycles (purple), the peptide abundance is reduced to <1% of its initial abundance.
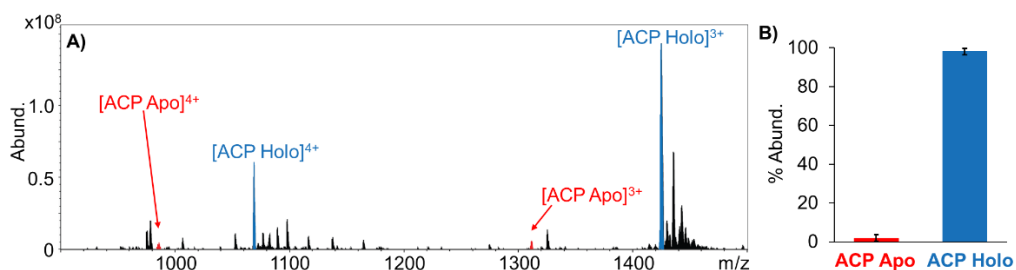
Figure 5.5: Example mass spectrum of Apo and Holo ACP active site peptide (**A**). Approximately 98% of detected ACP active site peptide was phosphopantetheinylated. Error bars correspond to ± σ.

When KirCAT and malonyl-SNAC are incubated with BryAM3, loading of malonyl onto the Holo ACP is observed (Figure 5.6). KirCAT was utilized as a malonyl specific trans-AT instead of native BryP trans-AT due to the difficulty of successful BryP expression and purification. Upon collisional activation, the phosphopantetheine+malonyl (Ppant+Mal) ejection ion is present, confirming successful addition of malonyl by the trans KirCAT.[24] From concentration dependent analysis (Figure 5.6), a maximum of 68% malonyl loading of Holo ACP was achieved at a 50 fold molar excess of malonyl-SNAC. Interestingly, at high malonyl-SNAC concentrations, malonyl addition was also observed for two BryAM3 cysteine containing peptides (Fig.5.6A). An example

mass spectrum of such a peptide can be seen in Figure 5.7. Upon removal of KirCAT in 100 fold molar excess of malonyl-SNAC, malonyl addition is absent for all observed tryptic peptides. KirCAT also does not successfully catalyze methylmalonyl addition to any BryAM3 peptides, as previously been reported.[20] To our knowledge, these results constitute the first discovery of aberrant cysteine acylation by a trans AT *in vitro*.
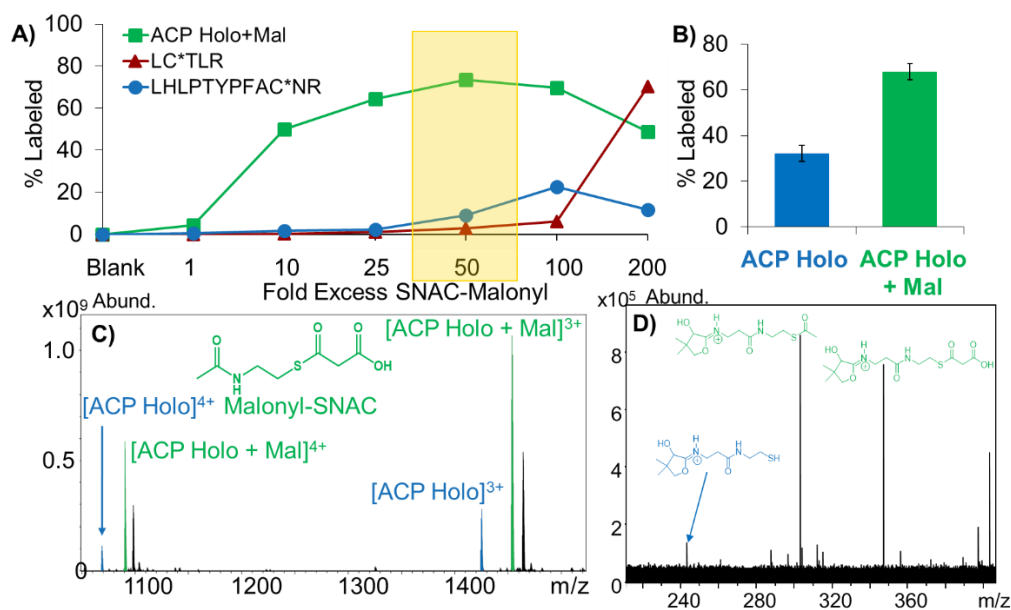
Figure 5.6: Concentration dependent analysis of malonyl loading onto Holo ACP, and two cysteine containing peptides via KirCAT (**A**). At a 50 fold molar excess of malonyl-SNAC, 68% of Holo ACP is loaded with malonyl (**B**). Example mass spectrum of malonyl loaded Holo ACP at Rt = 40.8 min (**C**) and Ppant ejection product ions upon collisional activation of the malonyl-bound ACP peptide (**D**).
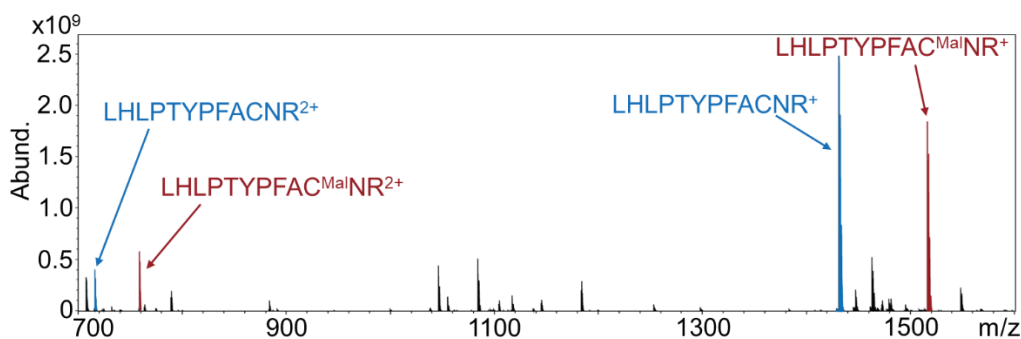
Figure 5.7: Example mass spectrum of a BryAM3 cysteine containing peptide (Rt = 21.4 min) that has been malonated in the presence of KirCAT at a 100 fold molar excess of malonyl-SNAC. Upon removal of KirCAT or substitution of malonyl-SNAC with methylmalonyl-SNAC, malonyl addition is absent for all tryptic peptides.

74

With successful loading of malonyl to Holo ACP, incubation of the malonyl-BryAM3 with the upstream triketide surrogate was completed. Unfortunately, at all concentrations studied, the TP-linked surrogate seemingly skipped KS selection and activation, instead directly adding to the Holo ACP (Figure 5.8). To confirm this observation, an intermediate TP-linked pentaketide from the pikromycin pathway was incubated with malonyl-BryAM3.[17, 18] Again, direct addition of the non-native pentaketide to the BryAM3 Holo ACP was observed. These results indicate that BryAM3 is highly selective for the native triketide for the activation and extension of the bryostatin intermediate, and that activated thiophenol-ketide intermediate substrates may not be ideal for correct BryAM3 KS enzymatic condensation.
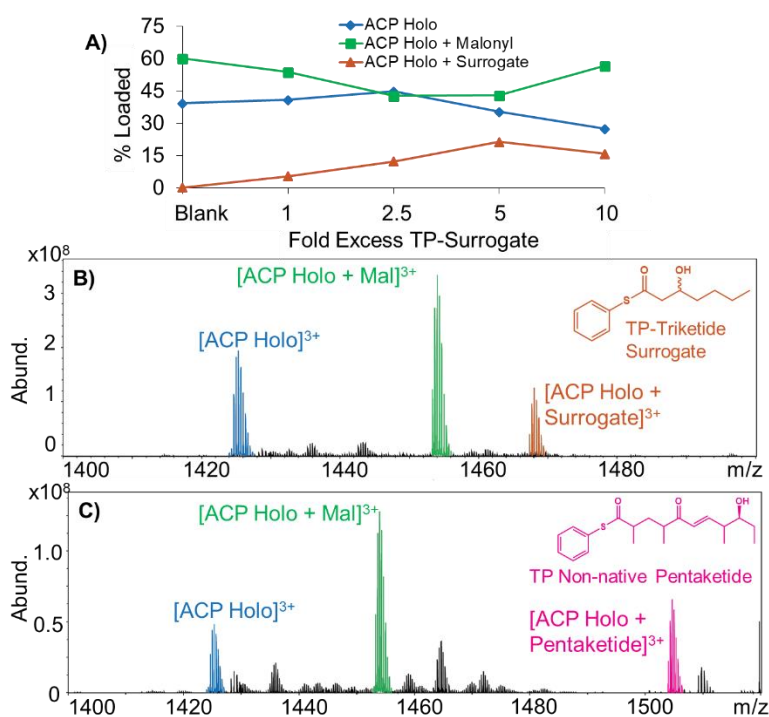

Figure 5.8: As the molar excess of TP-linked triketide surrogate is increased, Holo ACP is incorrectly loaded with the triketide surrogate (**A** and **B**). The addition of the TP-linked substrate to the malonyl loaded Holo ACP does not appear to displace the malonyl, instead adding directly to the Holo BryAM3 ACP. No condensation to generate a tetraketide is observed. With incubation of Mal-BryAM3 and a non-native pentaketide substrate, significant loading of the non-native substrate directly added to the BryAM3 ACP is observed (**C**).

5.4 Conclusions

The PKS BryAM3 was successfully monitored via optimized tryptic digestion and nLC-MS/MS. The nLC gradient was optimized for detection of large (>30 mer) active site peptides with minimal

run-to-run carryover. BryAM3 was successfully phosphopantetheinylated (98%) and accepted the native malonyl extender unit from the non-native trans AT, KirCAT, at 68% efficiency. KirCAT also attaches malonyl to cysteine residues, potentially altering the structure and function of BryAM3. Finally, TP-linked surrogate triketide and nonnative pentaketide substrates directly add to the BryAM3 Holo ACP, rather than undergoing KS activation and extension of the substrate. Future work includes generation of the native triketide substrate and application of other activated triketides for KS addition such as BryAM2 ACP-triketide or triketide-SNAC constructs. We are also interested in examining the unexpected malonation by KirCAT with other trans AT enzymes, such as BryP and phormidolide synthase PhmC or PhmD.[15, 25]

5.5 References

1. Newman, D. J., and Cragg, G. M. (2012) Natural Products As Sources of New Drugs over the 30 Years from 1981 to 2010, *J. Nat. Prod. 75*, 311-335.
2. Kim, E.-S., Bibb, M. J., Butler, M. J., Hopwood, D. A., and Sherman, D. H. (1994) Sequences of the oxytetracycline polyketide synthase-encoding otc genes from Streptomyces rimosus, *Gene 141*, 141-142.
3. Donadio, S., Staver, M. J., McAlpine, J. B., Swanson, S. J., and Katz, L. (1991) Modular Organization of Genes Required for Complex Polyketide Biosynthesis, *Science 252*, 675-679.
4. Kraft, A. S., Smith, J. B., and Berkow, R. L. (1986) Bryostatin, an activator of the calcium phospholipid-dependent protein kinase, blocks phorbol ester-induced differentiation of human promyelocytic leukemia cells HL-60, *Proc. Natl. Acad. Sci. U.S.A. 83*, 1334-1338.
5. May, W. S., Tyler, P. G., Ito, T., Armstrong, D. K., Qatsha, K. A., and Davidson, N. E. (1994) Interleukin-3 and bryostatin-1 mediate hyperphosphorylation of BCL2 alpha in association with suppression of apoptosis, *J. Biol. Chem. 269*, 26865-26870.
6. Trindade-Silva, A. E., Lim-Fong, G. E., Sharp, K. H., and Haygood, M. G. (2010) Bryostatins: biological context and biotechnological prospects, *Current Opinion in Biotechnology 21*, 834-842.
7. Hennings, H., Blumberg, P. M., Pettit, G. R., Herald, C. L., Shores, R., and Yuspa, S. H. (1987) Bryostatin-1, An Activator of Protein-Kinase-C, Inhibitys Tumor Promotion by Phorbol Esters in SENCAR Mouse Skin, *Carcinogenesis 8*, 1343-1346.
8. Nelson, T. J., and Alkon, D. L. (2009) Neuroprotective versus tumorigenic protein kinase C activators, *Trends Biochem. Sci. 34*, 136-145.
9. Nelson, T. J., Cui, C., Luo, Y., and Alkon, D. L. (2009) Reduction of β-Amyloid Levels by Novel Protein Kinase Cε Activators, *J. Biol. Chem. 284*, 34514-34521.
10. Khan, T. K., Nelson, T. J., Verma, V. A., Wender, P. A., and Alkon, D. L. (2009) A cellular model of Alzheimer's disease therapeutic efficacy: PKC activation reverses Aβ-induced biomarker abnormality on cultured fibroblasts, *Neurobiol. Dis. 34*, 332-339.

11. Sun, M.-K., Hongpaisan, J., and Alkon, D. L. (2009) Postischemic PKC activation rescues retrograde and anterograde long-term memory, *Proc. Natl. Acad. Sci. U.S.A. 106*, 14676-14680.

12. Way, K. J., Katai, N., and King, G. L. (2001) Protein kinase C and the development of diabetic vascular complications, *Diabetic Med. 18*, 945-959.

13. Keck, G. E., Poudel, Y. B., Cummins, T. J., Rudra, A., and Covel, J. A. (2011) Total Synthesis of Bryostatin 1, *J. Am. Chem. Soc. 133*, 744-747.

14. Sudek, S., Lopanik, N. B., Waggoner, L. E., Hildebrand, M., Anderson, C., Liu, H., Patel, A., Sherman, D. H., and Haygood, M. G. (2007) Identification of the Putative Bryostatin Polyketide Synthase Gene Cluster from "Candidatus Endobugula sertula", the Uncultivated Microbial Symbiont of the Marine Bryozoan Bugula neritina, *J. Nat. Prod. 70*, 67-74.

15. Lopanik, N. B., Shields, J. A., Buchholz, T. J., Rath, C. M., Hothersall, J., Haygood, M. G., Håkansson, K., Thomas, C. M., and Sherman, D. H. (2008) In Vivo and In Vitro Trans-Acylation by BryP, the Putative Bryostatin Pathway Acyltransferase Derived from an Uncultured Marine Symbiont, *Chem. Biol. 15*, 1175-1186.

16. Buchholz, T. J., Rath, C. M., Lopanik, N. B., Gardner, N. P., Håkansson, K., and Sherman, D. H. (2010) Polyketide β-Branching in Bryostatin Biosynthesis: Identification of Surrogate Acetyl-ACP Donors for BryR, an HMG-ACP Synthase, *Chem. Biol. 17*, 1092-1100.

17. Dutta, S., Whicher, J. R., Hansen, D. A., Hale, W. A., Chemler, J. A., Congdon, G. R., Narayan, A. R. H., Hakansson, K., Sherman, D. H., Smith, J. L., and Skiniotis, G. (2014) Structure of a modular polyketide synthase, *Nature 510*, 512-517.

18. Whicher, J. R., Dutta, S., Hansen, D. A., Hale, W. A., Chemler, J. A., Dosey, A. M., Narayan, A. R. H., Hakansson, K., Sherman, D. H., Smith, J. L., and Skiniotis, G. (2014) Structural rearrangements of a polyketide synthase module during its catalytic cycle, *Nature 510*, 560-564.

19. Stols, L., Gu, M., Dieckman, L., Raffen, R., Collart, F. R., and Donnelly, M. I. (2002) A New Vector for High-Throughput, Ligation-Independent Cloning Encoding a Tobacco Etch Virus Protease Cleavage Site, *Protein Express. Purif. 25*, 8-15.

20. Musiol, E. M., Greule, A., Hartner, T., Kulik, A., Wohlleben, W., and Weber, T. (2013) The AT(2) Domain of KirCI Loads Malonyl Extender Units to the ACPs of the Kirromycin PKS, *ChemBioChem 14*, 1343-1352.

21. Pfeifer, B. A., Admiraal, S. J., Gramajo, H., Cane, D. E., and Khosla, C. (2001) Biosynthesis of Complex Polyketides in a Metabolically Engineered Strain of E. coli, *Science 291*, 1790-1792.

22. Mellors, J. S., and Jorgenson, J. W. (2004) Use of 1.5-μm Porous Ethyl-Bridged Hybrid Particles as a Stationary-Phase Support for Reversed-Phase Ultrahigh-Pressure Liquid Chromatography, *Anal. Chem. 76*, 5441-5450.

23. Mitulović, G., Stingl, C., Steinmacher, I., Hudecz, O., Hutchins, J. R. A., Peters, J.-M., and Mechtler, K. (2009) Preventing Carryover of Peptides and Proteins in Nano LC-MS Separations, *Anal. Chem. 81*, 5955-5960.

24. Dorrestein, P. C., Bumpus, S. B., Calderone, C. T., Garneau-Tsodikova, S., Aron, Z. D., Straight, P. D., Kolter, R., Walsh, C. T., and Kelleher, N. L. (2006) Facile Detection of Acyl and Peptidyl Intermediates on Thiotemplate Carrier Domains via

Phosphopantetheinyl Elimination Reactions during Tandem Mass Spectrometry, *Biochemistry 45*, 12756-12766.

25. Bertin, M. J., Vulpanovici, A., Monroe, E. A., Korobeynikov, A., Sherman, D. H., Gerwick, L., and Gerwick, W. H. (2016) The Phormidolide Biosynthetic Gene Cluster: A trans-AT PKS Pathway Encoding a Toxic Macrocyclic Polyketide, *ChemBioChem 17*, 164-173.

Chapter 6

Conclusions and Future Directions

6.1 Dissertation Overview

Each chapter presented in this dissertation attempts to address modern proteomic challenges. In Chapter 2, the corona discharge suppression upon addition of the fluorosolvent TFE in negative ion mode nanoelectrospray ionization was examined. With addition of as little as 0.2% TFE to aqueous samples, nESI stability is greatly increased and corona discharge is suppressed. The addition of TFE does not alter observed analyte charge states. Upon addition of TFE to mobile phase solvents, an 18% protein sequence coverage increase is observed due to the elimination of corona discharge during negative ion mode nLC-MS proteomic analysis.

The compatibility of TFE with nLC-MS experiments allowed for interrogation of mobile phase pH and detection polarity effects on overall protein sequence coverage, as described in Chapter 3. Regardless of eluent pH and detection polarity, observed protein sequence coverages were maximized at low and high pH extremes, likely due to effective nLC separation of tryptic peptides. However, multiply phosphorylated peptides were only detected at alkaline pH in negative ion mode. Sulfated peptides could also only be detected effectively in negative ion mode, and most efficiently at pH 11.

Chapter 4 examined sulfopeptide alkylamine adducts for effective positive ion mode analysis. All seven alkylamines tested successfully and selectively adducted to sulfopeptides, preventing proton mediated elimination of the PTM. Adduction is observed at 0.05% TEA solution concentration over a range of pHs from 3-11. With slight collisional activation of adducted peptides, a

[SO$_3$+alkylamine] neutral loss is observed. This unique neutral loss was utilized to discover sulfopeptide standards in a complex tryptic peptide mixture at high and low separation pH via DIA nLC-MS/MS.

The PKS BryAM3 was studied via optimized nLC-MS/MS, as described in Chapter 5. A modified fast tryptic digestion protocol was developed to allow for detection of biosynthetic intermediates loaded onto active site ACP and KS peptides. For improved label-free quantitation of such active site peptides, a TFE wash cycle was implemented, reducing run-to-run carryover effects of incompletely digested protein. Using the trans AT KirCAT, malonyl was loaded onto BryAM3 Holo ACP at 68% and confirmed via Ppant ejection. KirCAT was also observed to unexpectedly add malonyl to non-active site cysteine containing peptides, potentially altering BryAM3 structure/function. Finally, thiophenol linked substrates were observed to skip KS loading and condensation with malonyl, instead adding directly to the Holo ACP.

6.2 Future Work and Development

6.2.1 Trifluoroethanol and Negative Ion Mode Corona Discharge Suppression Mechanism
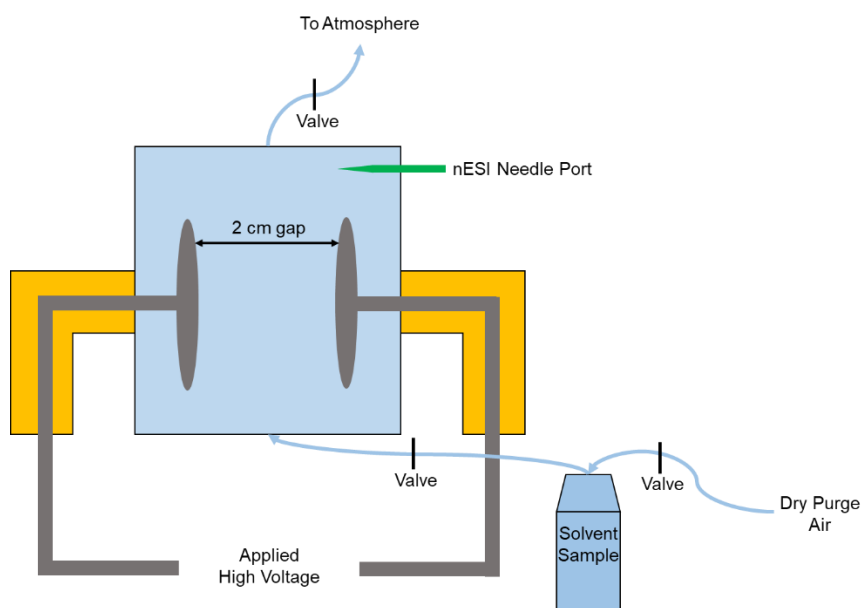
Figure 6.1: Sample instrument schematic for the examination of gas-phase dielectric constants of solvent systems utilized in negative ion mode nESI. Solvent gases can be introduced into the analysis chamber via bubbling of dry air through a solvent container or direct nESI of sample solvents. After gaseous sample solvents are introduced, the pressure in the chamber is equalized to 1 bar and the voltage is ramped until dielectric breakdown occurs.

While we have shown the utility of TFE in the suppression of corona discharge in Chapter 2, the exact mechanism of corona discharge suppression is not currently known. We postulate that the TFE molecule can act as an electron scavenger in the gas-phase, stemming plasma formation. To directly confirm the increase in atmospheric dielectric constant we have postulated, a device as seen in Figure 6.1 could be used to probe gas-phase dielectric constants of TFE laden nESI solutions. A solvent bottle would contain the solvent system of interest equilibrated at 1 bar with the analysis chamber. The bottle would then be closed and the potential would be ramped until dielectric breakdown occurs, providing a direct measurement of the dielectric barrier of the gas. With the measured gas-phase dielectric constants for TFE/water mixtures, we could assess the currently postulated mechanism of TFE corona discharge suppression.

6.2.2 Mobile Phase pH and Phosphoproteomic Coverage

In the work described in Chapter 3, multiply phosphorylated peptides were only detected at pH 11 with negative ion mode ionization. Previous uses of high pH mobile phases for negative ion mode proteomic experiments have been completed, however, the samples utilized were not examined with phosphopeptides included in the bioinformatic peptide search space.[55, 96, 98] A study by Brodbelt et al. utilized IMAC phosphopeptide enrichment strategies for improved negative ion mode phosphopeptide detection, but did not complete TiO_2 enrichment or examine the phosphopeptides at elevated pH in negative ion mode.[183] From our current results, alkaline pH would be ideal for the detection of highly phosphorylated peptides in negative ion mode. In the future, a HeLa cell lysate could be enriched for phosphopeptides via IMAC and TiO_2 enrichment strategies. This complex phosphopeptide sample could then be eluted with the five different mobile phase pHs at both polarities, as shown in Chapter 3. Due to the immense increase in sample complexity, CID or ETD fragmentation for positive ions and UVPD or NETD for negative ions would need to be completed for confident peptide identifications. The results of optimized alkaline negative ion mode nLC-MS in Chapter 3 indicates that novel multiply phosphorylated peptides would be preferentially discovered in the HeLa phosphoproteome.

6.2.3 Large Scale Sulfoproteome Analysis

Adduction of sulfopeptides with alkylamines provides the first facile, covalent modification-free, positive ion mode discovery of an organism's sulfoproteome. While previous studies have examined the sulfoproteome with semi-selective covalent modification, the DIA nLC-MS/MS

workflow demonstrated in Chapter 4 allows for sulfopeptide discovery without complex sample preparation. Also, because alkylamines selectively adduct to sulfopeptides at pH 3 and low concentrations (<0.1%), standard silica-based C18 stationary phases can be utilized, making adoption of this workflow possible with almost no modifications to existing instrumentation. Currently, sulfopeptide enrichment strategies such as WAX and MOAC have been developed but improvements to these strategies may be necessary when enrichment of an entire sulfoproteome enrichment is completed, due to the vast number of acidic peptides present in the sample.[137, 138]

With the addition of an Orbitrap Fusion Lumos instrument to our Chemistry department, MS^3 type experiments can be employed for sulfoproteome discovery with alkylamine-sulfopeptide adducts. For such experiments, first a high resolution MS scan would be completed in the Orbitrap. Next, low-energy DIA collisional activation would be completed, and the resulting fragment ions are analyzed in the Orbitrap to maximally resolve peptide ions. If an ion is observed to 1) decrease signal by ~80% from the MS to MS/MS scan and 2) a fragment ion peak appears in the MS/MS spectrum that is equivalent to the mass loss of the [SO$_3$+alkylamine], a CID or HCD ion-trap MS^3 event on the ion of interest would be completed to maximize Orbitrap duty cycle. With our FT-ICR instrument, DIA nLC-MS/MS analysis can only successfully flag sulfated peptides for peptide fragmentation in a separate analysis but, with the Orbitrap Fusion Lumos, the sulfopeptide flagging and fragmentation can be completed during the same analysis. The MS^3 approach will allow for unambiguous sulfopeptide identifications in half the time of the current MS^2 experiments.
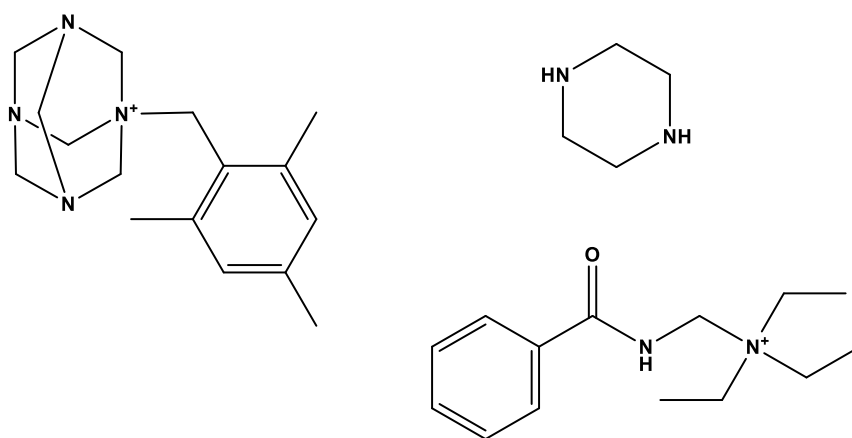

Figure 6.2: Example alkylamines for increased charging of sulfopeptides.

While sulfopeptides are selectively adducted by alkylamines, the sulfopeptide standards caerulein and gastrin I adduct more than one alkylamine. This phenomenon leads to ambiguity in the exact

location of the alkylamine binding location on the gas-phase sulfopeptide complex. Fragmentation of peptide cations via ECD can maintain labile PTMs and even gas-phase adducts.[88, 89, 260, 261] Alkylamine-adducted gastrin I is only observed in a 2+ charge state and upon electron irradiation for ECD analysis, only charge reduction and [SO_3+alkylamine] loss is observed. For improved ECD and alkylamine adduct location determination, the charge state of the gastrin I could be increased via quaternary amines and diamines (Figure 6.2).

6.2.3 Improvements for Future Polyketide Synthase *in vitro* Biosynthetic Experiments

In Chapter 6, KirCAT was observed to malonate non-active site cysteine containing peptides. This finding is, to our knowledge, the first reported instance of a trans-AT adding an activated acyl substrate to such thiol containing residues. More experiments are necessary to confirm this phenomenon. Incubation of KirCAT and malonyl-SNAC with standard peptides and protein digests with free cysteines should be completed. Also, examination of acylation promiscuity could be examined with other trans-ATs such as BryP, mycosubtilin synthetase FenF, and the recently discovered phormidolide synthase PhmC or PhmD.[254, 259, 262]

To successfully examine the β-branching and *O*-methylation events of BryAM3, addition of upstream triketide is necessary. Thiophenol linked surrogate substrates were not successfully activated and condensed with the malonyl extender unit, instead being directly loaded onto the Holo ACP. Optimization of the activated substrate is necessary to prevent undesired loading of the BryAM3 Holo ACP. SNAC or upstream BryAM2 Holo ACP linked substrates could be explored for efficient loading of the BryAM3 KS. Correct loading of the BryAM3 KS may occur with the native triketide substrate as well. These improvements/modifications are necessary to observe the native condensation and modification catalyzed by BryAM3.

6.3 References

1. Madsen, J. A., Xu, H., Robinson, M. R., Horton, A. P., Shaw, J. B., Giles, D. K., Kaoud, T. S., Dalby, K. N., Trent, M. S., and Brodbelt, J. S. (2013) High-throughput Database Search and Large-scale Negative Polarity Liquid Chromatography–Tandem Mass Spectrometry with Ultraviolet Photodissociation for Complex Proteomic Samples, *Mol. Cell. Proteomics 12*, 2604-2614.
2. McAlister, G. C., Russell, J. D., Rumachik, N. G., Hebert, A. S., Syka, J. E., Geer, L. Y., Westphall, M. S., Pagliarini, D. J., and Coon, J. J. (2012) Analysis of the acidic proteome with negative electron-transfer dissociation mass spectrometry, *Anal. Chem. 84*, 2875-2882.

3. Riley, N. M., Rush, M. J. P., Rose, C. M., Richards, A. L., Kwiecien, N. W., Bailey, D. J., Hebert, A. S., Westphall, M. S., and Coon, J. J. (2015) The Negative Mode Proteome with Activated Ion Negative Electron Transfer Dissociation (AI-NETD), *Mol. Cell. Proteomics 14*, 2644-2660.

4. Robinson, M. R., Taliaferro, J. M., Dalby, K. N., and Brodbelt, J. S. (2016) 193 nm Ultraviolet Photodissociation Mass Spectrometry for Phosphopeptide Characterization in the Positive and Negative Ion Modes, *J. Proteome Res. 15*, 2739-2748.

5. Hersberger, K. E. (2012) Metal-Oxide Enrichment and Gas-Phase Characterization of Sulfopeptides using Fourier Transform Ion Cyclotron Resonance Mass Spectrometry., University of Michigan.

6. Robinson, M. R., and Brodbelt, J. S. (2016) Integrating Weak Anion Exchange and Ultraviolet Photodissociation Mass Spectrometry with Strategic Modulation of Peptide Basicity for the Enrichment of Sulfopeptides, *Anal. Chem. 88*, 11037-11045.

7. Håkansson, K., Cooper, H. J., Emmett, M. R., Costello, C. E., Marshall, A. G., and Nilsson, C. L. (2001) Electron Capture Dissociation and Infrared Multiphoton Dissociation MS/MS of an N-Glycosylated Tryptic Peptide To Yield Complementary Sequence Information, *Anal. Chem. 73*, 4530-4536.

8. Stensballe, A., Jensen, O. N., Olsen, J. V., Haselmann, K. F., and Zubarev, R. A. (2000) Electron capture dissociation of singly and multiply phosphorylated peptides, *Rapid Commun. Mass Spectrom. 14*, 1793-1800.

9. Haselmann, K. F., Jørgensen, T. J. D., Budnik, B. A., Jensen, F., and Zubarev, R. A. (2002) Electron capture dissociation of weakly bound polypeptide polycationic complexes, *Rapid Commun. Mass Spectrom. 16*, 2260-2265.

10. Horn, D. M., Breuker, K., Frank, A. J., and McLafferty, F. W. (2001) Kinetic Intermediates in the Folding of Gaseous Protein Ions Characterized by Electron Capture Dissociation Mass Spectrometry, *J. Am. Chem. Soc. 123*, 9792-9799.

11. Aron, Z. D., Fortin, P. D., Calderone, C. T., and Walsh, C. T. (2007) FenF: Servicing the Mycosubtilin Synthetase Assembly Line in trans, *ChemBioChem 8*, 613-616.

12. Lopanik, N. B., Shields, J. A., Buchholz, T. J., Rath, C. M., Hothersall, J., Haygood, M. G., Håkansson, K., Thomas, C. M., and Sherman, D. H. (2008) In Vivo and In Vitro Trans-Acylation by BryP, the Putative Bryostatin Pathway Acyltransferase Derived from an Uncultured Marine Symbiont, *Chem. Biol. 15*, 1175-1186.

13. Bertin, M. J., Vulpanovici, A., Monroe, E. A., Korobeynikov, A., Sherman, D. H., Gerwick, L., and Gerwick, W. H. (2016) The Phormidolide Biosynthetic Gene Cluster: A trans-AT PKS Pathway Encoding a Toxic Macrocyclic Polyketide, *ChemBioChem 17*, 164-173.